DEVELOPMENT OF NEW LEAD-FREE SOLDERS FOR
ELECTRONICS INDUSTRY

A THESIS SUBMITTED TO
THE GRADUATE SCHOOL OF NATURAL AND APPLIED SCIENCES
OF
MIDDLE EAST TECHNICAL UNIVERSITY

BY
ANIL KANTARCIOĞLU

IN PARTIAL FULFILLMENT OF THE REQUIREMENTS
FOR
THE DEGREE OF MASTER OF SCIENCE
IN
METALLURGICAL AND MATERIALS ENGINEERING

NOVEMBER 2012

Approval of the thesis:

**DEVELOPMENT OF NEW LEAD-FREE SOLDERS FOR
ELECTRONICS INDUSTRY**

submitted by **ANIL KANTARCIOĞLU** in partial fulfillment of the requirements
for the degree of **Master of Science in Metallurgical and Materials Engineering
Department, Middle East Technical University** by,

Prof. Dr. Canan Özgen   _____
Dean, Graduate School of **Natural and Applied Sciences**

Prof. Dr. Cemil Hakan Gür   _____
Head of Department, **Metallurgical and Materials Engineering**

Assist. Prof. Dr. Yunus Eren Kalay   _____
Supervisor, **Metallurgical and Materials Eng. Dept., METU**

Examining Committee Members:

Prof. Dr. İshak Karakaya   _____
Metallurgical and Materials Engineering Dept., METU

Assist. Prof. Dr. Yunus Eren Kalay   _____
Metallurgical and Materials Engineering Dept., METU

Prof. Dr. Tayfur Öztürk   _____
Metallurgical and Materials Engineering Dept., METU

Prof. Dr. Cemil Hakan Gür   _____
Metallurgical and Materials Engineering Dept., METU

Dr. Caner Batıgün   _____
Welding Tech. and NDT Res./App. Center, METU

Date: *23.11.2012*

I hereby declare that all information in this document has been obtained and presented in accordance with academic rules and ethical conduct. I also declare that, as required by these rules and conduct, I have fully cited and referenced all material and results that are not original to this work.

Name, Last name : ANIL KANTARCIOĞLU

Signature   :

ABSTRACT

DEVELOPMENT OF NEW LEAD-FREE SOLDERS FOR ELECTRONICS INDUSTRY

KANTARCIOĞLU, Anıl

M.Sc., Department of Metallurgical and Materials Engineering

Supervisor: Assist. Prof. Dr. Yunus Eren KALAY

November 2012, 104 pages

Joining of electronic components onto the circuit boards is done by soldering operation, during production of all electronic devices. In many countries, including Turkey, traditionally used tin-lead (Sn-Pb) solder alloys have been restricted to be used in consumer electronics appliances because of the toxic effects of lead (Pb) within these alloys. Tin-silver-copper (Sn-Ag-Cu) based alloys have been developed as the most promising candidate that can replace the Sn-Pb alloys. However, various problems have emerged with the increasing trend in use of Sn-Ag-Cu solder alloys in electronics industry, namely large intermetallic compound formation, low wettability and thermal shock resistance. Many researches have been done in the past decade to overcome these problems. The solutions are based on changing the undercooling of the solder alloy; which was determined to be done by either changing the composition of the solder alloy by micro-alloying or changing the cooling rate during soldering operation.

In this thesis study Sn-3.5Ag-0.9Cu (wt. %) lead-free solder having the eutectic composition, was micro-alloyed with additions of aluminum (Al), iron (Fe) and titanium (Ti).

Experimental results were compared with commercially available near-eutectic Sn-40Pb (wt. %) solder, a commercially available Sn-3.0Ag-0.5Cu (wt. %) solder and also eutectic Sn-3.5Ag.0.9Cu (wt. %) and near-eutectic Sn-3.7Ag-0.9Cu (wt. %) solders that were produced for this thesis study. In the first stage of the study, the effects of 0.05 wt. % of Al, Fe and Ti micro-alloying were investigated. When preliminary results of mechanical and thermal test were compared, Fe was found to make positive effect on shear strength and undercooling. Further research was carried out to establish a relationship between the Fe compositions and solder properties. Therefore, 0.01, 0.03, 0.07 and 0.1 wt. % Fe additions were also studied and results were reported. 0.01 wt. % and 0.07 wt. % Fe added solders were found to have a smaller undercooling, resulting with dispersed intermetallic compound (IMC) and thus has highest shear strength. Different cooling rates; 0.017, 0.17 and 1.7 °C/sec were applied to solder-copper joints and microstructures were investigated. Large IMC-free microstructure was achieved by 0.01 wt. % Fe micro-alloyed solder, which was cooled with 1.7 °C/sec rate. Wetting of copper substrate was found to be improved by additions of Al, Fe and Ti compared to alloy with eutectic composition of Sn-Ag-Cu alloy.

Selected SAC+X alloys have been subjected to thermal shock experiments for crack formation analysis on the copper substrate-solder joints. The results showed that SAC+0.05Al solder has the higher thermal shock resistance, which no cracks were observed after 1500 cycles of thermal shock. In order to understand the insights of SAC performance, some of the lead-free solders were applied onto printed circuit boards for thermal shock resistance test. These results have indicate that the cracking may occur after thermal shock cycles due to process conditions of soldering operation (i.e. cooing rate), independent of the solder alloy composition.

Keywords: lead-free solders, Sn-Ag-Cu, mechanical properties, wetting, thermal shock resistance,

ÖZ

ELEKTRONİK SANAYİSİ İÇİN YENİ KURŞUNSUZ LEHİMLER GELİŞTİRİLMESİ

KANTARCIOĞLU, Anıl

Yüksek Lisans, Metalurji ve Malzeme Mühendisliği Bölümü

Tez Yöneticisi: Yrd. Doç. Dr. Yunus Eren KALAY

Kasım 2012, 104 sayfa

Tüm elektronik aygıtların üretiminde, bileşenlerin devre kartı ile birleştirilmesi lehimleme işlemi ile yapılamktadır. Geleneksel olarak kullanılan kalay-kurşun (Sn-Pb) lehim alaşımlarının tüketici elekroniği uygulamalarında kullanımı, alaşım içerisindeki kurşunun zehirli etkilerinden dolayı, Türkiye de dahil olmak üzere pek çok ülkede sınırlandırılmıştır. Geliştirilen kalay-gümüş-bakır (Sn-Ag-Cu) temelli alaşımlar, Sn-Pb alaşımlarının yerini alabilecek en ümit verici malzemeler olarak görülmektedir. Fakat, Sn-Ag-Cu lehim alaşımlarının elektronik sanayisinde kullanılma eğiliminin artmasıyla beraber, iri metallerarası bileşik oluşumu, düşük ıslatabilirlik ve düşük ısıl çok direnci gibi problemler ortaya çıkmıştır. Geçen on yılda, bu problemlerin çözümüne yönelik pek çok araştırma yapılmıştır. Varılan çözümler genel olarak alaşımın aşırı soğumasının azaltılması üzerine yoğunlaşmaktadır. Bu amaca yönelik olarak, alaşım kompozisyonuna mikro-alaşımlama yöntemi ile element eklenmesi ve katılaşma sırasındaki soğuma hızının ayarlanması yöntemleri çözümleri geliştirilmiştir.

Bu tez çalışmasında, Sn-3.5Ag-0.9Cu (% ağırlık) bileşimindeki kurşunsuz lehim alaşımları, ağırlıkça % 0.05 oranında aluminyum (Al), demir (Fe) ve titanyum (Ti)

elementleri ile mikro-alaşımlanmıştır. Alınan sonuçlar, ticari olarak piyasada bulunan Sn-40Pb (% ağırık) lehim, ticari olarak piyasada bulunan Sn-3.0Ag-0.5Cu (% ağırık) lehim ve bunun yanında bu çalışma için üretilen ötektik Sn-3.5Ag-0.9Cu (% ağırık) ve yakın-ötektik Sn-3.7Ag-0.9Cu (% ağırık) lehimleri ile karşılaştırılmıştır. Çalışmanın ilk aşamasında, ağırlıkça % 0.05 oranında Al, Fe ve Ti eklenmesi ile elde edilen sonuçlar analiz edilmiş ve Fe eklenmesinin alaşıma yaptığı olumlu etkiler bulunmuştur. Çalışmanın ileri aşamalarında, eklenen Fe oranını ile lehim özellikleri arasında doğrudan bir bağıntı kurulmaya çalışılmıştır. Bu sebeple, ağırlıkça % 0.01, 0.03, 0.07 ve 0.1 oranında Fe eklentilerinin yaptığı etkiler araştırılmış ve sonuçlar raporlanmıştır. 0.01 (% ağ.) Fe ile mikro-alaşımlanmış lehimin düşük aşırı soğuma ve sonucunda dağılmış metallerarası bileşik oluşumu ve daha yüksek kesme dayancına sahip olduğu görülmüştür. Alaşım-altlık birleşimlerine, 0.017, 0.17 ve 1.7 °C/sn olmak üzere farklı soğuma hızları uygulanmış ve içyapı üzerindeki etkileri araştırılmıştır. İri metallerarası bileşik bulundurmayan içyapıya 1.7 °C/sn hızında soğutulan 0.01 (% ağ.) Fe eklenmiş lehim alaşımında ulaşılabilmiştir. Bakır altlığı ıslatabilirlik özelliğinin, ötektik kompozisyona sahip Sn-Ag-Cu alaşımına kıyasla, Al, Fe ve Ti eklenmiş numulelerin tümünde geliştiği görülmüştür.

Seçilen SAC+X alaşımları, bakır altlık-lehim birleşimindeki çatlak oluşumlarının incelenmesi için ısıl şok deneylerine tabi tutulmuştur. Sonuçlar göstermiştir ki 1500 ısıl şok döngüsünden sonra çatlak gözlenmeyen SAC+0.05Al alaşımı ısıl şok direnci en yüksek olan alaşımdır. SAC alaşımlarının performansını derinlemesine anlyabilmek için kurşunsuz lehimlerin bazıları baskı devre kartları üzerine uygulanarak ısıl şok direnci sınamasına tabi tutulmuştur. Bunların sonuçları göstermiştir ki lehim alaşımının bileşiminden bağımsız olarak, lehimleme işlemi sırasındaki soğuma hızı gibi koşullara bağlı olarak belirli ısıl şok döngülerinden sonra çatlak oluşumu gözlenebilmektedir.

Anahtar Kelimeler: kurşunsuz lehim, Sn-Ag-Cu, mekanik özellikler, ıslatabilirlik, ısıl şok direnci

To My Family...

ACKNOWLEDGEMENTS

TABLE OF CONTENTS

LIST OF TABLES

TABLES

LIST OF FIGURES

NOMENCLATURE

MCM: Multi-Chip Module

PCB: Printed Circuit Board

RoHS: Restriction of Hazardous Substances

WEEE: Waste Electrical and Electronic Equipment

IMC: Intermetallic Compound

SAC: Sn-Ag-Cu (Tin-Silver-Copper)

SMT: Surface Mount Technology

PTH: Pin Through Hole

NEMI: National Electronics Manufacturing Initiative

JEITA: Japan Electronics & Information Technology Industries Association

BGA: Ball-Grid Array

BSE: Back-Scattered Electron Imaging

SEM: Scanning Electron Microscope

EDS: Energy Dispersive Spectroscopy

XRD: X-Ray Diffraction

ΔT: Undercooling (°C)

γ: Interfacial Energy

θ: Wetting (Contact) Angle (°)

A: Wetting Area (mm^2)

CHAPTER 1

INTRODUCTION

Soldering is a metallurgical technique which is used to join two (or more) metallic objects together by the use of a third alloy, known as solder alloy, which melts below 450 °C and also has a lower melting temperature than materials to be joint. Solder alloy is melted and applied on the joint area, then solidified to join the pieces together. This technique has been practiced for thousands of years by many civilizations. It is estimated that, soldering first emerged in Egypt around 3000 BC to join metals and gems to make jewelry. Some archeological remains of the Roman water piping system revealed that, soldering was also used to join lead pipes together. The word plumbing is derived from *plumbum*, which is the Latin word for lead and the origin of the symbol Pb for lead. It has also been used to make cooking ware, weapons and some tools by many other civilizations.

With the dawn of electronic age by 20th century, soldering has become an irreplaceable technique in the production of electronic devices. All the major electronics components such as resistors, capacitors, transistors and integrated circuits are connected to the printed circuit board (PCB) by soldering. In today's technology, portable electronic devices, modern automobiles, space vehicles, power plants are equipped with numerous soldered electronic components.

For many years, solder alloys containing the combinations of tin (Sn), lead (Pb), antimony (Sb), copper (Cu), silver (Ag), bismuth (Bi), indium (In), zinc (Zn), gold (Au), silicon (Si) and germanium (Ge) have been used in many industrial applications. Among these, tin-lead (Sn-Pb) solder alloys, particularly with compositions ranging between Sn_{95}-Pb_5 and Sn_2-Pb_{98} (wt. %) have been attracted much attention due to their low cost and low/moderate melting temperatures (183 to 316 °C). Eutectic $Sn_{63}Pb_{37}$ and near eutectic $Sn_{60}Pb_{40}$ are the most popular Sn-Pb

based solder alloys and they have been used traditionally in electronics industry due to their manufacturing practicality with reasonable mechanical and wetting properties. On the other hand, The European Union Waste Electrical and Electronic Equipment (WEEE) Directive, published in 2002 and Restriction of Hazardous Substances (RoHS) Directive of European Community, published in 2003 restricted the usage of certain toxic materials including Lead (Pb) in production of electronic devices used in European Union effective on 1 July 2006. Similar directives were adopted in Turkey, Japan, China, South Korea and California (USA). In Turkey, it was declared in the Official Gazette *(Resmi Gazete)* on 30th May 2008 and came into effect in June 2009 **[1]**. Some other countries and states are still debating to call out similar precautions. All the previously published directives strictly banned the use of lead (Pb) in any electronic equipment.

The toxic effects of lead have been known for many years. It has many adverse effects on vital systems in human body and it can affect physical, neurological functions; moreover, since lead strongly bonds to proteins, these negative side effects may appear in time with accumulation of small quantities in human body. Therefore, the use of lead has considerably decreased in recent years, which seriously effects several critical applications dependent on Pb such as soldering process in electronic industry. **Figure 1.1** shows the global consumption of lead-free solders over conventional tin-lead alloys. There is a clear increase in lead-free usage in recent years.
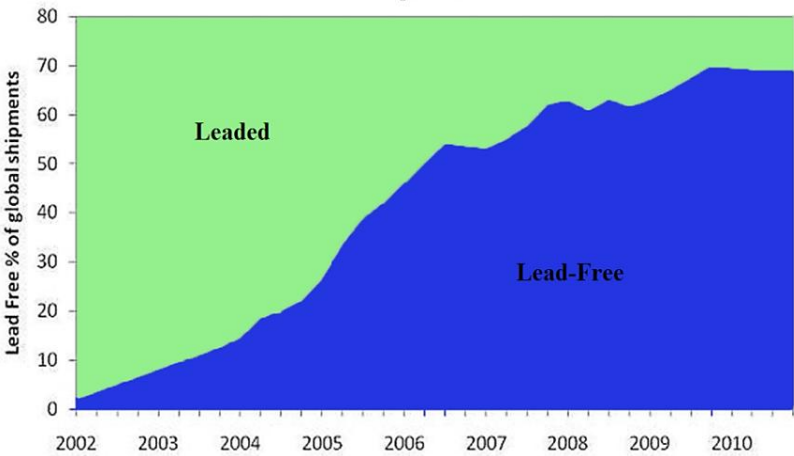
Figure 1.1. Lead-free soldering appliances by years **[2]**.

For the past decade, there has been a great interest in finding the best solder alloy system to substitute Sn-Pb alloys. So far, Sn-Ag-Cu based alloy system has been considered to be the best candidate. Even it has been already commercialized; Sn-Ag-Cu alloy system has several problems to be solved. One of the major problems is the formation of large *intermetallic compounds* (IMC) in these alloys. The presence of large IMCs greatly reduces the reliability of the solder joint. These IMCs act as stress concentrators and negatively effects mechanical properties of the solders. Another problem is the poor wetting of the solder alloys. To have a reliable solder joint, there must be a strong bonding between the solder and the surfaces to be jointed. To achieve this strong bond with smallest amount of solder volume, the solder alloy must wet the largest possible area. The importance of wetting of the solder alloy has increased vitally in the past decade since the sizes of the microelectronic devices have decreased drastically.

The main objective of the current thesis study is to conduct a fundamental study to investigate the microstructural evolution and its effects on mechanical and thermal properties of Sn-Ag-Cu based solder alloys due to the addition of a fourth alloying element and altering the solidification rate. The production is based on ternary eutectic Sn-Ag-Cu alloy. Based on the Hume-Rothery rules, that will be explained in **Chapter 2.3**, aluminum (Al), iron (Fe) and titanium (Ti) were selected to be added to this ternary eutectic alloys as fourth elements to enhance properties. Critical tests were designed to measure thermal, mechanical, microstructural and wetting properties of the solders. All tests and measurements were also applied and compared to near-eutectic $Sn_{60}Pb_{40}$ and Sn-Ag-Cu (SAC305) solders which are commercially available in the market. The organization of this thesis is as follows:

- In the *introduction* chapter, the background information was given, the aim and scope of this thesis study was declared.

- In the *literature review* chapter, a survey of the literature was presented by focusing the details on the past and current studies done by other researchers; as well as insights on the solder and soldering technologies.

- In the *experimental procedures* chapter, the production technique, microstructural, mechanical and performance tests were presented in detail.

- In the *results and discussion* chapter, the outcomes of the critical experiments were given and key points were discussed in terms of thermodynamic and materials properties.

- In the *conclusion and future recommendations* chapter, the conclusions of the study were derived and recommendations were given for future studies on lead-free solders.

CHAPTER 2

LITERATURE REVIEW

2.1. Introduction to Joining Processes

Joining is an essential step in manufacturing of products from smaller parts. There are numerous joining processes for different purposes. Mechanical joints can be formed by using fasteners and rivets for many applications. Welding, soldering, brazing, cementing, taping and gluing are some of the alternative joining methods.

Welding is a manufacturing method that usually metals or thermoplastics are joined by causing coalescence, which is often done by melting the work pieces and adding a filler material to form a pool of molten material (the weld pool) that solidifies to become a strong joint. Pressure may be applied in coherence with heat, or by itself, to produce the weld **[3]**. Unlike welding; soldering, as explained in **Chapter 1**, is done without melting the work pieces. Similarly, brazing is another joining method, where work pieces do not melt during the process. The difference between soldering and brazing is the melting temperatures of the filler materials; where in brazing, melting point of the filler materials are above 450 °C **[4, 5]**. Soldering, done below 450 °C is often called soft-soldering and brazing, done above that temperature is often called hard-soldering.

Soft-soldering is the preferred joining method in electronics industry, since low process temperatures are required during production of electronic assemblies.

2.2. Solders and Soldering in Electronics

Primarily, being a joining material, the solder alloy also serves as an electrical, thermal and mechanical support to the electronic circuits **[6]**. There are many requirements that a solder alloy must satisfy to become reliable and applicable for

all electronic assemblies. The basic requirements of solder alloys are generally described by defining the solder as a material that must wet and form intermetallic compounds at the interface with copper, nickel and other metallic substrates [7]. In that sense, basic properties of solder alloys were given in **Table 2.1**.

Table 2.1. Important properties of solder alloys [6].

Manufacturing Related Properties	Reliability and Performance Related Properties
Melting/liquidus temperature	Electrical conductivity
Wettability (of copper)	Thermal conductivity
Cost	Coefficient of thermal expansion
Environmental friendliness	Shear properties
Availability and number of suppliers	Tensile properties
Manufacturing using current processes	Creep properties
Ability to be fabricated as balls	Fatigue properties
Copper pick up	Corrosion and oxidation resistance
Recyclability	Intermetallic compound formation
Ability to be made into paste	

Electronic devices are being used at a wide range of temperatures. Some common ranges of temperature for specific products are given in **Table 2.2**. Thus, properties relevant to reliability and performance, which were given in **Table 2.1**, must be valid at any temperature in these temperature ranges. Therefore, solder alloys that are commonly used in these electronic equipment should be capable of satisfying the necessary reliability requirements as well.

Table 2.2. Temperature ranges of electronic products [8].

Temperature Range (°C)	Devices
-40 to 100	Most consumer electronics (TV, PC, freezer, washing machine, etc.)
-40 to 125	Reliable consumer electronics (mobile phone, notebook, etc.)
-40 to 150	Vehicles (especially in engine room) and factory equipment

2.2.1. Levels of Soldering

Electronic packaging consists of different levels, which are commonly known as "electronic packaging hierarchy" in electronics industry. Representations of those levels are shown in **Figure 2.1** and they can be described as follows [9]:

Level 0: Gate-to-gate interconnections on the chip. These connections are in nanometer scale and they are produced by unique techniques such as photolithography and ion implantation, during production of semiconductor components.

Level 1: Chip-to-module connections. These connections are in micron scale and located inside integrated circuit modules. Solders are used in this type of connections.

Level 2: Board level interconnections. These are the millimeter size connections where solders are used to join the electronic components onto the circuit board. This is the critical level for production and reliability of electronic devices. These connections are the source of most of the problems seen in electronics, which may result with failure of electronic devices.

Level 3: Board-to-board interconnections. These are usually socket type of connections, in which components are usually not joined but physical contacts of conductors are made for the flow of electrons. Connection between the graphics card and the mother board of a computer may be given as an example to this type connection.

Level 4: Connections between sub-assemblies. For complex electronics systems, many sub-assemblies, such as computers, detectors and controllers are connected to act as a one sophisticated system. This level represents such systems, which many assemblies are connected together.

Level 5: Connections between systems. These are the connections between separate devices. Connection between a computer and a printer may be example to this type of connections.
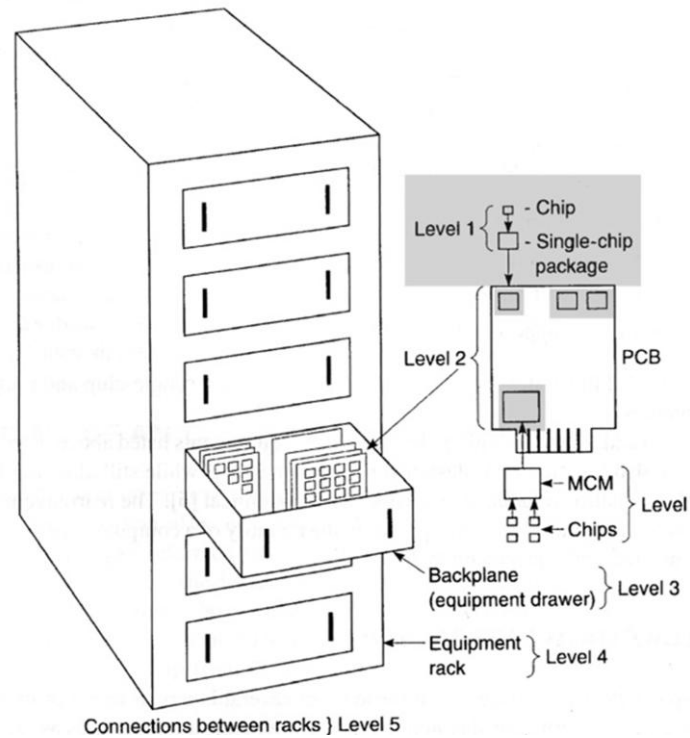
Figure 2.1. Levels of electronic packaging **[9]**.

The scope of this study includes *Level 2* type of connections, which connects module to circuit board with interconnections on millimeter scale.

2.2.2. Soldering Processes

There are two fundamental types of connections in joining the electronic component to PCBs: pin through hole (PTH) and surface mount technology (SMT) **[6]**. These connections are illustrated in **Figure 2.2** and **Figure 2.3**.
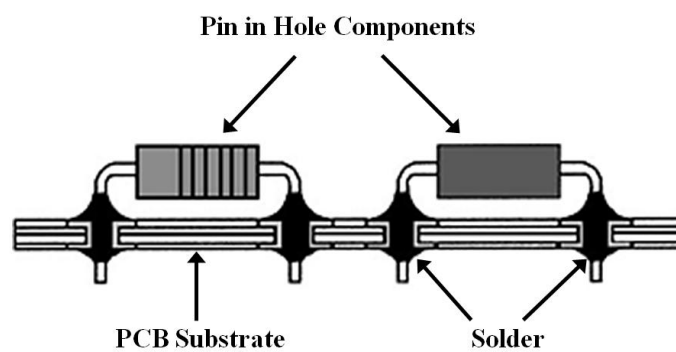
Figure 2.2. Cross-section of a pin through hole connection of a microelectronics component on a PCB **[6]**.
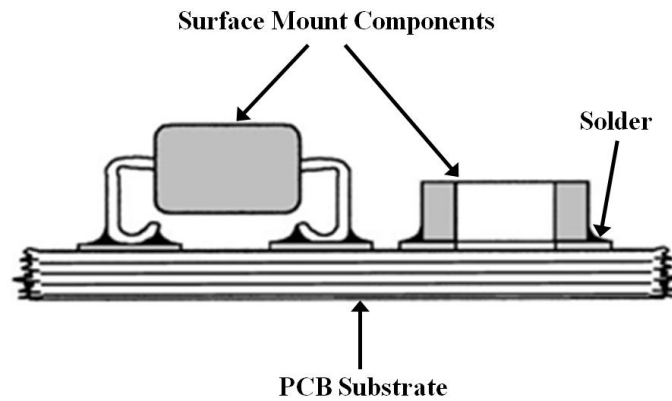
Figure 2.3. Cross-section of a surface mount connection
of a microelectronics component on a PCB [6].

These connections are formed by using different production methods. PTH types of connections are formed by wave soldering and SMT types of connections are formed by reflow soldering.

2.2.2.1. Wave Soldering

In wave soldering method, the assembled PCB is passed over a molten solder wave with a speed of 5-10 cm/s. Solder alloy wets both the surfaces of the pins of the electronic components and the surfaces of the conductor substrates and solidifies between them forming a solder joint. A schematic representation of this method is shown in **Figure 2.4**.
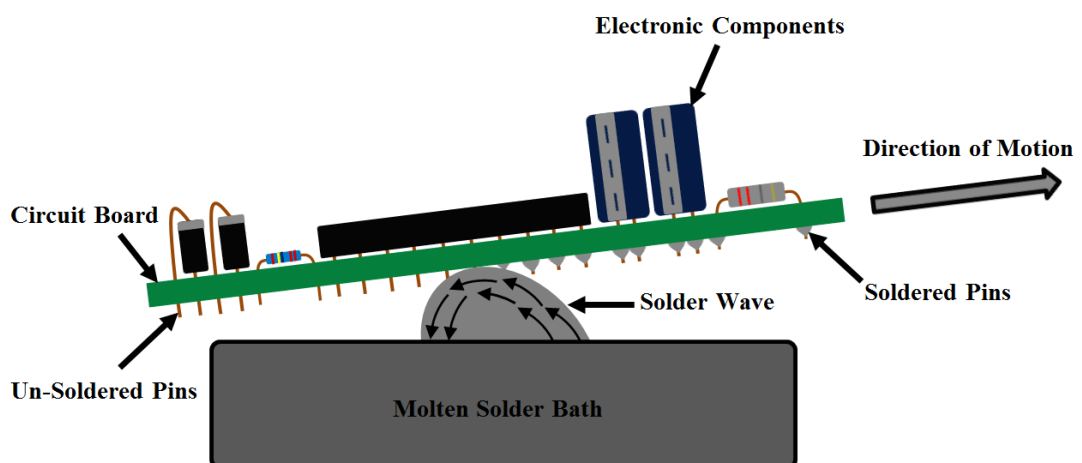
Figure 2.4. Wave soldering of a PCB.

Unlike reflow soldering of SMT, in this technique, the temperature profile cannot be controlled precisely during soldering operation, leading to undesired microstructures and possible cracks. Some surfaces on PCBs, which are not desired to come in contact with the solder such as previously soldered SMT components, are masked prior to this operation. This is called selective soldering.

2.2.2.2. Reflow Soldering

Reflow soldering method involves the use of a solder paste, which is a mixture of solder powder, solder flux and some other additives. The paste, that is in the form a cream, is applied onto the PCB prior to the assembly of electronic components. Subsequently, the components are placed onto the PCB and the electronic assembly is subjected to a controlled heat treatment in a furnace, which melts the solder in the paste. The joints are formed once the assembly is cooled down to room temperature **[6]**. In reflow soldering process, the cooling rate is high; thus even when the eutectic composition is used, completely eutectic microstructure usually cannot be reached **[10]**. The temperature profile that should be achieved during reflow soldering is shown in **Figure 2.5**. The heating rate should be maximum 3 °C/sec, since higher heating rates may create thermal shock for PCB and the electronic components on it. The peak temperature should be above 217 °C since the SAC based lead-free solders has melting temperatures above this temperature. Obviously, there is a limit for the peak temperature since all the electronics components on the PCB are also subjected to similar temperatures. The maximum reflow temperature is determined as 250 °C but slightly lower temperatures are usually preferred. The time that should be spent above the melting temperature is determined to be more than 40 seconds to wet the surfaces and form intermetallic layers at the interfaces but less than 120 seconds to avoid any catastrophic damage of the electronic components as well as to avoid oxidation of the solder alloy. Cooling rate of the joints is critical since ultimate microstructure of the solder will be determined at this step. Slow cooling, which is on the order of 1 °C/sec, must be applied from peak temperature to around 20 °C below the melting temperature of the solder. It should be noted that the solder will be solidified at a lower temperature than its melting temperature since it will undercool during solidification. Once solidified, higher cooling rates may be applied, not exceeding 3 °C/sec.
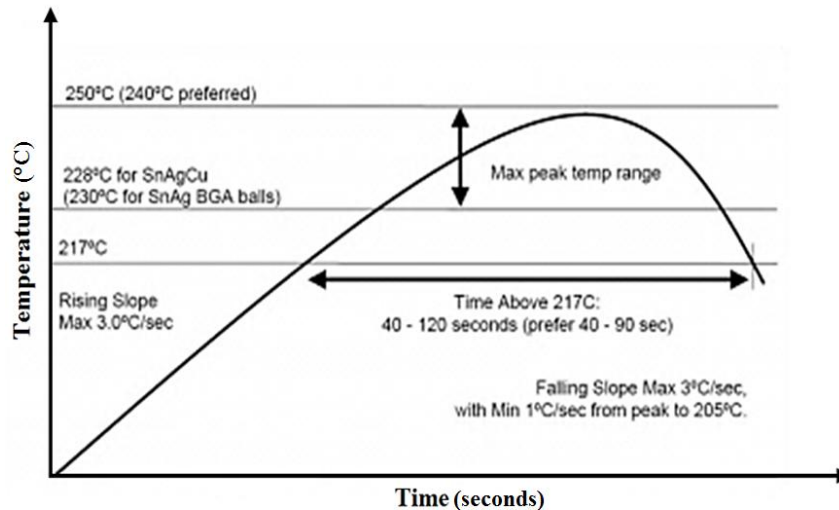
Figure 2.5. Temperature profile of solder during reflow operation **[11]**.

2.2.3. Traditional Pb-Sn Solders

Tin-lead (Sn-Pb) solders have been used in the electronics industry for decades. Their material properties are well known and the reliability of this alloy system is commonly accepted **[12]**. This alloy system owes its popularity to the unique properties of lead within the system. The effects of lead addition to tin are listed below:

a) The melting point of eutectic tin-lead system is considerably low compared to pure tin and pure lead. Pure tin and pure lead have melting points of 232 °C and 327 °C respectively, while eutectic tin-lead system melts at 183 °C **[13, 14]**. Binary phase diagram of tin-lead system is shown in **Figure 2.6**.

b) Addition of lead to tin reduces the surface tension; therefore the solder flows on the surface of the substrate and spreads better **[6, 14]**.

c) The wetting angle of pure tin on copper substrate is 35°, while wetting angle of eutectic tin-lead (63Sn-37Pb wt. %) solder on copper substrate is 11°. Addition of lead to pure tin greatly improves wetting **[14, 15]**.
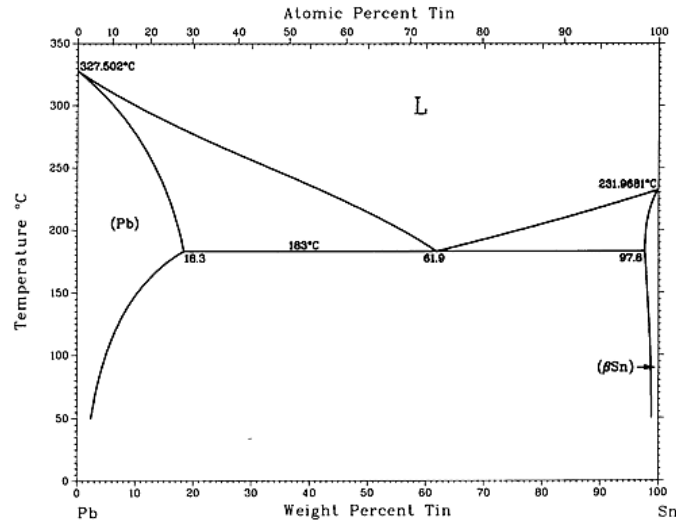
Figure 2.6. Pb-Sn binary phase diagram [16].

d) Lead forms solid solution with tin, but they do not form any intermetallic compound which may result in brittle phase formation in the matrix [7]. Microstructure of near-eutectic tin-lead system is shown in **Figure 2.7**.
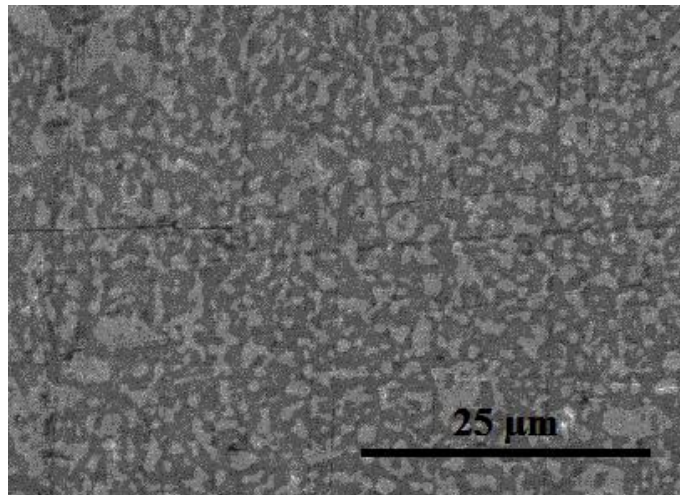
Figure 2.7. BSE image of near-eutectic Sn-40Pb alloy.

e) Allotropic transformation of β-Sn (tetragonal) to α-Sn (diamond cubic) upon cooling occurs below 13 °C. This transformation is known as tin pest. The occurrence of this transformation increases the bulk volume by 26 %, which would cause failure of any joints that were formed. Even small (0.1 wt. %) additions of lead into tin prevents the occurrence of this transformation [6].
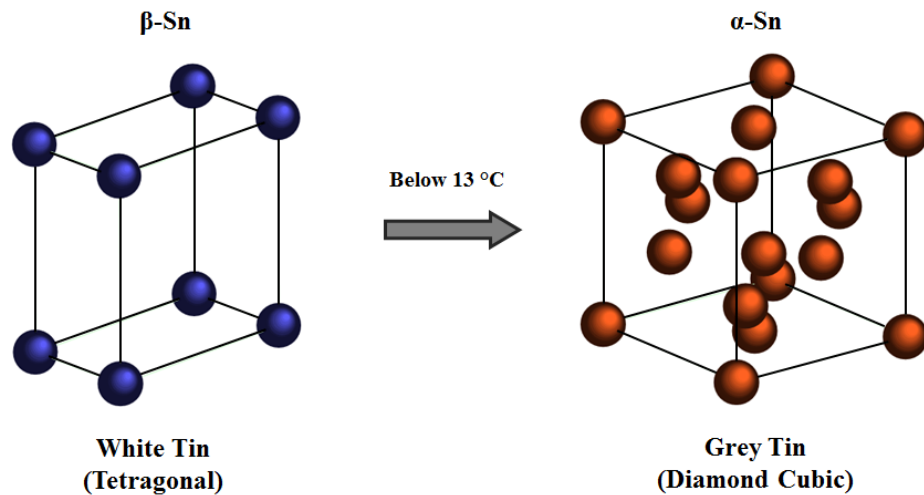
Figure 2.8. Allotropic transformation from β-Sn to α-Sn.

f) Lead improves some mechanical properties of tin, such as ductility **[13, 14]**.

g) Lead is an easy accessible element with relatively low cost.

These properties of lead-tin system made it the most reliable and popular solder alloy in electronics industry for many decades.

2.2.4. Why Lead-Free Solder?

Besides having unique properties, lead and lead compounds has been declared as one of the 17 toxic materials for human life **[17]**. Lead can accumulate in the body over time by forming strong bonds to proteins and inhibiting normal processing and functioning of the human system **[18]**. Lead poisoning occurs if the lead content of the blood is above 50 mg/dl **[19]**. There exist both direct and indirect risks. The direct risk includes electronic industry workers who are subjected solder vapor and fine lead-bearing particles during the production of electronic assemblies **[7]**. The indirect risk is due to the leaching of waste electronic assemblies by the effect of acidic rains and the contamination of underground waters **[20]**.

Due to these health concerns, Restriction of Hazardous Substances Directive, commonly known as RoHS, was adopted in February 2003 by the European Union. The RoHS directive took effect on 1 July 2006. In Turkey, a similar declaration was published in the Official Gazette (*Resmi Gazete*) **[1]** on 30th May 2008 and came

into effect in June 2009. Similar precautions were taken by some other countries like California/USA (January, 2007), China (March 2007) and Japan (July 2006). Therefore, intentional use of lead and lead products are prohibited in all consumer electronics in most of the developed countries.

2.2.5. Lead-Free Solder Alternatives

With the raise of public health care and environmental awareness, many alloys have been proposed to replace the traditional Sn-Pb solders. Most of the alternative solder alloys are still Sn based. Some of the major alloying elements include Au, Ag, Bi, In, Zn, Sb and Ge. Common properties of the binary systems are listed below:

Sn-Ag: Formation of large intermetallic Ag_3Sn plates is the main problem encountered in this binary alloy. Tin whiskering may also occur due to high tin concentration [6]. Binary phase diagram of Sn-Ag is shown in **Figure 2.9**.
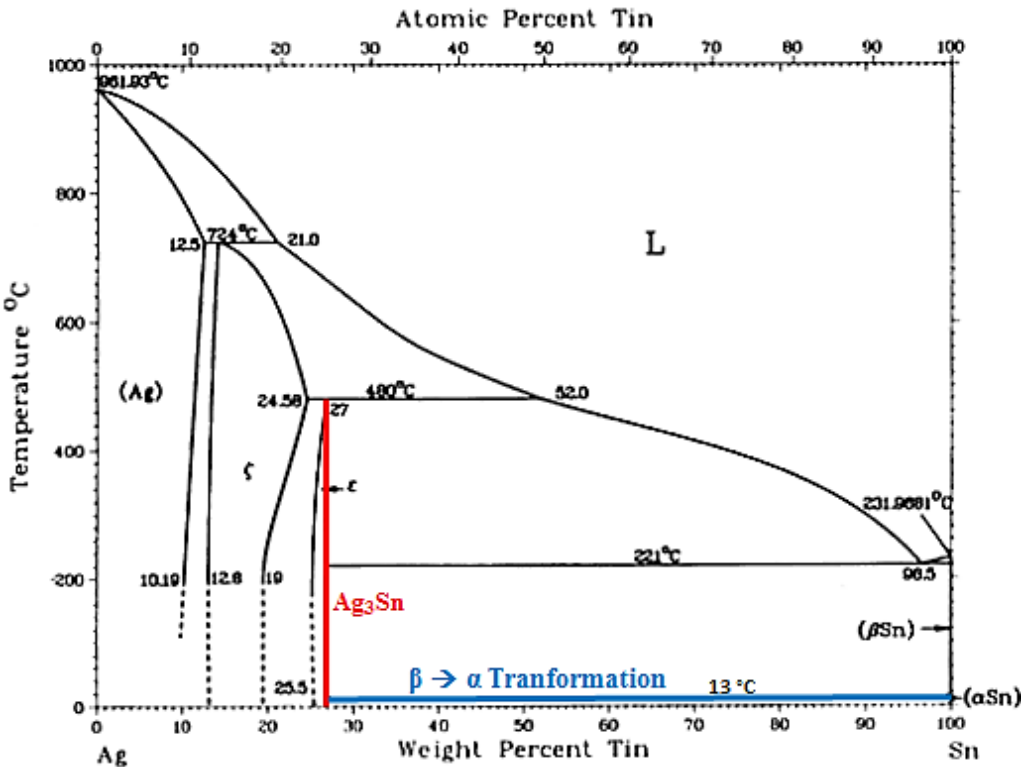
Figure 2.9. Sn-Ag binary phase diagram [21].

Sn-Zn: The eutectic temperature of this system is 198 °C, which is relatively close to traditional eutectic Sn-Pb system. Eutectic structure of this alloy is Zn-rich and Sn-rich lamellar phases.

Sn-Cu: Due to low alloying element concentration, tin whiskers may form and white tin to gray tin transformation may occur at low temperatures.

Sn-Bi: Low-temperature eutectic (138 °C) solder with high strength. It cannot be used in most of the electronic applications, where the operation temperatures reach to 150 °C.

Sn-In: This alloy is preferred in some SMT applications. The eutectic composition is In-49.1Sn and the eutectic temperature is 117 °C **[6]**. Like Sn-Bi eutectic alloy, due to low eutectic temperature, this alloy also cannot be used in most of the electronic applications.

Eutectic compositions of these alloys were considered as an alternative solder alloy, however, there are many problems with these alloys, namely as; intermetallic compound formation, tin whiskering, white tin to grey tin transformation, dewetting, high cost and high reactivity **[13]**.

The melting points and application fields of some of the well-known binary eutectic alloys are given in **Table 2.3**.

Table 2.3. Some well-known binary solders alloys.

Systems	T_m (°C)	Applications	Ref.
95Zn-5Al	382	Soldering of Aluminum	[4]
52In-48Sn	118	Glass Seals - Low Temperature Soldering	[22]
99.3Sn-0.7Cu	227	Electronics (Cheap Alternative)	[22]
96.5Sn-3.5Ag	221	Electronics (Hand Soldering Rework)	[23]
91Sn-9Zn	199	Soldering of Aluminum	[24]
63Sn-37Pb	183	Electronics (Toxic)	[25]
95Sn-5Sb	235	Plumbing and Radiator Repair	[26]
80Au-20Sn	280	Sophisticated Electronic Applications	[27]
58Bi-42Sn	138	Thermoelectric Applications	[28]
97In-3Ag	143	Cryogenic Applications	[29]
87.5Au-12.5Ge	356	Die Attachment of Electronic Chips	[30]

In order to overcome the problems encountered in binary solder alloys, ternary alloy systems have been developed. Some of the important ternary alloys were listed in **Table 2.4** with their melting temperatures.

Table 2.4. Compositions and melting points of some ternary solder alloys.

Alloy Composition (wt. %)	Melting Point (°C)	Ref.
Bi - 26In - 17Sn	79	[31]
Bi - 41.7Sn - 1.3Zn	127	[32]
Sn - 56 Bi - 1Ag	137	[32]
Sn - 57Bi - 1.3Zn	127	[32]
Sn - 6Zn - 6Bi	127	[32]
Sn - 2.8Ag - 20In	178	[33]
Sn - 25Ag - 10Sb	233	[34]
Sn - 3.5Ag - 1Zn	217	[35,36]
Sn - 9Zn - 10In	178	[36,37]

Solders that are currently being used in most of the consumer electronics are based on Sn alloys. Sn-Ag-Cu based ternary alloys are the most widely used lead-free solder alloy systems.

2.3. Sn-Ag-Cu Solders

In all ternary solder alloys, eutectic and near-eutectic Sn-Ag-Cu (SAC) alloys seem to be the most promising alloy systems to replace traditional Sn-Pb alloys. They were first discovered in 1996 by a research group at Ames Laboratory in USA **[38]**. SAC alloys have very high thermal shock resistance and mechanical vibration resistance and they can operate at temperatures up to 150°C **[39, 40]**. Their thermo-mechanical properties are better than traditional Sn-Pb solders **[41, 42]**.

The calculated ternary eutectic composition is Sn-3.7Ag-0.9Cu (wt. %) as shown in **Figure 2.10**. The ternary eutectic composition was experimentally determined as Sn-3.5Ag-0.9Cu (wt. %) and the eutectic temperature is 217 °C **[43, 44]**. Eutectic phases are Sn, Ag_3Sn and Cu_6Sn_5.
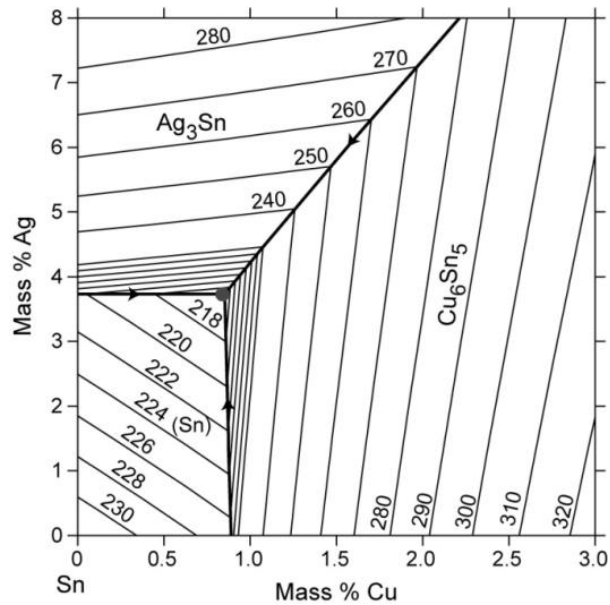
Figure 2.10. Sn-rich part of Sn-Ag-Cu ternary system **[45]**.

The eutectic temperature of SAC alloy is 34°C higher than that of the eutectic Sn-Pb solders. This explains why SAC alloys has better thermo-mechanical properties and how they can operate at higher temperatures. SAC solders were reported to have fine and stable microstructures and higher shear strength compared to Sn-Pb alloys **[46]**. During solidification, depending on the cooling rate, various phases may form. Reaching fully eutectic microstructure is usually not possible since the eutectic point will deviate due to faster cooling rates applied during solidification. Because of these deviations; β-Sn, Ag_3Sn and Cu_6Sn_5 may form at various amounts in both eutectic and near-eutectic SAC solders. Currently, there are two SAC solder compositions that were indicated for the electronics manufacturers by two different organizations. National Electronics Manufacturing Initiative (NEMI) recommends Sn-3.9Ag-0.6Cu alloy **[47, 48]** and Japan Electronics and Information Technology Industries Association (JEITA) recommends Sn-3.0Ag-0.5Cu alloy **[49, 50]**. These alloys lie in the near-eutectic composition region, where, near-eutectic SAC alloy compositions fall into the composition range between Sn-3.8Ag-0.7Cu and Sn-4.0Ag-0.5 Cu **[51]**. Although SAC compositions are widely used in electronics industry and recommended by NEMI and JEITA, several problems with these alloys exist. The performance and reliability related properties of SAC solders and the existing problems will be explained in the following chapters.

2.3.1. Microstructures of SAC Alloys

The microstructures of SAC solders are extremely sensitive to compositional changes. Comparing the microstructures of Sn-3.7Ag-0.9Cu and Sn-3.6Ag-1.0Cu, in **Figure 2.11**, one can clearly see the changes in microstructure caused only by replacing 0.1 wt. % Ag with 0.1 wt. % Cu. The amount of eutectic phase has increased while the amount of β-Sn has decreased. However, many Cu_6Sn_5 intermetallic compounds (IMCs) were observed in the matrix. The properties of the intermetallic compounds are clearly different from its constituent elements **[52]**. The amount, size and distribution of the intermetallic compounds must be controlled since almost all the intermetallic compounds are hard and brittle phases. Large or localized IMCs can cause embrittelment of the solders joints. However, small amounts of intermetallic compounds can improve the mechanical and thermal properties of the solders. Hardness and fatigue resistance can also be improved by homogenous distribution of small IMC **[52]**.

Ag_3Sn is the other IMC that can form in the matrix of the SAC solders. It is formed as large plates, sometimes referred as blades; usually seen as the least desirable phase since it degrades the mechanical properties of the solders **[53, 54]** and cause catastrophic failures of electronic components. Composition and the cooling rate are found to be the most effective parameters on the size and dispersion of Ag_3Sn particles **[55]**. Pro-eutectic Ag_3Sn particles are appreciably larger than the eutectic Ag_3Sn particles which are small, typically needle or round in shape **[8]**. Large Ag_3Sn plates can extensively affect the mechanical properties of the solder alloys by locally inhibiting the plastic deformation **[55]** and causing stress concentration at the interface between the Ag_3Sn plate and the surrounding β-Sn **[56]**.

Thus, formation of the large Ag_3Sn plates should be prevented to maintain the integrity of the solder joint in the presence of any mechanical or thermal loads during its service life. The composition of the solder alloy and the cooling rate during solidification are the most effective parameters on the formation of large Ag_3Sn plates.
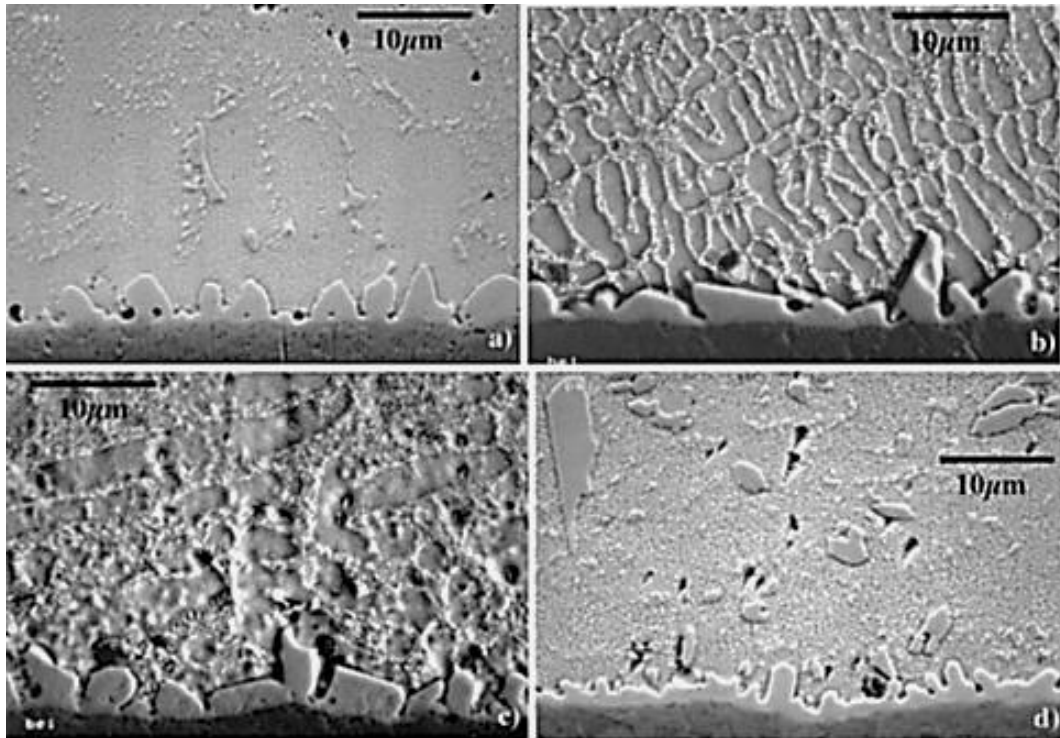
Figure 2.11. Back-scattered electron (BSE) images of solder joints made from:
a)Sn-3.0Ag-0.5Cu, **b)**Sn-3.9Ag-0.5Cu, **c)**Sn-3.7Ag-0.9Cu **d)**Sn-3.6Ag-1.0Cu **[57]**.

2.3.1.1. Effect of Composition on Microstructure

a. Effect of Silver Content

It was suggested that the formation of large Ag_3Sn plates is effectively reduced if the silver content of the solder is less than 3 wt. % even at very low cooling rates (≤ 0.02 °C/s). It was also reported that, the compositions with silver content ≤ 2.7 wt. % does not allow the nucleation and growth of Ag_3Sn phase unless there is an undercooling of 20°C **[51]**. Ag has a limited solubility in Sn. Therefore, all the Ag that is not dissolved in the Sn is considered to form Ag_3Sn IMCs. It was found that an increase in the Ag content from 3.0 wt. % to 3.8 wt. % results an increase of 28 vol. % in the Ag_3Sn content **[10]**. Similarly, formation of large Ag_3Sn blades were observed due to change in Ag content from 3.0 wt. % to 3.9 wt. % as shown in **Figure 2.12**. **Table 2.5** shows the effect of Ag content on the number of large Ag_3Sn plates.
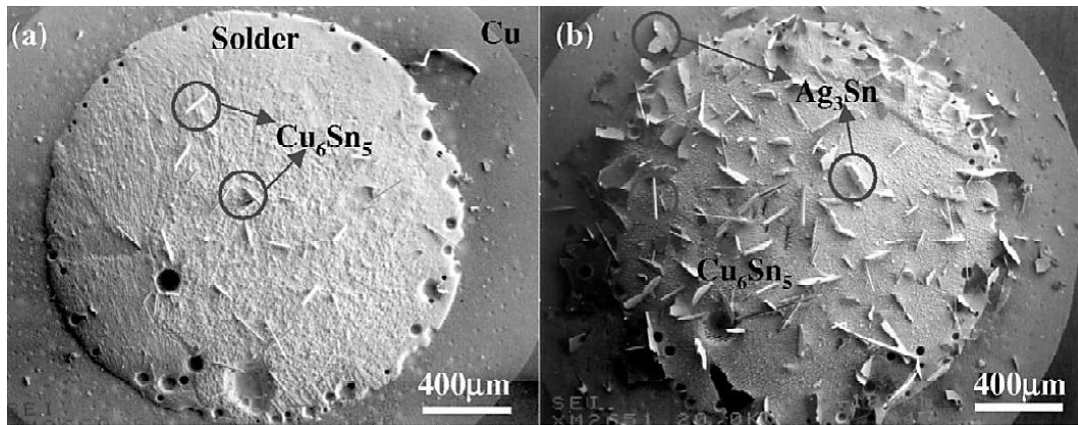
Figure 2.12. Results of microscopic examination of
a) Sn-3.0Ag-0.5Cu and **b)** Sn-3.9Ag-0.5Cu [58].

Table 2.5. Number of large Ag_3Sn plates in SAC solders solidified at
0.02 °C/s cooling rate (adapted from [51]).

Alloy Composition (wt. %)	Number of large Ag_3Sn plates
Sn-3.8Ag-0.7Cu	76/100
Sn-3.4Ag-0.9Cu	10/100
Sn-3.0Ag-0.9Cu	6/100
Sn-2.5Ag-0.9Cu	1/100
Sn-2.0Ag-0.9Cu	0/100

b. Effect of Copper Content

Copper content is less effective than silver content on the formation of large Ag_3Sn plates. Alloys having the compositions of Sn-3.8Ag-0.35Cu and Sn-3.8Ag-0.7Cu do not exhibit a difference in the amount and size of Ag_3Sn IMCs. Small amounts of copper atoms are enough to lead the nucleation of Ag_3Sn plates. Therefore, after a critical copper composition, further addition of copper atoms does not alter the nucleation rate of Ag_3Sn plates. On the other hand, copper content is more effective on the formation of large Cu_6Sn_5 rods [51]. Depending on the composition, Cu_6Sn_5 phase can also form in Sn matrix in the form of fine precipitates having 5-50 nm diameters [10].

c. Effect of fourth alloying element

The effect of minor element addition to SAC solders is still not fully understood [59]. Micro-alloying with elements of Si, Ni, Ti, Mn, Cr, and Ge can suppress the formation of large IMC by promoting the formation of β-Sn [60]. Hume-Rothery [61] rules are commonly used for the selection of fourth element that will be added to SAC solder to replace Cu in the alloy. According to Hume-Rothery rules [62]:

1) The atomic radii difference of the solute and solvent atoms must not be higher than 15 %.

2) The crystal systems of solute and solvent must match.

3) The valances should be the same for complete solubility.

4) Solute and solvent should have similar electronegativities.

In addition to Hume-Rothery rules, Darken-Gurry [63] maps are commonly used to further narrow down the possible elements that can enhance the microstructure of the lead-free solder alloys [64]. The intention in modification of microstructure with fourth element addition is to decrease the undercooling of the alloy during solidification. Nucleation of β-Sn phase requires a high undercooling, which also makes the nucleation of pro- eutectic Ag_3Sn possible [53].

Effect of minor element additions on microstructure is shown in **Figure 2.13**. It can be seen that, even if added at small concentrations; the minor elements can also form their own IMC in the matrix, which can also cause some reliability problems for the solder alloy. In the work of K.S. Kim et al. [65], they intended to determine the effects of the addition of 0.1 wt. % of Ti, Mn, Fe, Ni and Co to the Sn-3.0Ag-0.5Cu solder alloy. They found that the addition of Ti causes primary β-Sn grains and the eutectic structure to be finer and fine precipitates of intermetallic compounds of Ti to form in the matrix. However, the chemical compositions of those IMCs in the matrix were not reported. They also found that, by the addition of Mn, fine precipitates with considerable amount of Sn, Mn and Cu forms. They indicated that, those precipitates can be seen both in the eutectic regions and β-Sn grains. For the addition of Fe, they concluded that it forms large, irregular shaped $FeSn_2$ IMCs in the eutectic network. They reported that no refinement in β-Sn grains was achieved with Fe addition. The addition of Ni was concluded with

similar precipitates if Mn, such that Ni, Sn and Cu was detected in those fine precipitates, formed in both β-Sn grains and the eutectic network. Co addition was reported to form both fine and large rod-like $CoSn_2$ IMCs. They concluded that the additions of Ti, Ni and Mn, which forms fine precipitates, should improve the strength and undercooling of the solder alloys. Some result of this study was summarized in the **Table 2.6**.
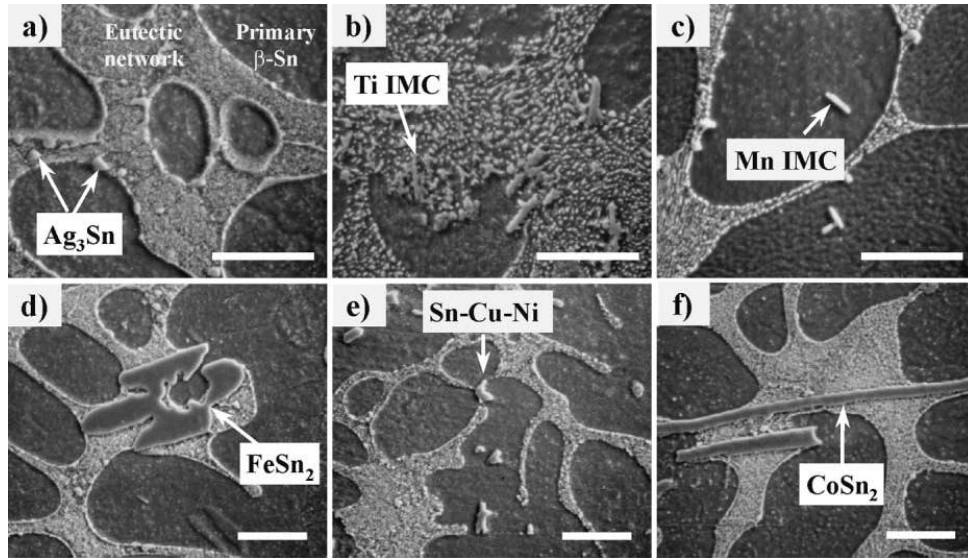
Figure 2.13. Effect of micro-alloying on microstructures of:
a) Sn-3.0Ag-0.5Cu, **b)** Sn-3.0Ag-0.5Cu -0.1Ti, **c)** Sn-3.0Ag-0.5Cu-0.1Mn,
d) Sn-3.0Ag-0.5Cu-0.1Fe, **e)** Sn-3.0Ag-0.5Cu-0.1Ni, **f)** Sn-3.0Ag-0.5Cu-0.1Co
(Bars indicate 10 μm) **[65]**.

Table 2.6. The results of the microstructural analysis **[65]**.

Alloying Element	Precipitate Composition	Formed In	Size
Ti	N/A	Eutectic + β-Sn	N/A
Mn	Mn-Sn-Cu	Eutectic + β-Sn	< 2μm
Fe	$FeSn_2$	Eutectic	> 10 μm
Ni	Ni-Sn-Cu	Eutectic + β-Sn	N/A
Co	$CoSn_2$	Eutectic	> 50 μm

Similar work was also carried out by L.W. Lin et al. **[66]**. They intended to improve the microstructure of the Sn-1.0Ag-0.5Cu (wt. %) solder alloy with the additions of 0.15 wt. % and 0.5 wt. % of Mn and Ti. They also compared the results with the Sn-3.0Ag-0.5Cu alloy. **Figure 2.14** shows the microstructures achieved as a result of those additions.
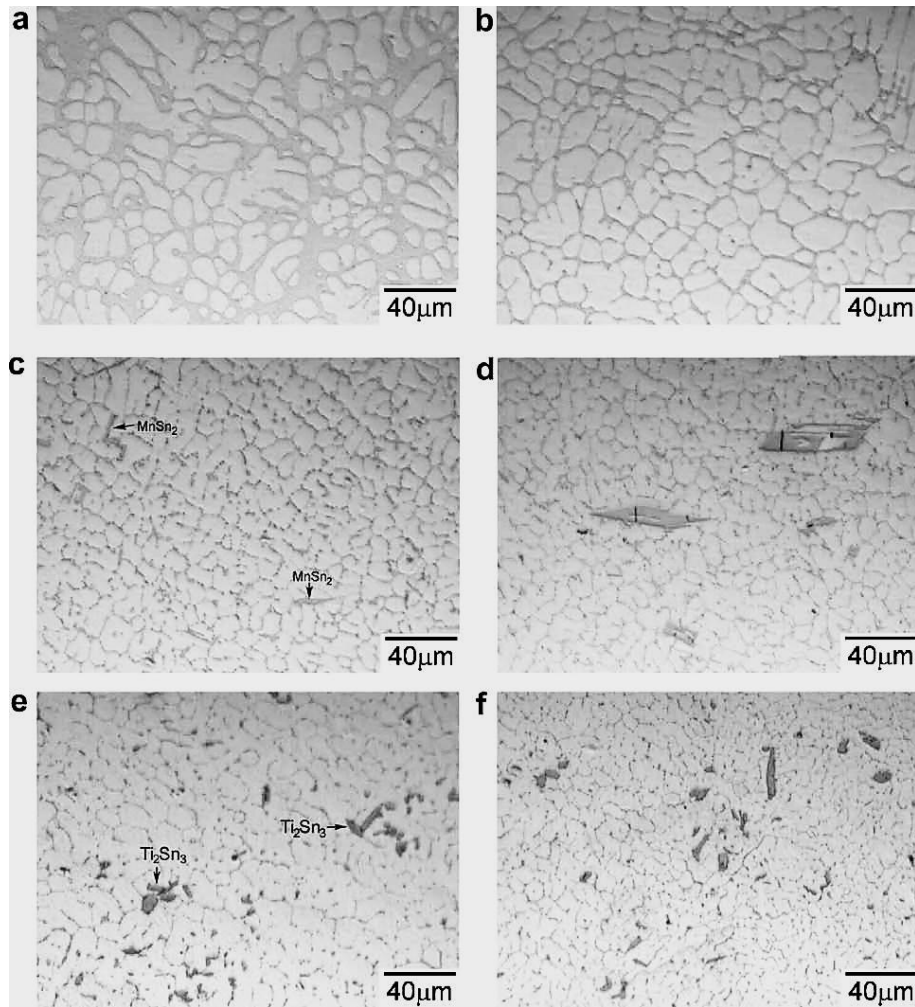
Figure 2.14. Effect of micro-alloying on microstructure of :
a) SAC305, **b)** SAC105, **c)** SAC105+0.15Mn,
d) SAC105+0.5Mn, **e)** SAC105+0.15Ti, **f)** SAC105+0.5Ti **[66]**.

By looking at the microstructures shown on **Figure 2.14.a** and **Figure 2.14.b**, one can easily say that even before the micro-alloying, Sn-1.0Ag-0.5Cu alloy exhibit far less eutectic network than Sn-3.0Ag-0.5Cu alloy. The structure of Sn-1.0Ag-0.5Cu alloy is highly dominated by β-Sn grains.

As a result of Mn addition, $MnSn_2$ IMCs were formed. IMCs are finer for 0.15Mn added alloy, compared to 0.5Mn added alloy, with sizes of ~15 μm and ~50 μm respectively. Both alloys have finer β-Sn grains compared to Sn-1.0Ag-0.5Cu and Sn-3.0Ag-0.5Cu alloys, where no further refinement was observed after 0.15Mn addition. These microstructures may be seen in **Figure 2.14.c** and **Figure 2.14.d**.

By the addition of Ti, Ti_2Sn_3 IMCs were formed. These IMCs has no specific shape and size, which can be seen on **Figure 2.14.e** and **Figure 2.14.f**. Both alloys have finer microstructures compared to Sn-1.0Ag-0.5Cu and Sn-3.0Ag-0.5Cu alloys. It is observed that the β-Sn grains were further refined with the addition of 0.5Ti. Moreover, 0.5Ti modified alloy has the finest β-Sn grains in all the compositions that were reported in this work.

The works of K.S. Kim et al. **[65]** and L.W. Lin et al. **[66]** showed that, micro-alloying elements may cause the formation of IMCs while refining the β-Sn grains. Refinement on the microstructure would affect the mechanical properties in a positive way, however depending on the size, morphology and distribution of the IMCs, the mechanical properties may be affected negatively as well.

I.E. Anderson et al. **[67]** has worked on various compositions of lead-free solders. The base alloy composition was chosen as Sn-3.5Ag-0.95Cu (wt. %) and modifications were done by adding 0.05-0.25 (wt. %) of alloying elements Ni, Co, Fe, Mn, Zn and Al. The main objective of this work was stated as the suppression of blade-shaped, pro-eutectic Ag_3Sn IMC particles. They reported that the micro-alloying of the base alloy with 0.05Al was the most effective which successfully suppressed the Ag_3Sn blade formation, this also being the addition with the lowest fourth element concentration. Addition of 0.25Al was as successful as 0.05Al addition. However, compositions having higher than 0.15Al were not totally Ag_3Sn-free. 0.10Mn, 0.15Mn, 0.21Zn, 0.25Zn additions were also successful in reaching the blade-free microstructures. Additions of Fe and Co did not give satisfactory results at compositions of 0.10, 0.15 and 0.25.

The effect of micro-alloying on undercooling was determined in another work of I.E. Anderson et al. **[68]** which, the effects of 0.05 (wt. %) Co addition on Sn-3.5Ag-0.95Cu (wt. %) alloy were investigated. Two melting-solidifying cycles were done by DSC with the heating and cooling rate of 1.5 °C/s. For the base alloy, the undercooling was determined as 28 and 32 °C on the first and second runs, respectively; whereas, undercooling of the micro-alloyed alloy was determined as 6 °C in both cycles. The corresponding DSC curves are shown in **Figure 2.15** and **Figure 2.16**.
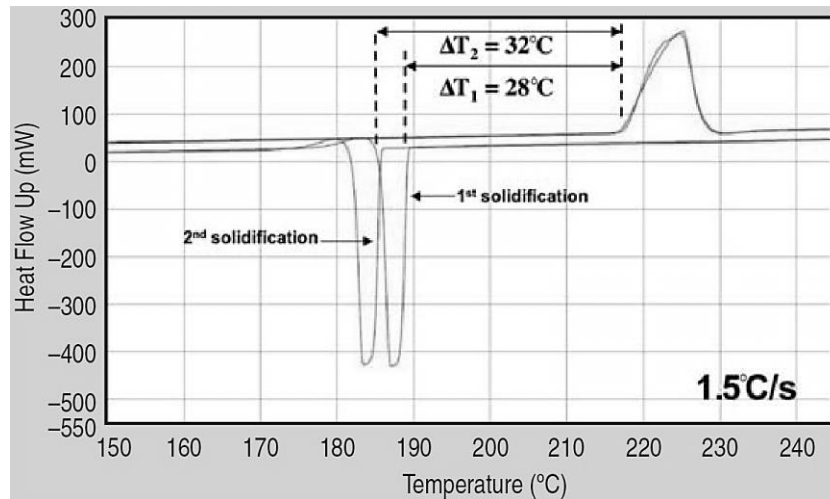
Figure 2.15. DSC curves for Sn-3.5Ag-0.95Cu alloy **[66]**.
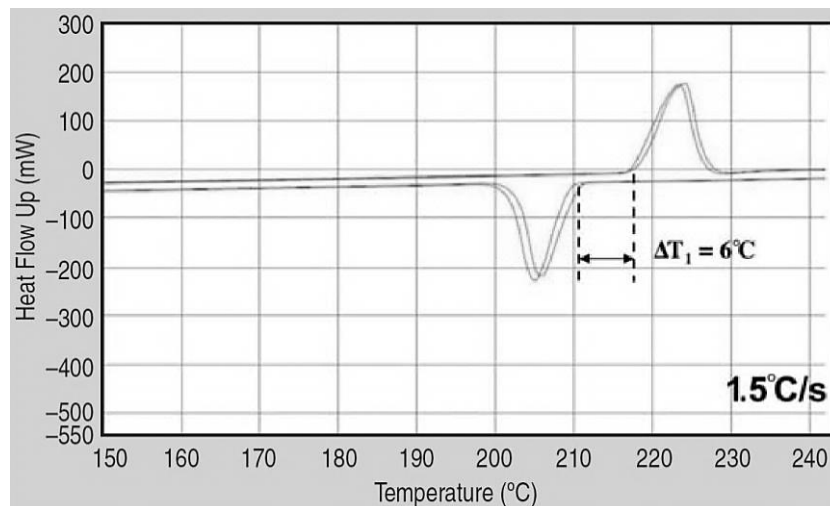
Figure 2.16. DSC curves for Sn-3.5Ag-0.95Cu-0.05Co alloy **[68]**.

2.3.1.2. Effect of Cooling Rate on Microstructure

Experimentally, during reflow soldering, the formation of large Ag_3Sn plates can be controlled if cooling rates of the joints are at least 1.5 °C/s **[51]**. However, cooling rate may not be precisely controlled on all of the joints during manufacturing process, since different joint sizes are available on a single electronic package and those will cool with different rates. Generally, cooling rates of commercial surface mount and ball-grid array joints are on the order of 1.5 and 0.17 °C/s, respectively **[68]**.

25

2.3.2. Mechanical Properties of SAC Alloys

Mechanical properties of the solder alloys have great importance for electronics industry since electronics circuits are subjected to various mechanical loads during their service. These mechanical loads are mainly originated due to the coefficient of thermal expansion (CTE) difference between the different types of materials used in the electronic devices. The circuit board, which is a non-metallic material, essentially has a different CTE than the metallic leads of the electronic components. When those materials are joined by using a solder, which also has a different CTE than other two materials, there will be a dimensional and geometrical mismatch between these materials. When the electronic device is switched on and off, the mechanical loads will form cycling stresses on the solder joints and the joints may fail if the solder alloy does not possess the required mechanical properties such as ductility, shear strength and hardness [6].

Compared to traditional Sn-Pb solders, with their higher melting temperatures, SAC alloys are expected to have better shear properties at ambient temperatures and higher resistance to thermal fatigue at high temperatures [59]. On the other hand, mostly because of the formation unwanted IMCs, mechanical properties are not fully reliable. Therefore, mechanical properties of solder alloys highly depend on chemical composition and hence the microstructure.

In a previous work [57], where shear strengths of a binary eutectic Sn-3.5Ag solder, four different near-eutectic SAC solders and two micro-alloyed solders were compared; 0.2 wt. % Fe modified solder was found to have the highest shear strength, where 0.3 wt. % Co modified alloy is the second strongest alloy. On the other hand, the yield point of that solder was observed a lower stress than the Sn-3.6Ag-1.0Cu solder. The weakest alloy composition was determined as Sn-3.0Ag-0.5Cu, which is the lead-free alloy composition that is recommended by JEITA [47, 50]. Sn-3.9Ag-0.6Cu solder alloy, which is the composition recommended by NEMI [47] was found to be the second weakest solder together with Sn-3.7Ag-0.9Cu near-eutectic composition. This shows that, micro-alloying may increase the shear strength of the near-eutectic SAC compositions considerably with minor decrease in their yield strengths. The results are shown is **Figure 2.17**.
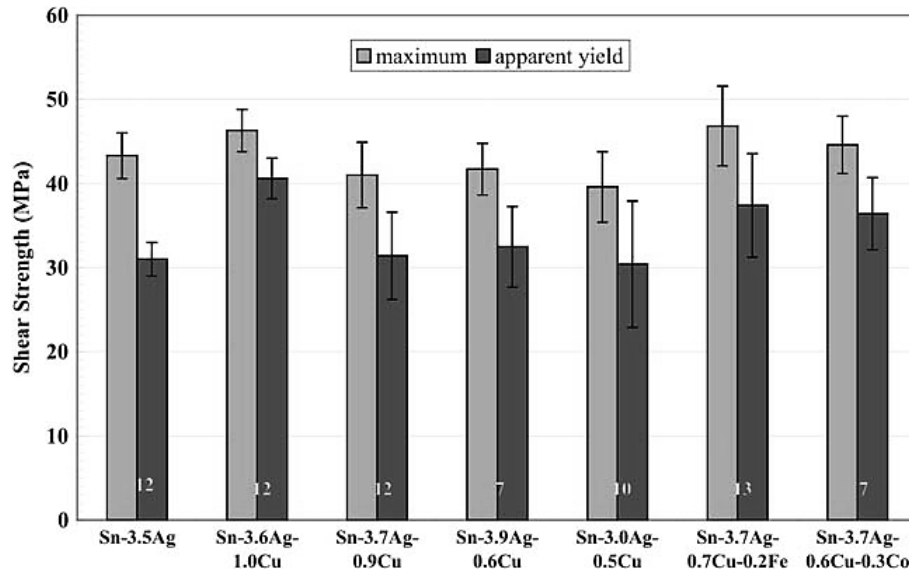
Figure 2.17. Shear strength of some lead-free solder alloys [57].

In the work done by K.S. Kim et al. [65] for which, microstructures were shown in **Figure 2.13**, tensile properties of the alloys were tested at room temperature. Ultimate tensile strengths (UTS) of the alloys were determined at 3.5 x 10^{-3} s^{-1} strain rate and results were shown in **Figure 2.18**.

The 0.1Fe (wt. %) modified alloy was determined as the strongest one. Although the size and morphology of the IMCs formed in Mn, Ni and Co modified alloys were observed to be different, those alloys have nearly the same strength under tensile loading.
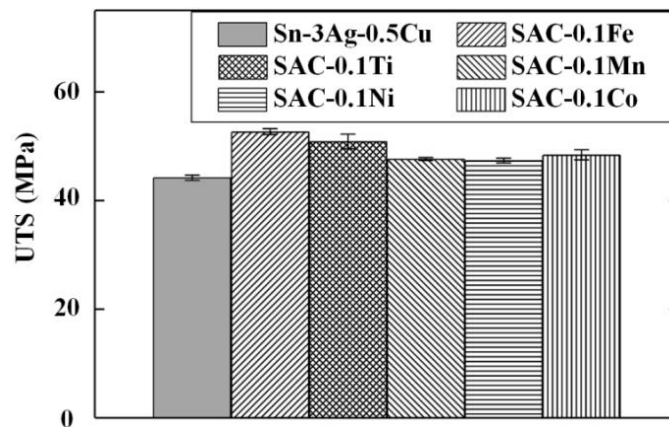
Figure 2.18. UTS of solders made from Sn-3.0Ag-0.5Cu-X [65].

All the modified alloys have higher tensile strength than the base alloy of Sn-3.0Ag-0.5Cu, which clearly shows that fourth alloying addition is an effective way of altering the microstructure and improving the mechanical properties of the solder alloys.

Solders may also be subjected to shear loads at the temperatures up to 200 °C. Therefore, their shear strength at the high temperatures is critical when reliability of the joints is concerned. As it can be seen in **Figure 2.19**, the alloys loose more than 50 % of their shear strength at 150 °C. However, at 150 °C all the alloys have shear strength very close to each other, which is about 18 MPa. It should be noted that standard deviations for Sn-3.6Ag-1.0Cu and Sn-3.0Al-0.5Cu alloys are significantly higher than the other alloys.
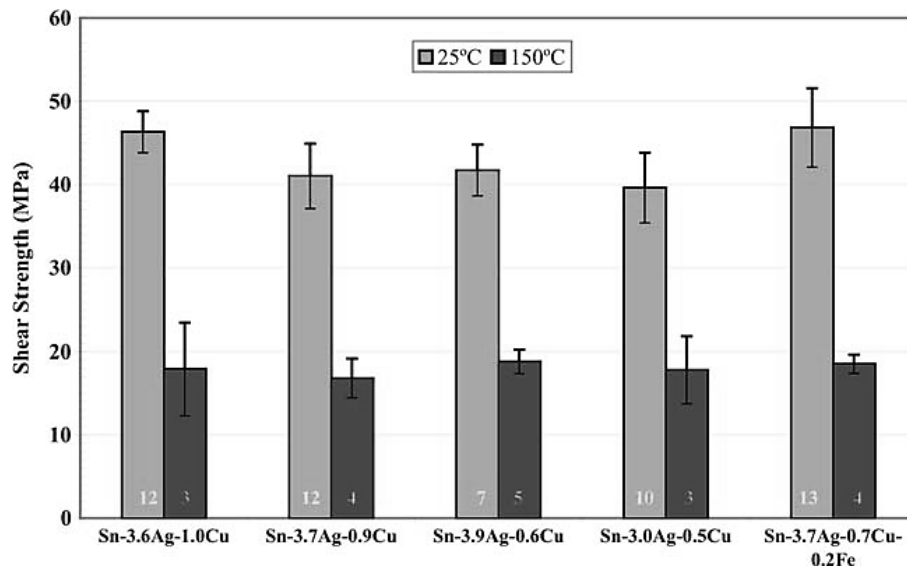
Figure 2.19. Shear strength of some lead-free solder alloys at 25°C and 150°C **[57]**.

The solder matrix (i.e. Sn dendrites + ternary eutectic phases) and IMCs usually determines the shear strength, but the solder-substrate interface phase does not have a significant effect on the shear strength. The shear strength is most affected by the large and localized intermetallic phases like Ag_3Sn plates **[10]**. The type of IMC is also an important factor, besides its morphology and distribution. By the addition of a fourth element to overcome the large Ag_3Sn and Cu_6Sn_5 formation problems, new types of IMCs may be formed in the structure, which can be more detrimental than

28

the Ag_3Sn and Cu_6Sn_5 phases. As the hardness of the IMC increases, the ability to bear the loads consistently with the matrix decreases and the probability of crack formation at the stress concentration zones increases. The hardness of the $MnSn_2$ and Ti_2Sn_3, which may form by the addition of Mn and Ti to SAC solders, is given in **Figure 2.20**. In that specific case, Mn and Ti were added to suppress the formation of unwanted Ag_3Sn plates; however, relatively large $MnSn_2$ and Ti_2Sn_3 were formed.
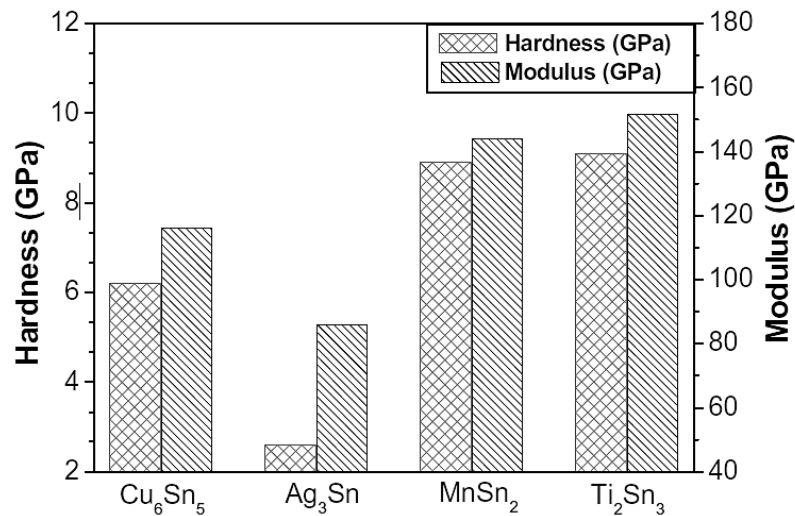
Figure 2.20. Hardness and modulus of IMC [66].

2.3.3. Solder-Substrate Interface of SAC Alloys

The growth of the intermetallic layer takes place during freezing of the solder by the attachment of solute atoms onto the nucleated layer. The solute atoms which cannot diffuse and attach to the interface layer, nucleates and grows in the matrix to form IMC crystals [52]. Like in many other growth controlled processes, the growth of interface layer is a diffusion controlled mechanism and it depends on the time and temperature. The interface thickness is calculated using the parabolic function of:

$$Thickness = D.t^{1/2}$$

Where, **D** is the diffusion coefficient, which is an empirical, temperature dependent parameter and **t** is time [52]. On the **Figure 2.21**, it can be seen that Sn-3.7Ag-0.6Cu-0.3Co alloy which has thicker interface layer at 100 hours, grew with a

higher growth rate than the other two alloys. According to Hume-Rothery [61] rules, the maximum mismatch for solid solubility is 15%. When the atomic radius of Cu is compared with Fe and Co, it is found that the radius mismatch is calculated as 0.3% for Fe and 1.9% for Co [69]. This explains the nature of detected Fe and Co in the Cu_6Sn_5 interface, when chemical analysis of the interface layer is done.
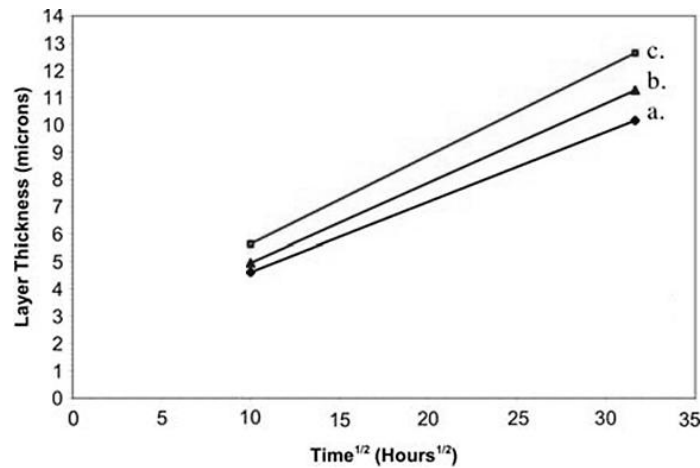
Figure 2.21. Interface layer thickness of solders: **a)** Sn-3.7Ag-0.9Cu, **b)** Sn-3.7Ag-0.7Cu-0.2Fe and **c)** Sn-3.7Ag-0.6Cu-0.3Co [60].

In a study, carried out by K.S. Kim et al. [65], 0.1 (wt. %) of Co, Ni, Ti, Mn and Fe were added to base solder alloy of Sn-3.0Ag-0.5Cu, the effects of those element on the interface thickness and morphology of the scallops at the interface were investigated. They determined the average interface thickness as 10 μm. They indicated that the interface is thicker and the scallops at the interface are deeper and more elongated in the 0.1Ti modified solder. They observed no change in the morphology with the additions of Mn and Fe. On the other hand, they pointed that the interfaces are relatively thin (~2-3 μm) and flat for the Co and Ni modified solders.

The results of reactions between Cu and Sn-2.5Ag-0.8Cu solders, micro-alloyed with 0.03 wt. % of Fe, Co, Mn and some of their combinations were investigated by Y.W. Wang et al. [70]. The resulting interface microstructures were shown in **Figure 2.22**. As small as 0.03 wt. % micro-alloying made extreme effects on the interface thickness of solder-copper joints. The thicknesses of the interfaces reached

to 3-4 times of the thickness of the interface formed by the base alloy. Thicker interfaces form when the alloying element concentration increases. The solders modified with 0.03Fe+0.03Ni and 0.03Co+0.03Ni additions have the thickest interfaces. 0.03Fe+0.03Ni modified alloy has deeper Cu_6Sn_5 scallops than any other composition. There are many trapped solder regions at the interface in all of the modified alloys which look like black holes at the interface, since they were etched away during metallographic preparation. The concentrations of those trapped solders are highest for the 0.03Co+0.03Ni modified alloy.
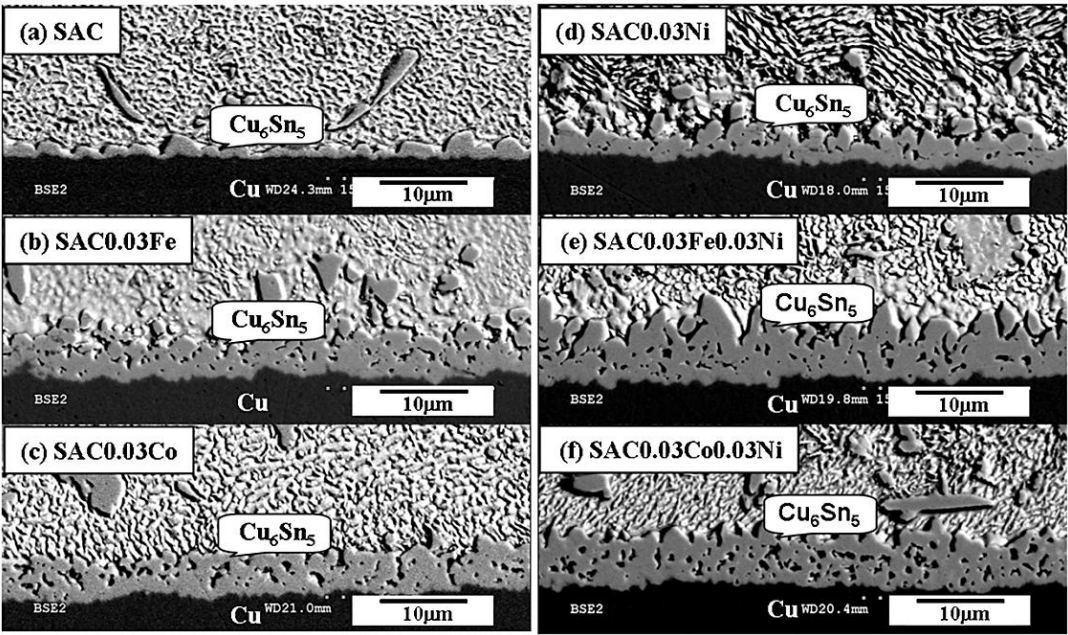
Figure 2.22. SEM images of joints made by modified solder alloys [70].

The soldering technique also affects the interface properties extensively. Therefore, there is a great difference between the joints formed with wave soldering and reflow soldering techniques; although, the peak temperature reached in two techniques is the same. However, contact time of liquid solder and the substrate is different. In wave soldering it is typically 2 seconds, whereas in reflow soldering it may be an order of magnitude longer [52]. The SEM images of solder joints produced by two different soldering techniques are shown in **Figure 2.23**.
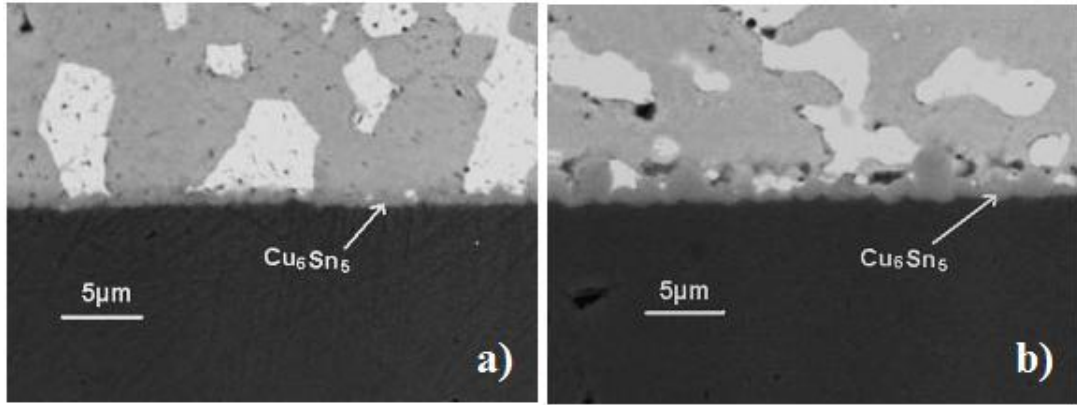
Figure 2.23. Cross-sections of the joints produced by:
a) wave soldering and **b)** reflow soldering methods **[52]**.

The difference in the interface thickness can be clearly seen by looking at the two images; in which, the joint formed by reflow soldering technique has a significantly thicker interface layer.

Another important parameter, affecting the interface layer thickness is the interface chemistry. Different coatings may be used on the substrate to enhance the wetting and solderability. While changing the wetting properties, the coatings also alter the diffusion rate between the solder and the substrate. In **Figure 2.24**, the effect of organic soldering preservative (OSP) and Nickel-Gold (Ni-Au) surface coatings is shown for different compositions of SAC solder alloys. For all compositions, Ni-Au coated substrates form a thinner interface in the as-reflowed state.
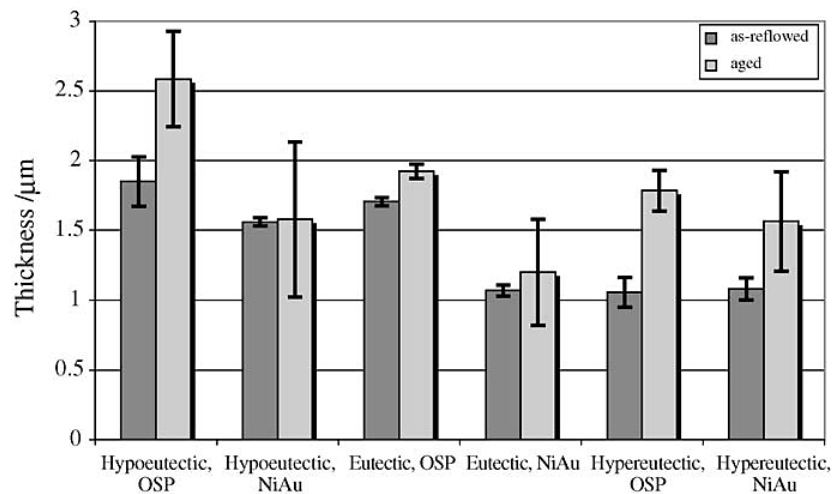
Figure 2.24. Effect of surface coating on interface layer thickness **[47]**.

2.3.4. Wetting of SAC Alloys

Wetting means the spreading of a liquid over a surface by the effect of interfacial energies along the drop–substrate contact line. Two conditions of wetting are shown in **Figure 2.25**. The equation of these energies may be expressed by means of Young's Equation as: $\gamma_{int} = \gamma_{sub} - \gamma_{surf} \cos\theta$, where γ_{int} is the metal/substrate interfacial energy; γ_{surf} and γ_{sub} are the surface–vapor interfacial energies (i.e. surface energies) of the metal and the substrate, respectively; and θ is the contact angle [71].

Figure 2.25. Poor and good wetting conditions.

A reliable solder joint requires a good wetting with a low wetting angle [8]. Wetting and solderability is affected by the IMC formed at the solder-copper interface during soldering operation. Generally good wetting is the indication of an IMC formation at the solder-substrate interface [6, 72]

Compared to traditional Sn-Pb solders, SAC solders forms a joint with higher contact angle, which means SAC solders has poorer wetting than Sn-Pb solders [6]. Some alloying additions to SAC system slightly improve the wetting ability. For example, when added in small amounts (< 1 wt. %) Bi [73] and Zn [74, 75] improves wetting.

The most effective parameters on wetting are soldering temperature, type of substrate and type of soldering flux. In **Table 2.7**, the effect of soldering temperature and type of soldering flux was compared for different alloy compositions by using copper as soldering substrate for all solders. The alloys were grouped as *a,b* and *c* for the ease of comparison.

Table 2.7. Wetting angles of some solder alloys (adapted from **[47]**).

Group	Alloy Composition (wt.%)	Soldering Temperature (°C)	Flux Type*	Wetting Angle (°)	Reference
a_1	Sn-37Pb	215	RMA	22	[76]
a_2	Sn-37Pb	215	WS	12	[76]
a_3	Sn-37Pb	215	NC	31	[76]
b_1	Sn-9Zn	245	RA	83	[77]
b_2	Sn-9Zn	260	RA	77	[77]
b_3	Sn-9Zn	290	RA	72	[77]
c_1	Sn-9Zn-0.05RE	260	RA	59	[77]
c_2	Sn-9Zn-0.1RE	260	RA	65	[77]

*RMA: rosin mildly activated, RA: rosin activated, WS: water soluble, NC: no-clean

In group *a*: effect of flux type on wetting angle was compared,

In group *b*: effect of soldering temperature on wetting angle was compared,

In group *c and b_2*: effect of *Rare Earth* element addition on wetting was compared.

According to the previous table, results can be summarized as:

a) When the data in group *a* are considered, WS type flux results the smallest wetting angle and RMA type flux results the highest wetting angle for eutectic Sn-Pb solder.

b) According to data in group *b*, the higher soldering temperature results smaller the wetting angle.

c) According to data in group *c* and *b_2*, rare earth addition improves the wetting at minor concentrations; however, this effect is lost as the concentration of the RE increases.

As pointed out by M. Abtew and G. Selvaduray **[6],** the comparison of lead-free solder wetting data is difficult since experimental parameters such as temperature, surface properties of the substrate and flux may differ with each researcher.

2.3.5. Undercooling of SAC Alloys

The term *undercooling* defines a temperature difference, which a liquid material should be super-cooled below its melting temperature, until it starts to solidify. Thus, it is the temperature difference between the melting and solidification temperatures of a material. For SAC alloys, undercooling defines the temperature difference needed to start the nucleation of β-Sn phase. The high undercooling (>15 °C) necessary for nucleation of β-Sn phase also gives the opportunity for nucleation of pro-eutectic Ag_3Sn for most near-eutectic SAC alloys [57]. Undercooling of the solder alloys is an important concept in understanding and controlling the nucleation and growth of the IMC that forms in the bulk alloy. Studies show that the undercooling for SAC alloys of various compositions is in the range of 35 °C (for Sn-3.8-0.7Cu near-eutectic alloy) and 18 °C [78]. Unlike SAC systems, the eutectic and near eutectic Sn-Pb alloys undercools only 3-4 °C, therefore they yield a more uniform eutectic microstructure at a broader range of cooling rates. While 5-10 °C/s cooling rate results a fine eutectic microstructure in eutectic Sn-Pb alloys, eutectic composition of SAC alloy forms fine Sn dendrites in ternary eutectic matrix [54]. Micro-alloying of SAC alloys greatly affects the level of undercooling, as well as the resulting microstructure. Detailed information on the effects of fourth element addition on undercooling was discussed **Chapter 2.2.**

Table 2.8. Melting temperatures and undercooling of some SAC solders [51].

Alloy (wt. %)	Melting Temperature (°C)	Undercooling (°C)
Sn-3.8Ag-0.7Cu	216.9	28.6
Sn-3.4Ag-0.9Cu	217.0	18.0
Sn-3.0Ag-0.9Cu	216.8	21.9
Sn-2.5Ag-0.9Cu	216.8	34.3
Sn-2.0Ag-0.9Cu	216.9	29.3

2.3.6. Thermal Shock Resistance of SAC Alloys

Thermo-mechanical fatigue and creep is usually the reason for failure of electronic packages during their operations. Switching on/off and environmental effects create temperature fluctuations. This causes variation of strains acting on the solder joints because of the difference in coefficient of thermal expansion (CTE) of the different materials in electronic packages. As a result of cycling loading, thermal fatigue may

cause failure of the joints **[79]**. Most of critical electronic equipment works with zero-tolerance for such electrical circuit failures. The thermal expansion coefficients of the components of a typical surface mount electronic assembly are shown in **Figure 2.26**. FR4 laminate is the most common type of PCB material used in the consumer electronics industry.
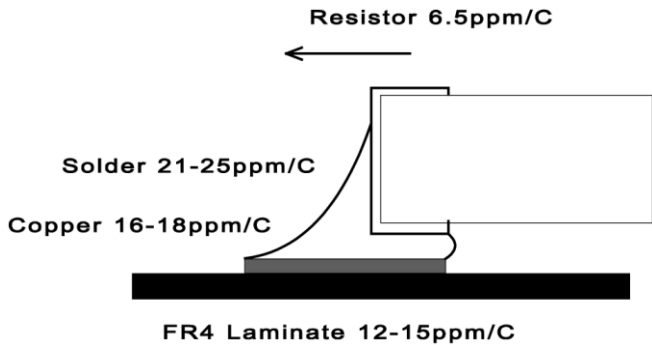
Figure 2.26. Thermal expansion coefficients of the components **[80]**.

The source of thermal stresses was previously explained in **Chapter 2.2**. Thermal stresses can cause failure of a solder by initiation and propagation of micro-cracks that may initiate from any irregularities at the matrix, interface or the surface of the solder joint due to thermal cycling at high cooling and heating rates **[6]**.

The effects of thermal shock cycles on SAC solder with the composition of Sn-3.8Ag-0.7Cu (wt. %) was focused in the study of M.R. Harrison et al. **[7]**. They tested the solders by joining 1206 type surface mount resistors onto the circuit boards. The cycles were carried out between -25 and 125 °C, with 3 minutes dwell time at cold and hot baths on each cycle. The crack initiation and propagation is shown on **Figure 2.27**.
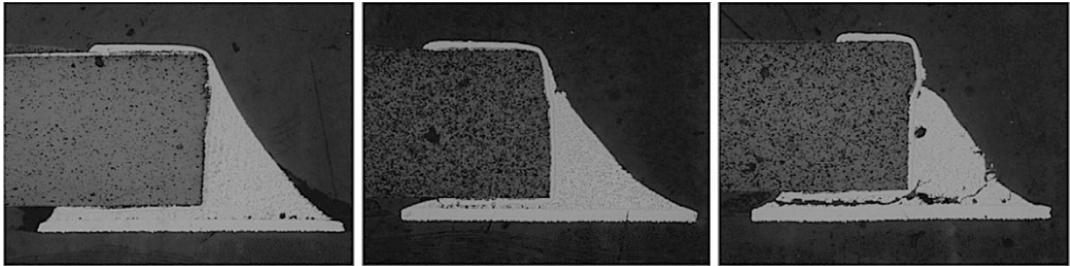
Figure 2.27. Joints after 0, 1000 and 2000 cycles of thermal shock **[7]**.

Thermal cycles, between -40 and 125 °C were applied to the printed circuit boards (PCBs) in the study of P. Arulvanan et al. [12]. The test was conducted at a heating-cooling rate of 0.17-0.23 °C/sec with a dwell time of 15 minutes at two boundary temperatures. Under these conditions, no cracks were observed at 500 cycles, however, at 1000 cycles, the cracks were visible at the solder-substrate interface. Fragmentation of the joints was observed only in certain locations after 2000 cycles. However, after 3000 cycles, fragmentation was dominant in all of the samples. **Figure 2.28** shows the cracking in the joints after 1000 and 3000 cycles of thermal cycling.
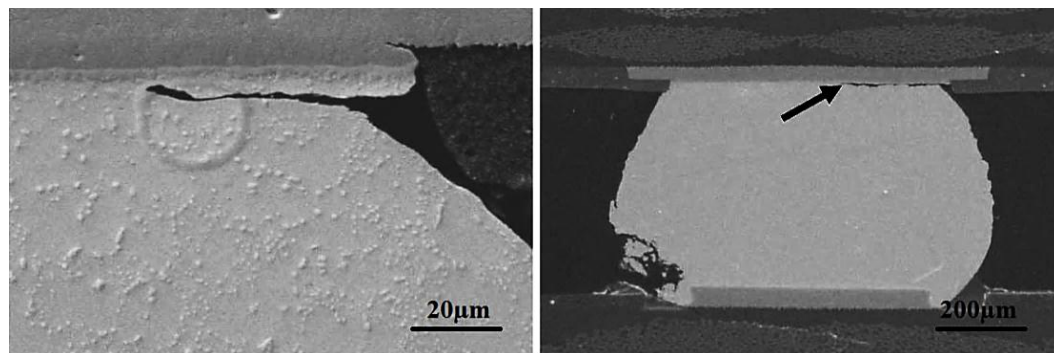
Figure 2.28. The cracking at the interface of joints after:
a) 1000 and **b)** 3000 cycles **[12]**.

Ball-grid array (BGA) type of joints having the composition of Sn-3.0Ag-0.5Cu were tested between -40 °C and 125 °C at 6, 15 and 35 °C/min heating and cooling rates to see the effect of ramp rate on the failure mode of thermally cycled joints. The results at 3000 cycles were shown in **Figure 2.29**. At the 6 °C/min and 15 °C/min ramp rates, the cracking started with the rupture of bulk solder and then peeling at the interface proceeded. At the 35 °C/min ramp rate both bulk solder and the interface ruptured. At the lower ramp rates, the solders are subjected to high temperatures for longer times, therefore metallic reactions at the interface region continue **[81]**. Therefore, heating and cooling rates of thermal cycling is important for characterizing the solders joints for their thermal resistance. The appropriate ramp rates should be selected during testing of the solder joints for the specific application.
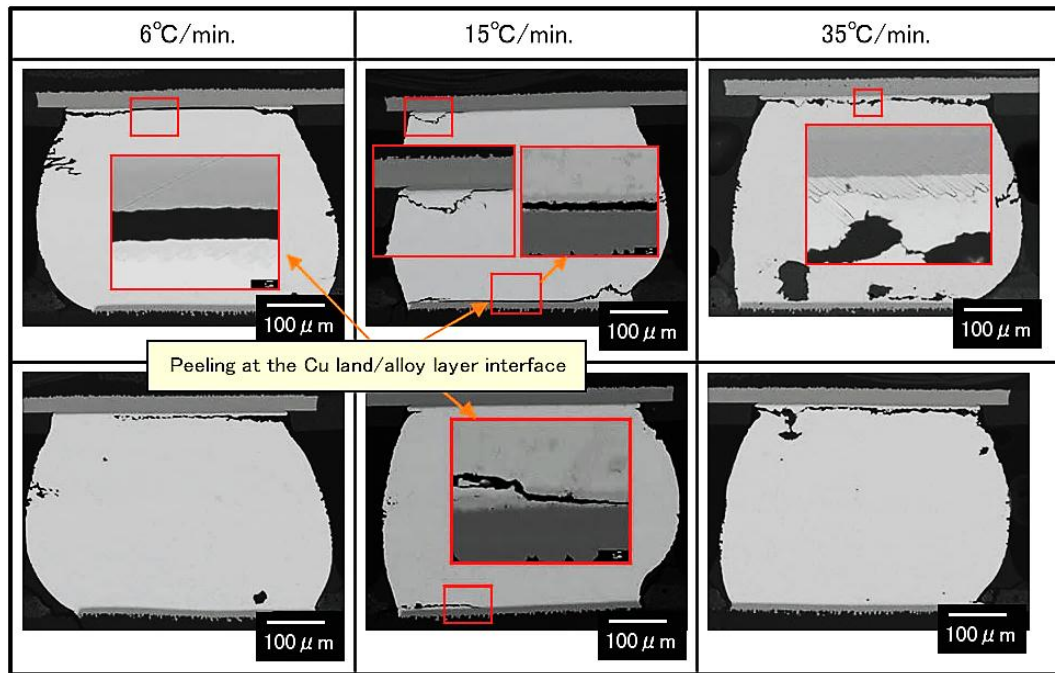
Figure 2.29. Cross-section of the BGA joints **[81]**.

Since cracks would initiate and propagate at the stress concentrated regions; IMCs, such as Ag_3Sn plates and Cu_6Sn_5 rods may provide sites for crack formation as a result of thermal shock. Since, occurrence of these IMCs depends on the alloy composition and related microstructure; the thermal shock resistance of solder alloys greatly depends on the alloy composition.

CHAPTER 3

EXPERIMENTAL PROCEDURES

3.1. Production of Alloys

The production of lead-free solder alloys start with the weighing of raw materials in accurate amounts to create a batch. The raw materials that were used in this research were supplied by Alfa Aesar[®]. The purity and the form of raw materials were shown in **Table 3.1.** The pure elements were weighed, using Radwag[®] AS220 analytical balance having a precision of 0.1 mg.

Table 3.1. The raw materials.

Material	Purity	Form and Size
Sn	99.99+ %	Shots, 3 mm
Ag	99.9 %	Wire, 0.5 mm diameter
Cu	99.9 %	Shots, 1-10 mm
Al	99.999 %	Wire, 1 mm diameter
Fe	99.99 %	Irregular pieces, 3.125-6.25 mm
Ti	99.99 %	Granules

The production set-up (shown in **Figure 3.1**) used in this research is a custom made, atmosphere control system. It is capable of reaching the vacuum level of 10^{-3} mbar (~100 Pa) with a mechanical rotary pump. The vacuum and gas controls are manual and the vacuum level is detected with a digital vacuum sensor. The position of the sensor was specially adjusted so that it will always detect the vacuum level of the materials during the whole alloying process. High purity (99.998 %) argon was used as the inert gas. The system consists of two butterfly valves (one at the Ar gas side and one at the vacuum pump side), one needle valve (at the Ar gas side, to send the gas precisely) and one vent valve (to vent the system by letting air flow into the system). The system is able to evacuate the glass tubes having 12 mm diameter. Quartz tubes were preferred, since the temperature of the tube during melting will rise more than 1000 °C and quartz can easily resist at that temperature levels. The

tubes are attached to the system and made air-tight by two O-rings at their end. Since heat conduction of quartz is very low, while temperature of the tip is around 1000 °C the other end of the tube can still remain at room temperature and the O-rings remain safe. To ensure this, the length of the quartz tubes was chosen to be 150 mm. The tubes were cleaned with ethanol prior to use and each tube was used only once to avoid contamination.
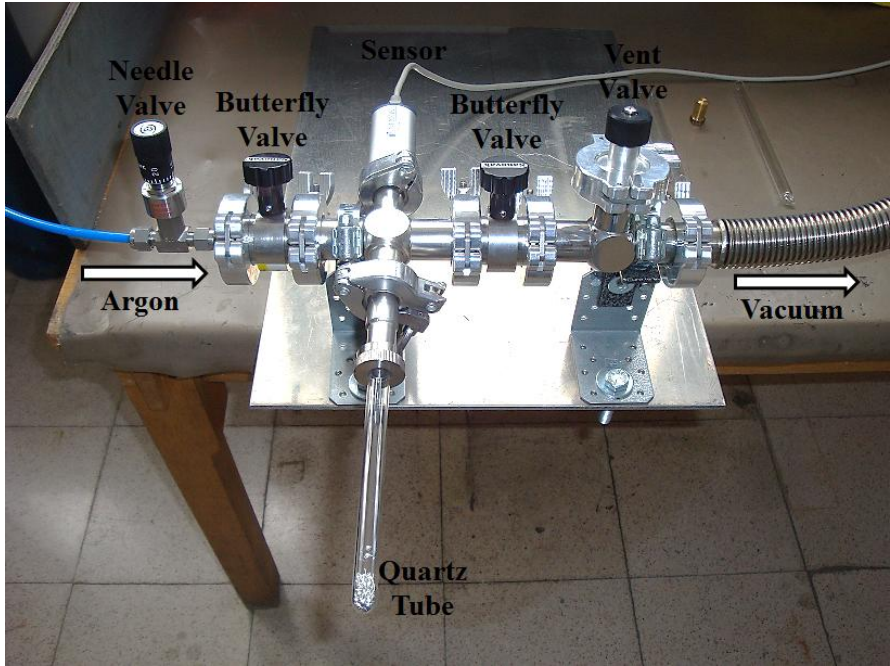
Figure 3.1. The alloy production set-up.

Chemical compositions of the alloys that were produced in this set-up are listed in **Table 3.2**.

Table 3.2. Names and chemical compositions of produced solder alloys.

	Alloy Notation	**Composition (wt. %)**
First Group	SAC (Eutectic)	Sn-3.5Ag-0.9Cu
	SAC (Near-Eutectic)	Sn-3.7Ag-0.9Cu
	SAC + 0.05Al	Sn-3.5Ag-0.9Cu-**0.05Al**
	SAC + 0.05 Fe	Sn-3.5Ag-0.9Cu-**0.05Fe**
	SAC + 0.05 Ti	Sn-3.5Ag-0.9Cu-**0.05Ti**
Second Group	SAC + 0.01Fe	Sn-3.5Ag-0.9Cu-**0.01Fe**
	SAC + 0.03 Fe	Sn-3.5Ag-0.9Cu-**0.03Fe**
	SAC + 0.07 Fe	Sn-3.5Ag-0.9Cu-**0.07Fe**
	SAC + 0.1 Fe	Sn-3.5Ag-0.9Cu-**0.1Fe**

3.1.1. Alloying Operation

After weighing, pure elements were inserted into a quartz tube and the tube was attached to the melting set-up. The steps that were followed to have an inert atmosphere in the system are as follow:

1) Close gas side valve, close needle valve, close vent valve and open pump side valve.
2) Run the pump until the vacuum level reaches to ~3×10^{-2} mbar
3) Close pump side valve, open gas side valve and slowly open the needle valve to start sending Ar gas.
4) Send the gas until vacuum level drops to ~100 mbar.
5) Repeat steps 1-4 by setting the vacuum level to ~2×10^{-3} mbar in step 2.
6) Repeat steps 1-4 by setting the vacuum level to ~1.5×10^{-3} mbar in step 2.
7) Close pump side valve, open gas side valve and slowly open the needle valve to start sending Ar gas.
8) Send the gas until vacuum level drops to ~1-10 mbar.
9) Close all valves.

After these steps, the desired inert atmosphere inside the system and the tube is reached and melting can be conducted. A propane flame torch, which can reach ~1500 °C, was used as the source of heat for melting. The flame was directly applied to the tip of the tube, where the raw materials were located. No temperature measurement was done during melting but melting and mixture of the elements were visually observed. Once melting was conducted, further heat was applied and the color of the melt was monitored. This high temperature is needed to ensure the melting and homogenization of materials having high melting temperatures, such as Ag (962 °C) and Cu (1085 °C). Fe and Ti have even higher melting points which are 1536 °C and 1670 °C, respectively. However, their weight percentages in the alloys are very low (< 0.1 %) and they are dissolved, well below their melting temperatures.

After melting and alloying process, the melt alloy was cooled and solidified by water quenching. The water was poured onto the tip of the quartz tube where the melt was located. After solidification was completed, the tube was turned upside

41

down without venting the tube and melting process was repeated. In total, the alloy was melted and solidified for three times to ensure homogenization of the elements. However, after last melting process, the alloy was air cooled instead of water quenching. For solders, the cooling rate during primary production is not critical since they will be re-melted at the time of their use in joining metal pieces.
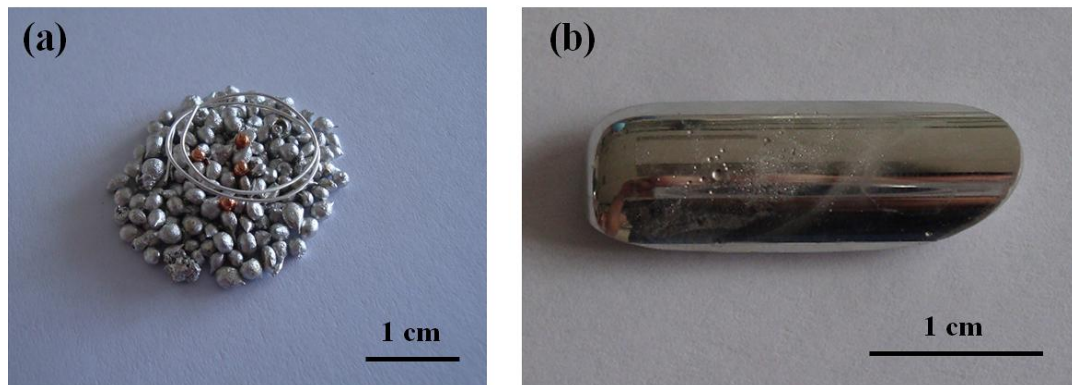
Figure 3.2. a) Batch of raw materials and **b)** produced lead-free solder alloy.

3.1.2. Inspection of Solder Ingots

The weight of pure elements and the weight of alloy that were measured after alloying process must be similar if no materials were vaporized or lost during the melting process Also, chemical elemental analysis is necessary to observe the chemistry after producing ingots of solder alloys. All alloys were inspected by their weight and chemistry prior to any testing or analysis.

Weight Loss Calculation

For determination of weight loss, the alloys were weighed and compared with the weight of the batch. Then, percent weight loss was calculated by using **Equation 1**. In all alloys that were produced, the weight loss was less than 0.025 wt. %.

$$\% \, WL \; = \frac{weight \; of \; the \; batch - weight \; of \; alloy}{weight \; of \; the \; batch} \; x \; 100 \qquad \textbf{(Equation 1)}$$

Chemical Composition Analysis

For confirmation of chemical compositions, energy dispersive spectroscopy (EDS) attached to a scanning electron microscope (FEI® Nova NanoSEM 430) was used. The surfaces of the alloys were grinded and polished to have a flat surface before conducting EDS analysis. This is necessary to obtain correct results from EDS, since rough surfaces may lead to incorrect measurements. The analyses were performed at 20 kV and a spot size of 6. The working distance between the sample surface and the pole piece was 5 mm. EDS was conducted at six random areas on the surface and averages of compositions were calculated. The results were compared with the weight percentages of the pure elements in the batch.

3.2. Thermal Analysis

Thermal analysis was performed to determine the melting and solidification temperatures and thus the level of undercooling for the solder alloys at different compositions. Differential scanning calorimeter (Perkin Elmer® Diamond DSC) was used for this purpose. Samples were cut to 10 mg pieces and they were melted in Pyrex tubes, under Argon atmosphere and solidified to have a uniform shape. By surface tension, solder alloys form spheres when they are melted. Diameter of these solder spheres are ~1.3 mm. The pans and lids for DSC analysis were made of copper. The inner surface of the pans and the lids were covered with solder flux, which acts as a wetting agent and prevents oxidation of solder, where the most common type of flux used in electronics (soft-soldering) is rosin-based, made from the rosin from selected pine trees **[82]**. The solder discs were placed in the middle of the pans and the lids were closed and pinched at eight points to secure the lids. All the analyses were performed between 30 °C and 250 °C under N_2 atmosphere. After each run of thermal scan, a subsequent run was conducted with empty crucibles to calculate the baseline. A common heating-cooling DSC profile that was followed in this study can be listed as:

1)   Hold for 2.0 minutes at 30.00 °C

2)   Heat from 30.00 °C to 250.00 °C at ΔT °C/minute

3)   Hold for 1.0 minute at 250.00 °C

4)   Cool from 250.00 °C to 30.00 °C at ΔT °C/min

Here, ΔT is the cooling and heating rate, which was chosen as 0.017, 0.17 and 1.7 °C/sec for different samples. Melting temperatures were determined from the on-set points of isothermal scans. This will be discussed in details in **Chapter 4.2**.

3.3. Microstructural Analysis

The solder samples were grouped with respect to solidification rate, undercooling and composition for detailed microstructural analysis. These samples were first grinded and polished then etched with a solution of 60 ml HCl, 15 ml H_2O, 15 ml HNO_3, 15 ml CH_3COOH for 10 seconds to reveal the microstructure of the alloy. Scanning electron microscope (FEI$^®$ Nova NanoSEM 430) was used for microstructural analysis. Secondary electron detectors, namely Everhart-Thornley Detector (ETD) and Through Lens Detector (TLD), were used for topographical contrast and back-scattered electron detector, namely low voltage high contrast detector (VCD), was used for chemical contrast. The microstructural analysis was conducted to detect and quantify intermetallic compounds (i.e. Ag_3Sn and Cu_6Sn_5) and morphology of the phases (i.e. eutectic and dendritic) and to measure the interface thickness between the solder and substrate.

3.4. Mechanical Analysis

In this part of the study, two methods were used for determination of mechanical properties of the solder alloys that were produced. In shear test, two copper plates were joined by the solder and then by applying tensile load to those copper plates, the shear strengths of the alloys were calculated. For hardness test, Vickers micro-hardnesses of the alloys were measured by simply applying a load with an indenter and measuring the size of the indent that the applied load has caused. The details of these two mechanical testing methods that were used in this study are explained below.

3.4.1. Single-Lap Joint Shear Test

Shear test specimens were prepared by reflowing the solder alloys on copper plates. In this experiment, copper plate having ASTM B 187 standards was used. A bulk copper plate, having the dimensions of 700 mm x 700 mm x 1.5 mm was cut down to smaller plates with dimensions of 50 mm x 12 mm x 1.5 mm. The overlap length of plates was set to 12 mm. The geometry of specimens is shown in **Figure 3.3**. Four specimens were prepared for each alloy compositions. Surfaces of the copper plates were grinded with 1200 mesh grinding paper and cleaned with methanol to avoid any oxide layer on the surface. Reflowing operation was done at 250 °C for 30 seconds. All joints were air cooled to room temperature. After cooling, the overlap lengths were measured to verify the 12 mm target length. Any deviation from this number would greatly affect the shear strength. Shear test is conducted on INSTRON® 5582 Universal Testing Machine at an extension rate of 0.1 mm/min. The maximum load each specimen could bear was divided by the overlap area, which is 144 mm^2. Shear tests were repeated four times for each alloy compositions. The average values and standard deviations of the results were calculated.
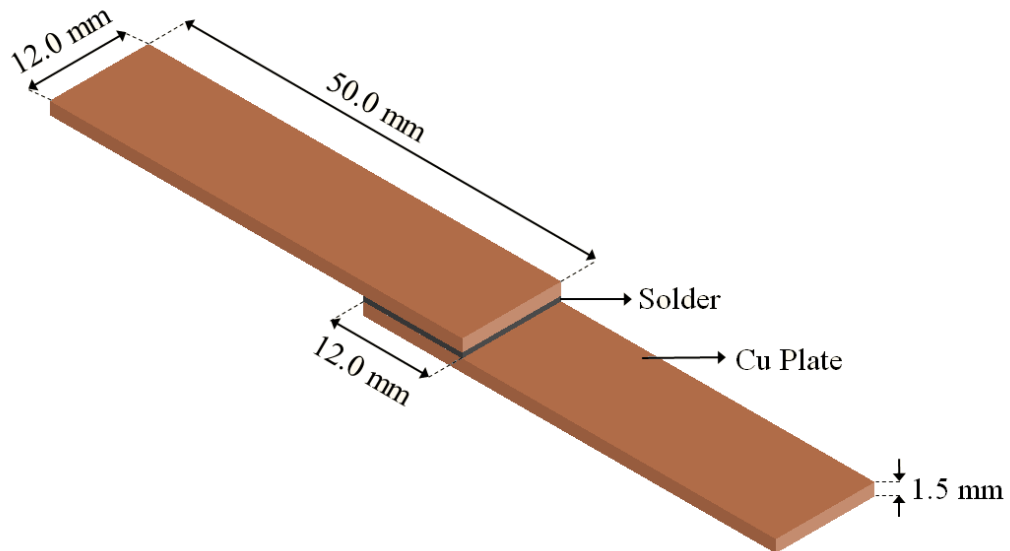

Figure 3.3. Single-lap joint shear specimen geometry.

3.4.2. Hardness Test

Hardness test specimens were carefully grinded to have flat surfaces, since inclined surfaces would lead to irregular indent geometries and consequently give false results. Hardnesses of the specimens were measured with SHIMADZU® HV-2 Micro-Vickers Tester. The load was set to 980.7 mN with a dwell time of 15 seconds. Ten consecutive indentations were performed for each specimen with 50 microns distance between each indent mark. The highest and lowest hardness values were neglected and the remaining eight were used in calculations. The average and the standard deviation of eight values were calculated and tabulated.

3.5. Wetting Analysis

For wetting measurements, samples were cut to 10 mg pieces and they were melted in Pyrex tubes, under argon atmosphere and solidified to have uniform, spherical solders. Copper pieces with dimensions of 10 mm x 10 mm x 1.5 mm were prepared. Their surfaces were grinded and polished to remove any oxide layer. Then soldering flux (Stannol® - Kontakt Lötpaste) was evenly applied on the surface of each copper chip. The spherical solder pieces were placed on the surface of the copper pieces. These pieces were kept at 250 °C on a hot plate and melting of the solder alloys was observed. After the melting was observed, they were kept at that temperature for another 15 seconds and air cooled to room temperature. For each composition, two sets of specimens were prepared for wetting area and angle measurements.

3.5.1. Wetting Area Measurement

Wetting area measurements were performed on the specimens having the geometry shown in **Figure 3.4**. Macro photographs of the samples were taken from the top of the samples and analyzed with image processing software (ImageJ). The areas covered by the solder alloys (shown **A** in **Figure 3.5**) were analyzed and measured in "mm^2" unit.

Figure 3.4. Geometry of the wetting area measurement specimen.
(* Arrow shows the point of view)
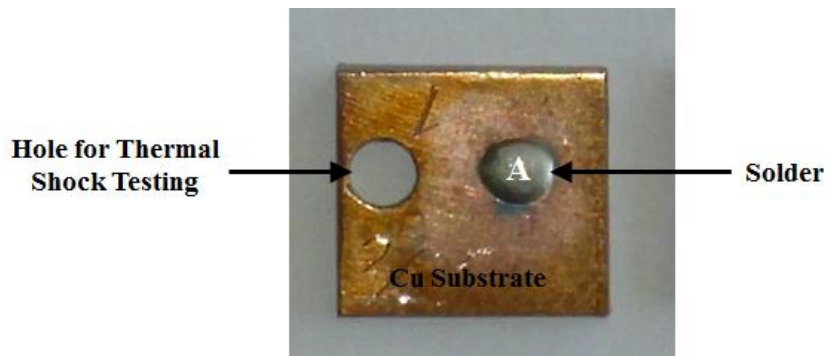
Figure 3.5. The photograph taken from a lead-free solder/copper joint
for wetting area measurement

3.5.2. Wetting Angle Measurement

The samples that were used in wetting area measurements were cut in half to prepare the wetting angle measurement specimens. After cutting, the cross sections of the samples were grinded and polished to have a completely flat surface. Wetting angle measurements were performed on the samples having the geometry shown in **Figure 3.6**. Scanning electron microscope (SEM) images at 80 magnifications were taken from the cross-section of these samples and the wetting angle θ, as shown in **Figure 3.7** was measured from both left and right sides of the samples. Unless the angles measured from the both ends are in close proximity (within 1.5 degrees), the measurement is considered invalid. **Figure 3.7** shows a valid measurement, where θ_1 and θ_2 has values close to each other, whereas in **Figure 3.8**, an invalid measurement was shown, which the angles θ_1 and θ_2 has a difference larger than 1.5 degrees.

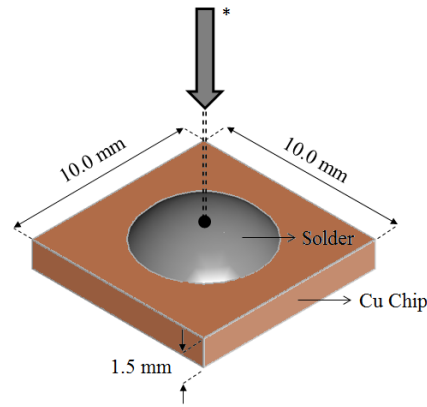**Figure 3.6.** Geometry of the wetting angle measurement specimen.
(* Arrow shows the point of view)

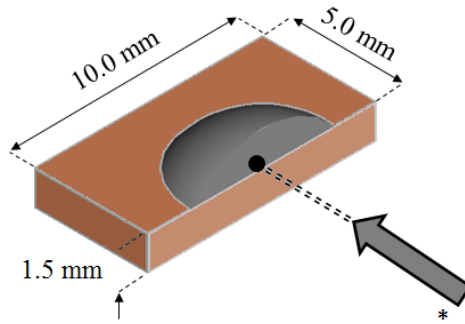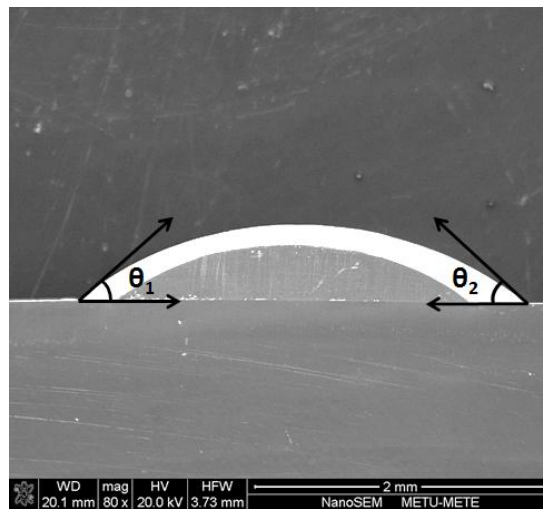**Figure 3.7.** SEM image taken from a lead-free solder/copper joint for wetting angle measurement. Valid measurement, where $\theta_1 \approx \theta_2$.
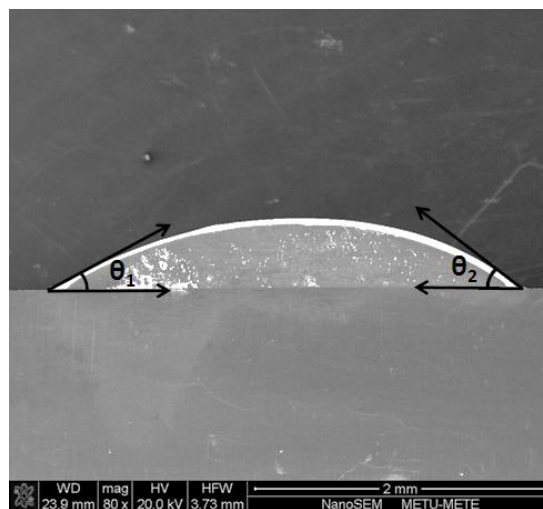
Figure 3.8. SEM image taken from a lead-free solder/copper joint for wetting angle measurement. Invalid measurement, where $\theta_1 \neq \theta_2$.

3.6. Thermal Shock Analysis

Thermal shock resistance of solder alloy was tested by mainly two different methods within the same temperature range. Those techniques are explained below.

3.6.1. Solder-Copper Joint Thermal Shock Resistance Test

A thermal shock set-up, illustrated in **Figure 3.9**, was designed and built for this study. The set-up mainly consists of a cold chamber, a hot chamber, a motor and an electronic control unit. The cold chamber contains liquid ethanol at -30 °C. The hot chamber is a tube furnace, which was held at ~140 °C. The samples and a *K-type* thermocouple were attached at the tip of a steel rod having a diameter of 4 mm. The thermocouple is connected to a temperature controller. The rod was fixed to a set of rails which are moving along the vertical axis. A 300 rpm DC motor and a ball screw were used to move the system up and down. The DC motor was controlled with a programmable logic controller (PLC). The PLC was programmed so that the user can enter the number of cycles to be performed and the desired time at the hot and cold chambers. The temperature controller was connected to the PLC, so that the motion of the system could be triggered when the samples has reached at the desired temperature.
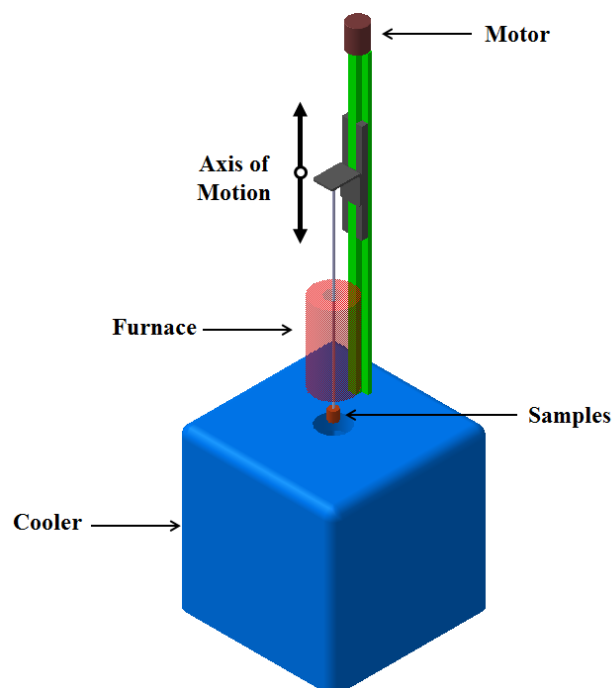
Figure 3.9. The thermal shock set-up.

Specimens continuously move between the cold and hot chamber for a pre-determined time and speed. Two specimens were tested for each alloy composition. All the specimens were tested together so that they would be exposed to the same thermal conditions. Each thermal cycle took 3 minutes with the temperature profile shown in **Figure 3.10**. The specimens were taken out at every 500 cycles for detailed investigation with SEM, for possible initiation and propagation of micro-cracks as a result of severe thermal shock cycles.
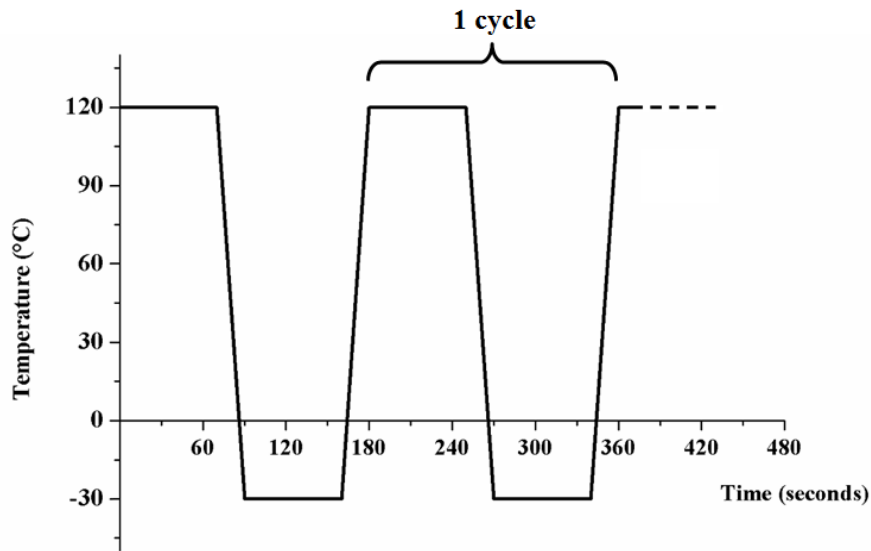
Figure 3.10. Temperature profile of samples during thermal shock test.

3.6.2. Performance Test on Printed Circuit Boards

Thermal shock resistances of the lead-free solders were also tested on printed circuit boards (PCBs) to simulate the service conditions of the solder joints. This part of the study was collaborated with ARÇELİK. Vötsch® VT3 7012 S2 thermal shock test chamber which is shown in **Figure 3.11** was used.

The PCBs were cycled between two chambers, which were constantly held at -40 and +85 °C. The dwell time at each chamber was 15 minutes. Each solder composition was applied onto four PCBs. At each 100 cycles, one of those four PCBs was removed from the test system for detailed investigation of crack propagation and microstructural change formed as a result of severe thermal cycling. **Figure 3.12** shows the PCB and the resistor soldered onto it, which was used in this test.

Figure 3.11. Thermal shock test chamber used by Arçelik.
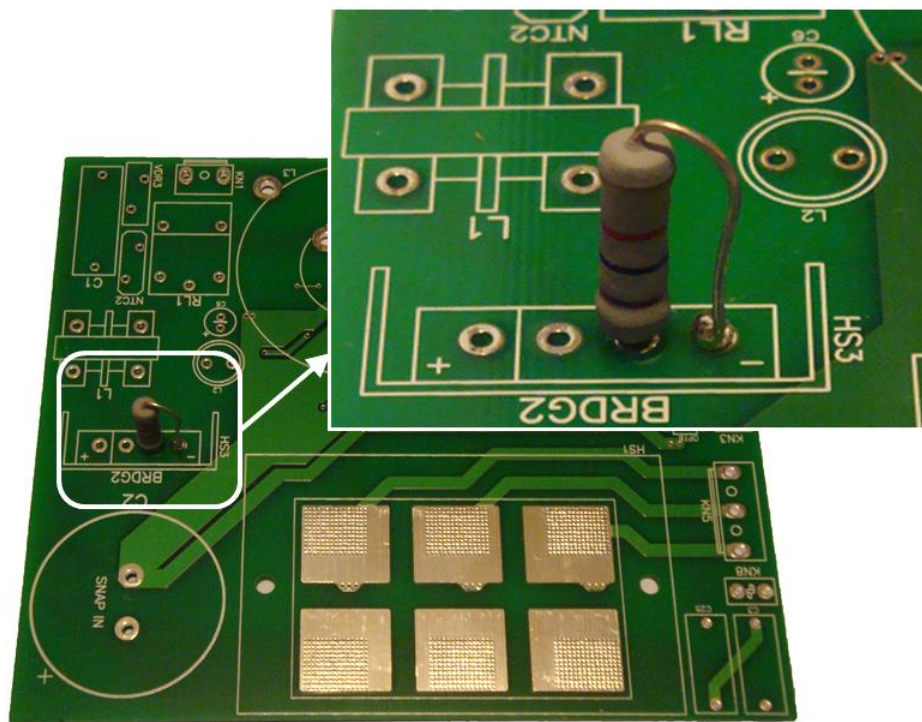
Figure 3.12. PCB and resistor, that were subjected to thermal shock test.

CHAPTER 4

RESULTS AND DISCUSSION

4.1. Thermal Analysis

The melting temperature (T_m) and solidification temperature (T_s) were measured by using differential scanning calorimeter (DSC). Heating and cooling rate of the experiment was set to 0.17 °C/sec. The melting temperatures of the alloys are in the range of 217.1 - 217.9 °C; which shows, melting temperature just slightly depends on the type of alloying element and its overall composition.

On the other hand, there is a strong dependence of alloying element composition on the solidification temperature. This also affects the undercooling which is the difference between melting and solidification temperatures, indicated with **ΔT** on the plot shown in **Figure 4.1**.
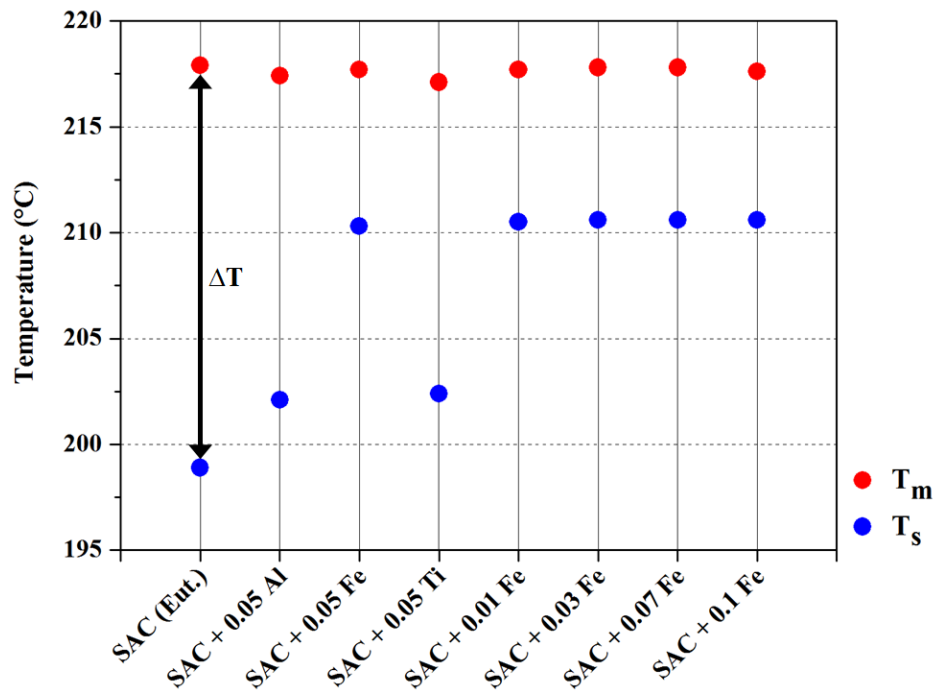
Figure 4.1. Melting (T_m) and solidification (T_s) temperatures of the alloys. Their difference is undercooling, shown with **ΔT.**

While undercooling of eutectic SAC alloy was measured as 19 °C, it was measured as 7 °C for SAC+0.1Fe solder. Al and Ti additions were less effective and had similar impacts; which, undercooling was measured as 15.3 °C and 14.7 °C respectively. Fe is the most effective element on decreasing the undercooling. Measured undercoolings of the alloys are given in **Table 4.1**. The shapes of melting peaks are similar for all the alloys; however, having sharper peaks, eutectic SAC, SAC+0.05Al and SAC+0.05Ti alloys solidifies at a shorter temperature range than all Fe micro-alloyed samples. Therefore; eutectic SAC, SAC+0.05Al and SAC+0.05Ti alloy compositions may be expected to have coarser microstructures. On the other hand, a broad crystallization peak close to melting on-set indicates a refinement of microstructure upon solidification. The corresponding DSC curves are shown in **Figure 4.2** and **Figure 4.3**.
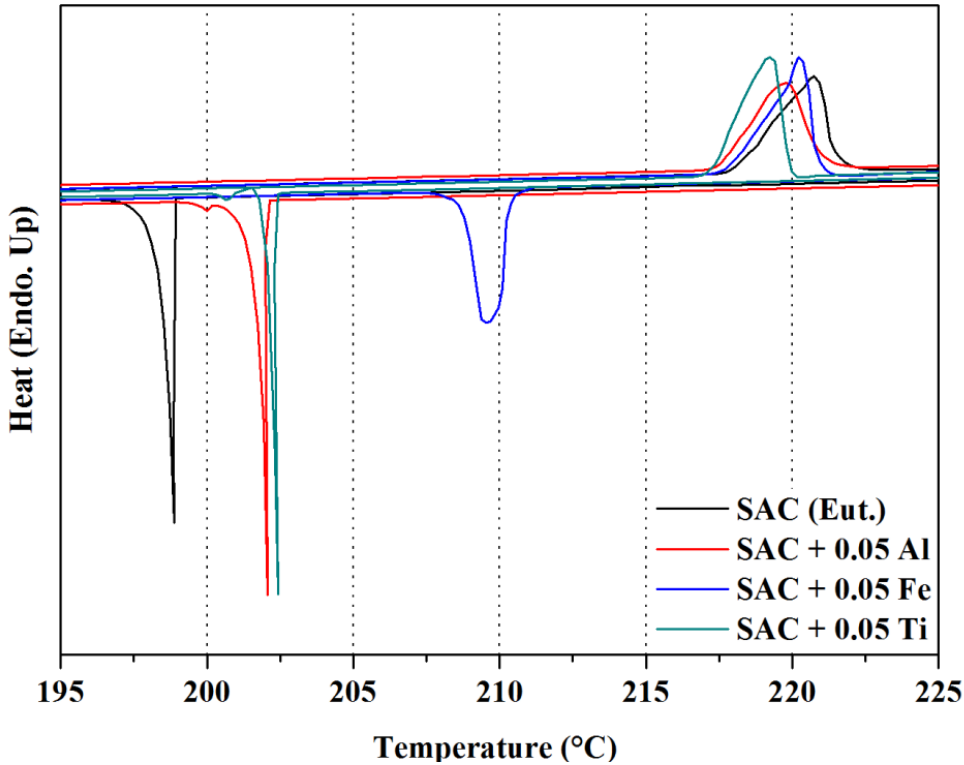
Figure 4.2. DSC curves of selected first group alloys.
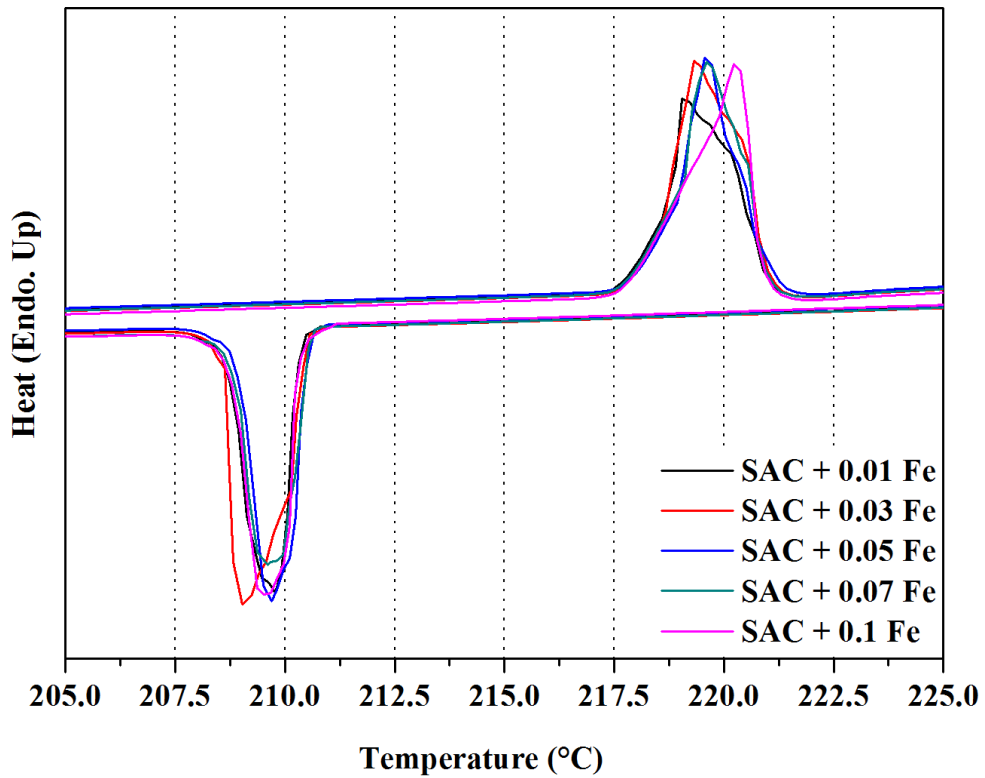
Figure 4.3. DSC curves of second group alloys.

Table 4.1. Measured melting, solidification temperatures and undercoolings for solders cooled with 0.17 °C/sec.

Alloy	T_m (°C)	T_s (°C)	ΔT (°C)
SAC (Eutectic)	217.9	198.9	19
SAC + 0.05 Al	217.4	202.1	15.3
SAC + 0.05 Fe	217.7	210.3	7.4
SAC + 0.05 Ti	217.1	202.4	14.7
SAC + 0.01 Fe	217.7	210.5	7.2
SAC + 0.03 Fe	217.8	210.6	7.2
SAC + 0.07 Fe	217.8	210.6	7.2
SAC + 0.1 Fe	217.6	210.6	7.0

4.1. Microstructural Analysis

In the first part of study, the effect of SAC composition on the level of undercooling was analyzed. In this section, effects of SAC composition and the cooling rate on microstructure evolution is investigated.

4.1.1. Effect of Composition on Microstructure

As-cast solder ingots were analyzed with X-ray diffraction for the confirmation of the phases. IMC phases such as $FeSn_2$ or Ti_2Sn_3 that may form between Sn and micro-alloying elements are absent in this study. **Figure 4.4** shows the corresponding XRD pattern of as-cast ingots. Indexing shows that Ag_3Sn, Cu_6Sn_5 and β-Sn are the only phases formed in these samples.
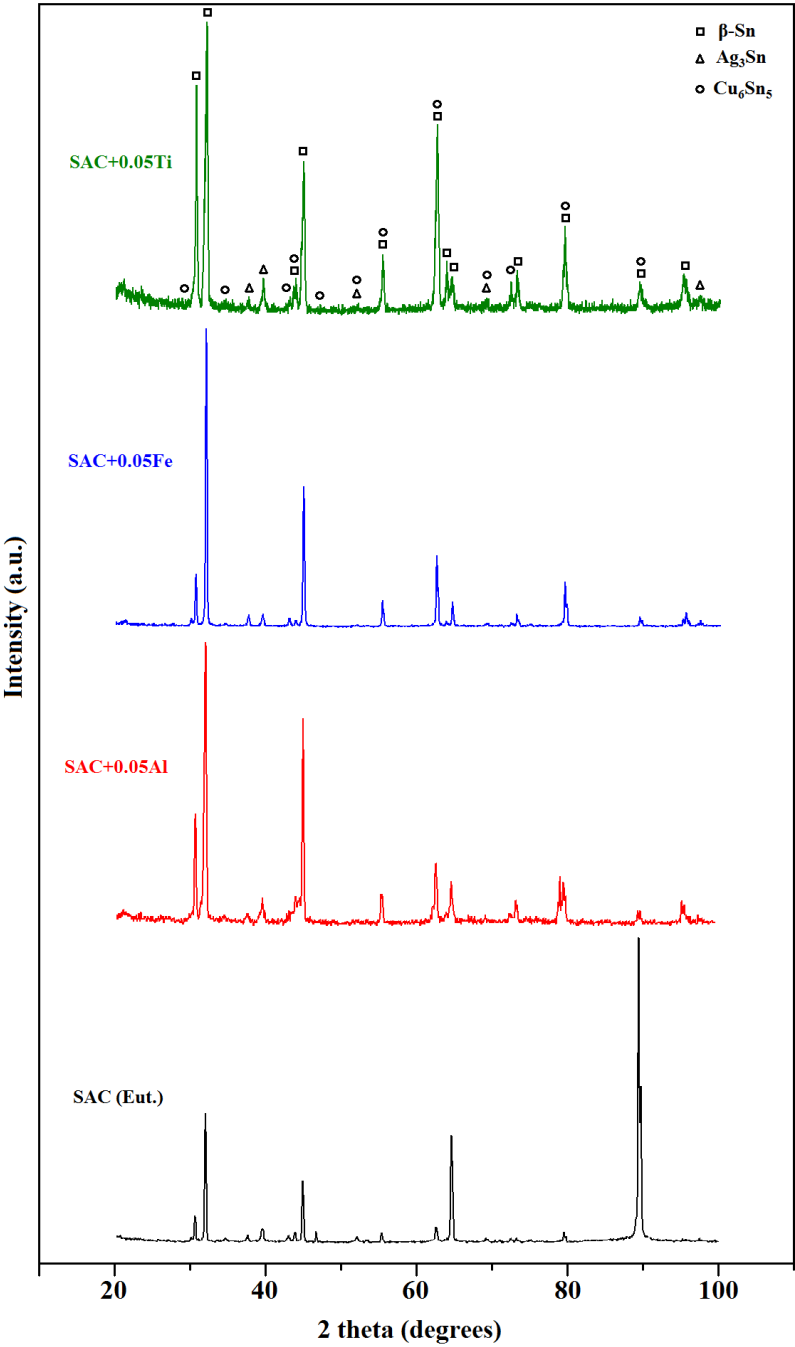
Figure 4.4. XRD spectrums of as cast solder ingots.

All solder specimens were subjected to the same cooling conditions before any further microstructural analysis. Five types of microstructure have been commonly observed in SAC and SAC+X alloys investigated in this study. Their morphologies and some characteristic properties were tabulated in **Table 4.2.** Among these microstructures, pro-eutectic Ag_3Sn were only observed in eutectic SAC, SAC+0.05Al and SAC+0.03Fe alloys for which the largest Ag_3Sn sizes were measured as 53 μm, 38 μm and 44 μm, respectively. On the other hand, Cu_6Sn_5 IMCs were detected in all of the samples. β-Sn dendrites were observed in all of the samples except eutectic SAC and SAC+0.1Fe alloys. They are finer in SAC+0.01Fe, SAC+0.03Fe and SAC+ 0.05Al and getting coarser in the SAC+0.05Fe and SAC+0.05Ti. The amount of eutectic phase is higher in SAC+0.01Fe. Cu_6Sn_5 at the interface is thickest for eutectic SAC alloy and it decreases with micro-alloying. Thinnest interface was observed in SAC+0.01Fe and SAC+0.05Fe.

When morphologies of IMCs were considered, large pro-eutectic Ag_3Sn plates and Cu_6Sn_5 rods were only seen in eutectic SAC alloy. Between these two IMC, Ag_3Sn is seen as the major cause poor mechanical and wetting properties. One might ask why a eutectic composition solidifies into so large IMC upon cooling. In order to answer this question the phase diagrams and undercooling values should be carefully investigated. **Figure 4.5** shows the ternary and binary phase diagrams of Sn-Ag-Cu and Sn-Ag, respectively.
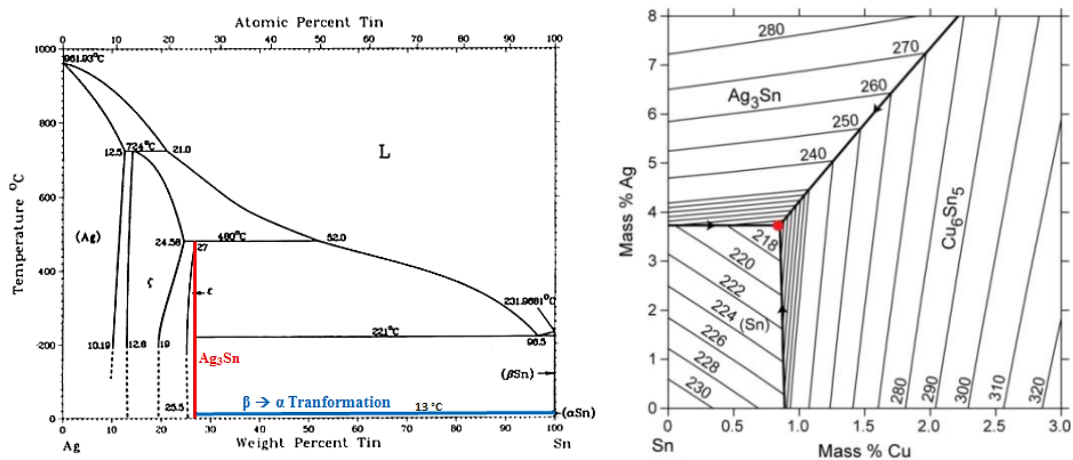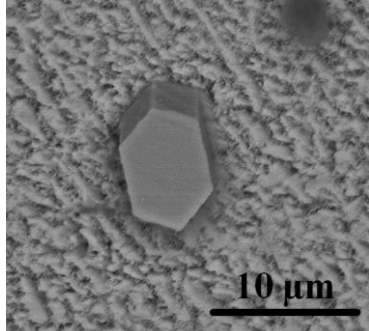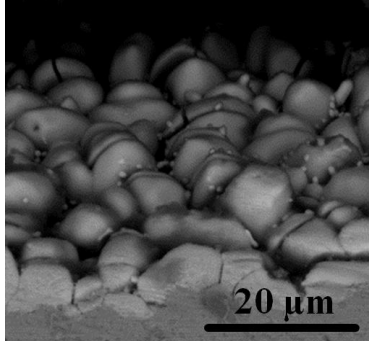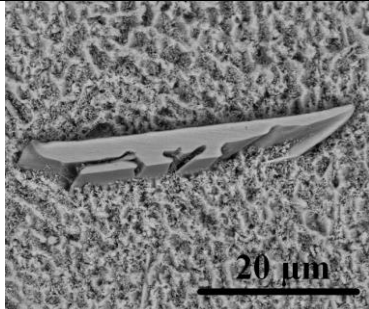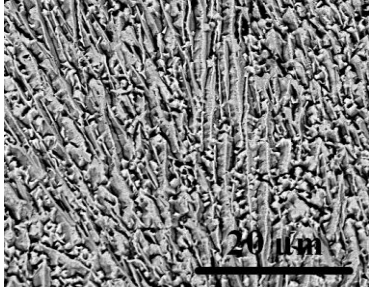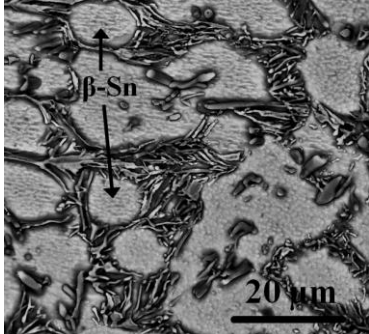
Figure 4.5. Sn-Ag binary phase diagram **[19]** and Sn-rich part of SAC system **[43].**

Table 4.2. BSE images and lattice parameters of phases seen in SAC solders.

Phase	BSE Image	Lattice Parameter (Å)
Cu$_6$Sn$_5$ (In matrix) *(Faceted)*	10 μm	a=4.206 c=5.097 (Hexagonal) **[83]**
Cu$_6$Sn$_5$ (at interface) *(Faceted)*	20 μm	a=4.192 c=5.037 (Hexagonal) **[84]**
Ag$_3$Sn (Pro-Eut.) (Faceted)	20 μm	a=5.9689, b=4.7802, c=5.1844 (Orthorhombic) **[85]**
Ternary Eutectic	20 μm	N/A
β-Sn (Pro-Eut.) (Non-Faceted)	β-Sn 20 μm	a=b=5.8314 c=3.1815 (Tetragonal) **[86]**

When slow cooling is applied, if primary Ag_3Sn forms just before the eutectic reaction, the eutectic Ag_3Sn crystals nucleate adjacent to the primary-Ag_3Sn crystals since their crystalline orientation match. Further growth of this primary and eutectic Ag_3Sn phases during solidification leads to the formation of bulk Ag_3Sn IMC.

First phase to come out from the liquid is Cu_6Sn_5. After the nucleation of primary Cu_6Sn_5 phase, growth of these particles initiates and they start to eject Ag to the liquid. As the growth continues, the ejected Ag atoms gradually accumulate near Cu_6Sn_5 particles and Ag rich regions are formed in the liquid. This phenomenon shifts the local concentration to the Ag rich side of the phase diagram (**Figure 4.5**) and when the concentration reaches to the Ag_3Sn formation line of the phase diagram, pro-eutectic Ag_3Sn IMC starts to form. Since Ag_3Sn and Cu_6Sn_5 are both faceted phases, Ag_3Sn can heterogeneously nucleate on the Cu_6Sn_5. This theory also explains why large Ag_3Sn next to the Cu/solder interface is commonly observed as in **Figure 4.11**.

Table 4.3. Results of microstructural analysis of the produced lead-free solders.

Alloy	Number of IMC / mm²	Largest Cu_6Sn_5 (μm)	Largest Ag_3Sn (μm)	Interface Thickness (μm)
SAC (Eutectic)	30	176	53	4.5
SAC + 0.05 Al	338	72	38	4.0
SAC + 0.05 Fe	21	30	-	3.0
SAC + 0.05 Ti	9	68	-	4.0

A common practice to suppress the nucleation (or refine the size) of any IMC in SAC is the micro-alloying with fourth elements. Hume-Rothery Rules were applied for the selection; accordingly, parameters which define the ability to form substitutional solid solution, which are electronegativities and atomic radii of the elements were tabulated and shown in **Table 4.4**. In this study Al, Fe and Ti were selected according to their abilities to form solid solution with copper. The representative Darken-Gurry map and the solubility properties of Al, Fe and Ti are given in **Figure 4.6**.

Table 4.4. Electronegativities and atomic radii of selected elements.

	Al	Fe	Ti	Cu	Sn	Ag	Ref.
Electro-negativity	1.61	1.83	1.54	1.90	1.96	1.93	**[87]**
Atomic radius (pm)	125	140	140	135	145	160	**[88]**
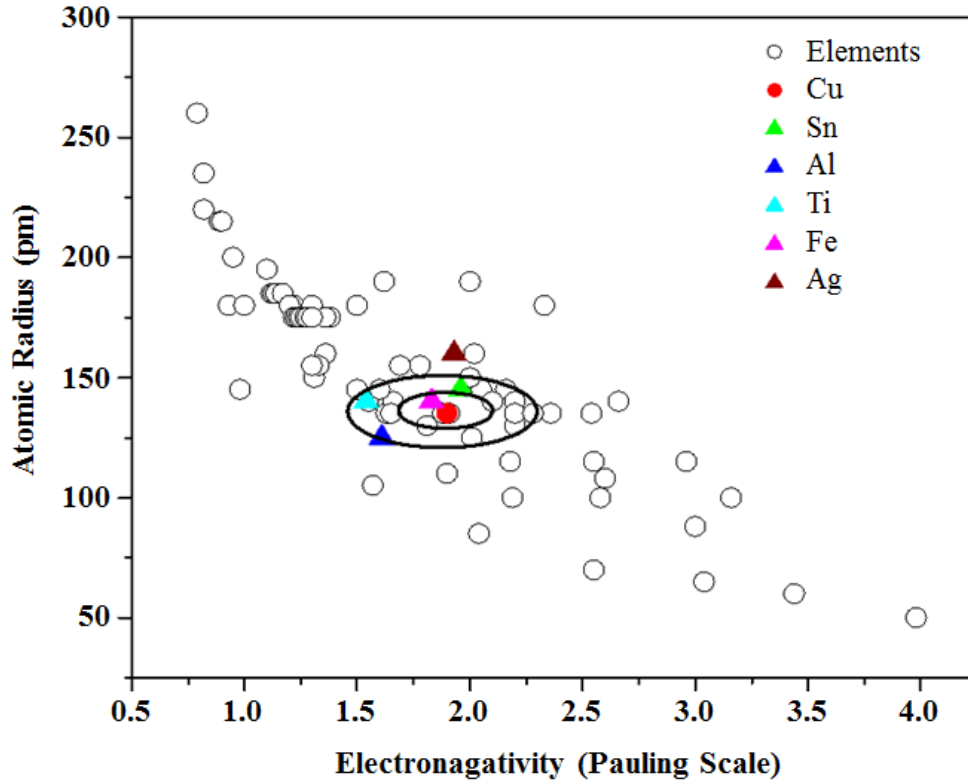
Figure 4.6. Darken-Gurry map for Cu.

According to Hume-Rothery Rules, Fe has the highest tendency of making substitutional solid solution with Cu since they have the closest electronegativity and atomic radius values. This makes two fundamental effects in the formation of resultant microstructure.

First of all, additions of *transition metals* (i.e. Al, Fe, Ti) changes the alloy composition, such that the solidification path of the liquid alloy moves towards the eutectic point. Changing the composition also affects the solidification temperature and the undercooling values greatly. The measured undercooling values from DSC are in good agreement with this argument. By addition of Fe, the minimum undercooling was reached, which is 7 °C while undercooling of the eutectic alloy

was 19 °C. This shows that by minute amounts of Fe, the undercooling of eutectic lead-free solder alloy can be decreased by 12 °C (63 %). The addition of other elements had similar impacts on decreasing the undercooling but not as effective as Fe. The decrease in the undercooling was found to be 3.7 °C (19 %) and 4.3 °C (23 %), respectively.

The second effect of fourth element addition is the refinement of microstructure. This is due to the decrease in the undercooling as well as the limited diffusion of Cu. **Figure 4.7** and **Figure 4.8** shows the resultant microstructures after fourth element additions. The bare eutectic compositions contain large pro-eutectic Cu_6Sn_5 and Ag_3Sn phases. For the formation of large Cu_6Sn_5, large amount of Cu atoms must diffuse near the Cu_6Sn_5 nuclei since matrix is originally poor in Cu. If the added fourth element acts as a barrier to the diffusion of Cu to large distances, then Cu_6Sn_5 crystals can no longer grow into large particles but many Cu_6Sn_5 crystals form in many sites and grows less with small amount of Cu that diffuse only in small distance. Similarly, for the formation of large Ag_3Sn, Ag must diffuse large distances since matrix is poor in Ag. If diffusion of Ag is hindered and it undergoes into eutectic reaction, it forms many nano-sized Ag_3Sn crystals. Also this phenomenon may decrease the undercooling of the alloy during solidification, since these added elements will acts as inoculants which would act as sites for heterogeneous nucleation and formation of Cu_6Sn_5 and Ag_3Sn may start at many sites simultaneously. Then solidification can take place with decreased undercooling since less energy is involved in heterogeneous nucleation. When **Figure 4.7** and **Figure 4.8** are observed, Fe added compositions, especially SAC+0.01Fe and SAC+0.07Fe alloys seem to form many small Cu_6Sn_5 crystals. However, no trend was observed with variation in Fe concentration and number of Cu_6Sn_5 crystals that were formed. Al addition was less effective since higher undercooling was achieved and larger Cu_6Sn_5 particles were observed. Note that the observations are not limited to images in **Figure 4.7** and **Figure 4.8** but at least 8 images of different locations for each composition were evaluated for microstructural analysis of the solders.
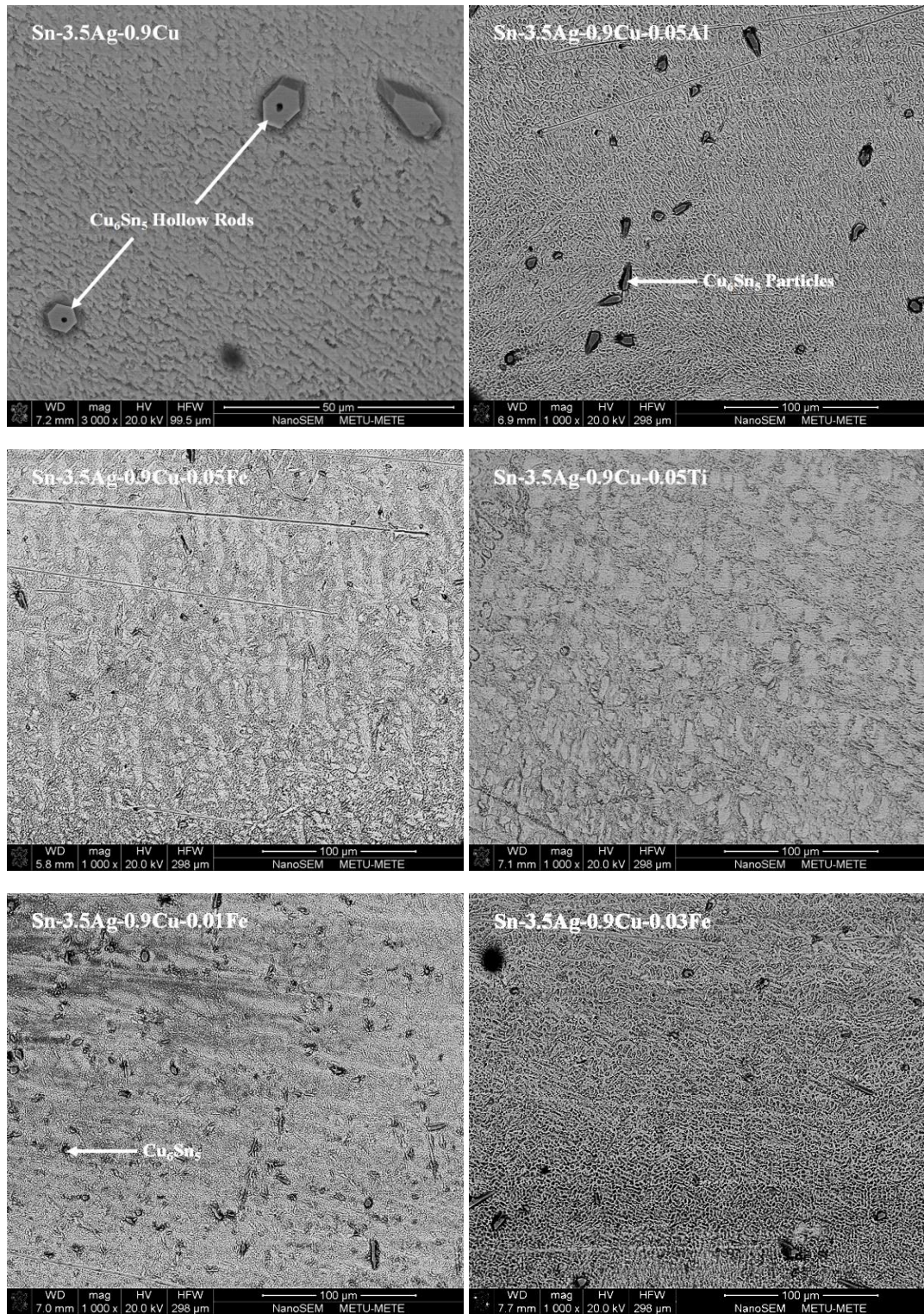
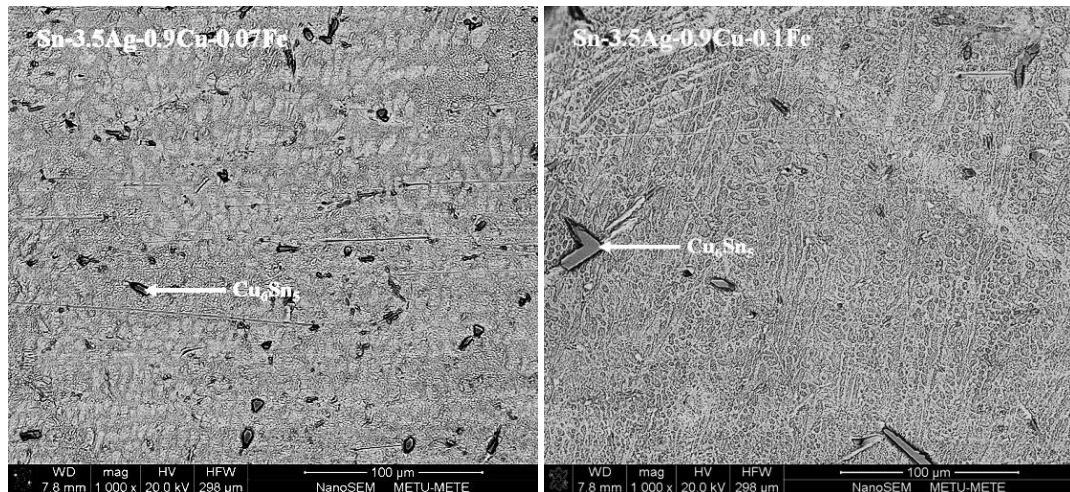**Figure 4.7.** Back-scattered SEM images of produced solders.

Figure 4.8. Back-scattered SEM images of produced solders (continued).

In summary, addition of Fe gives the lowest undercooling with the most desirable microstructure. Good dispersion of relatively small Cu_6Sn_5 IMCs was achieved. Previous studies **[65, 66]** have indicated the tendency of β-Sn nucleation on IMC. The addition of fourth element should retard the growth of any large IMC by acting as a potential heterogeneous nucleation sites for the nucleation of pro-eutectic Sn. Fe being the most suitable element to be substitutionally exist in Cu, it also behaves as the most effective additive in the alloy.

The interface between substrate and solder is important in the means of reliability of the solder joint which directly affects the operation performance of whole electronic device. The solder-copper interfaces of the alloys were shown in the **Figure 4.9**. Interface thickness was found to be slightly dependent on the compositions of the solder alloys; where, interface thickness is highest for eutectic SAC alloy. This may be explained by the undercooling of the alloys; which eutectic SAC alloy was found to have highest undercooling. Higher undercooling of the alloys enables the contact of copper substrate and the liquid solder for longer times. Since growth of interface is diffusion controlled process, high mobility of the atoms in liquid phase results with larger intermetallic compound between the substrate and the solder matrix. This is also explained in **Chapter 2.2**, where reflow soldered samples have considerably thicker interfaces than wave soldered samples, since these processes have different temperature profiles. In this case, although the cooling rates are exactly the same, undercooling values are significantly different. The undercooling
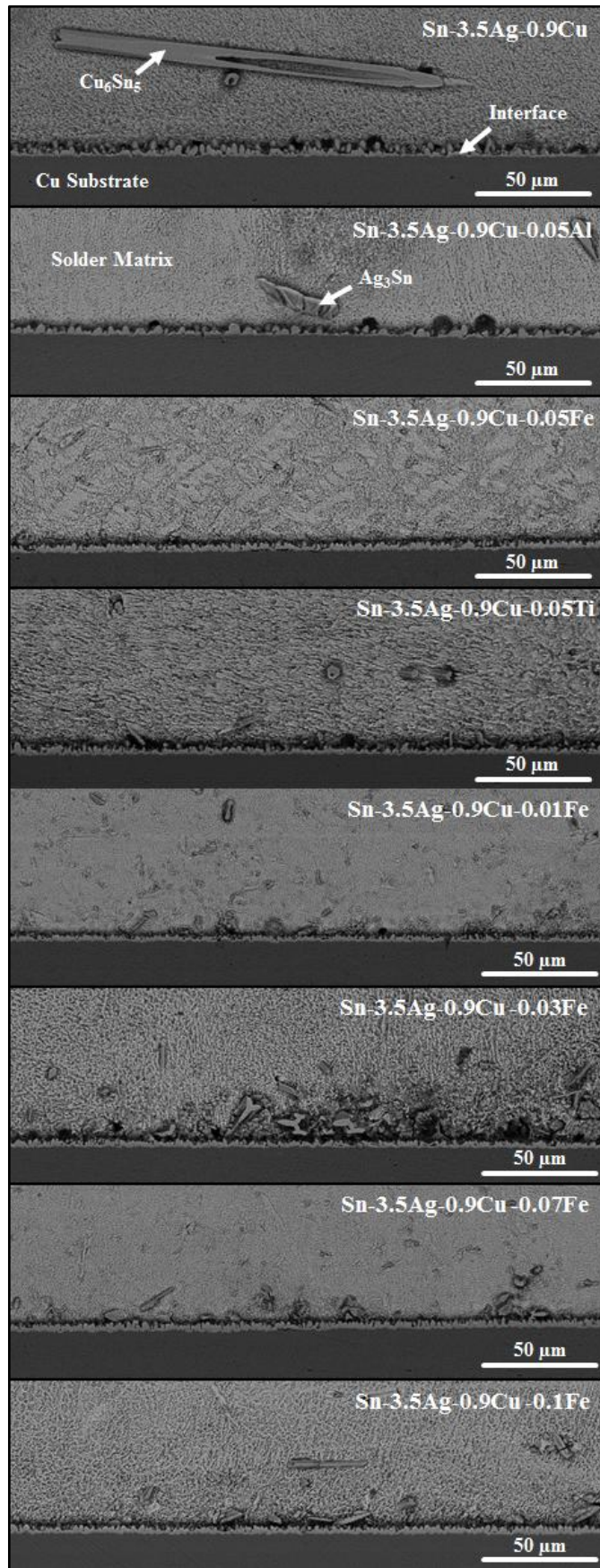
Figure 4.9. BSE images of substrate/interface/matrix of solder alloys.

of eutectic SAC alloy is 19 °C, while the undercooling of SAC+0.01Fe alloy is 7.2 °C. No direct relationship was found between Fe concentration and the interface thickness, which the undercoolings of Fe alloys are equal.

Significant microstructural observations are quantified in **Table 4.3**. The quantitative data derived here were calculated from at least 8 different area of interest. It should be noted that since microscopy is a 2-dimensional technique the measured numbers and dimensions of IMCs do not truly represent their real size, but only gives a rough estimate.

4.1.2. Effect of Cooling Rate on Microstructure

In addition to alloy composition, cooling rate of solder alloy affects the resultant microstructure, as well. Several soldering applications are performed under different cooling rates. For example surface mount and ball-grid arrays solders require 1.5 and 0.17 °C/sec of cooling rates, respectively.

X-ray mapping of Sn, Ag and Cu was done to determine the distribution of elements in matrix, interface and IMCs. **Figure 4.10** shows elemental map of the area in **Figure 4.11.a**. By looking at **Figure 4.10.a**, Sn can be said to have distributed homogenously in the matrix. The concentration of Sn of this alloy is 95.5 wt. %. However, Sn in the Ag_3Sn phase is only 26.8 wt. %. Therefore, Ag_3Sn plates were found to be darker regions in the Sn map, which means matrix is richer in Sn.
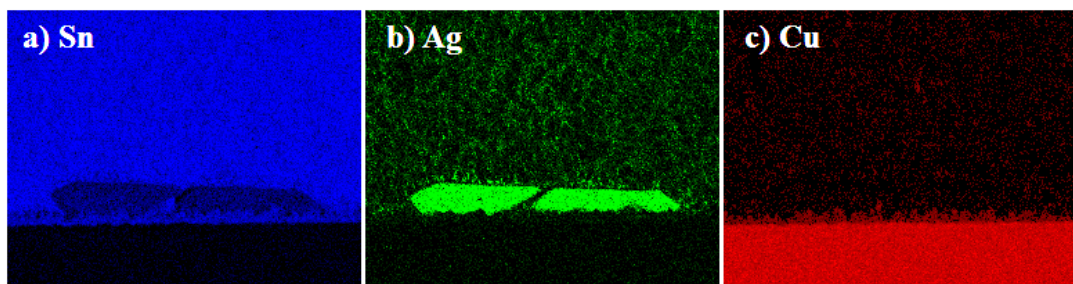

Figure 4.10. Elemental X-ray maps of a) Sn, b) Ag and c) Cu.

The map of Ag shown in **Figure 4.10.b** reveals that the β-Sn phase is poor in Ag, where dark regions in the matrix are β-Sn and green regions are ternary eutectic

phase. The Ag concentration of this alloy is 3.5 wt. %; where, Ag concentration of Ag_3Sn plates are 73.2 wt. %, therefore Ag_3Sn IMCs appears brightly green in the elemental map of Ag. Since substrate is pure Cu, it appears bright red as seen in **Figure 4.10.c**. The Cu concentration of this alloy is 0.9 wt. % and Cu concentration of Cu_6Sn_5 at the interface is 39.1 wt. %, therefore the interface appears brighter compared to matrix but darker compared to substrate.

In order to test the effects of cooling rates, SAC+0.01 and SAC+0.1Fe solders were solidified at 0.017 and 1.7°C/sec cooling rates. Microstructures of the solder joints were shown in **Figure 4.11** and **Figure 4.12**. Interface thickness of the solders cooled at 0.017 °C/sec is significantly higher than 1.7 °C/sec cooled solders. Dependence of interface thickness on composition is less on slow cooled solders. Large Ag_3Sn plates were seen on 0.017 °C/sec cooled SAC+0.01Fe, SAC+0.1Fe solders. Aspect ratio of the plates was found to be 4.5:1 and 5.5:1 for 0.017 °C/sec cooled SAC+0.01Fe and SAC+0.1Fe solders, respectively. Relatively small and dispersed Cu_6Sn_5 particles were observed for 1.7 °C/sec cooled SAC+0.1Fe solder. Therefore, alloy composition and cooling rate should be considered together to achieve the desired microstructure. The growth of Ag_3Sn nuclei are affected critically with the cooling rate, where slower cooling rates favors the growth of large Ag_3Sn plates. It is a well-known fact that undercooling is cooling rate dependent and increasing the cooling rate increases the amount of undercooling.

Attributing to previous solidification experiments, it is well accepted that the accessible undercooling can be increased by increasing the cooling rate. A good example is the bulk amorphous metallic systems where very large amount of undercooling is achieved by using rapid solidification techniques. The microstructural investigations suggest that by increasing the cooling rate, the formation of unwanted Ag_3Sn is suppressed. However, this might be seen contradicting with the previous results as the undercooling is increasing with cooling rate. This can be explained by classical solidification theory. At low undercoolings, the driving force for the non-faceted primary phases (i.e. pro-eutectic Sn) is lower and can be ignored. On the other hand, this is not quite true for faceted phases such as Ag_3Sn. The growth of the faceted phase can be easily triggered by any of the catalyst effect (such as the re-entrant angle). Actually, if the

BSE images in **Figure 4.11** are carefully investigated, it is seen that faceted Ag_3Sn phase grown near Cu_6Sn_5 interface. Most probably, Ag_3Sn nucleate on Cu_6Sn_5 by decreasing the surface energy and since the cooling rates are low it can easily grow to bulk facets by a diffusion process. When the cooling rate increases, undercooling also increases since diffusion is a time dependent process and β-Sn phase cannot nucleate heterogeneously on faceted IMCs, which can nucleate with small undercoolings.
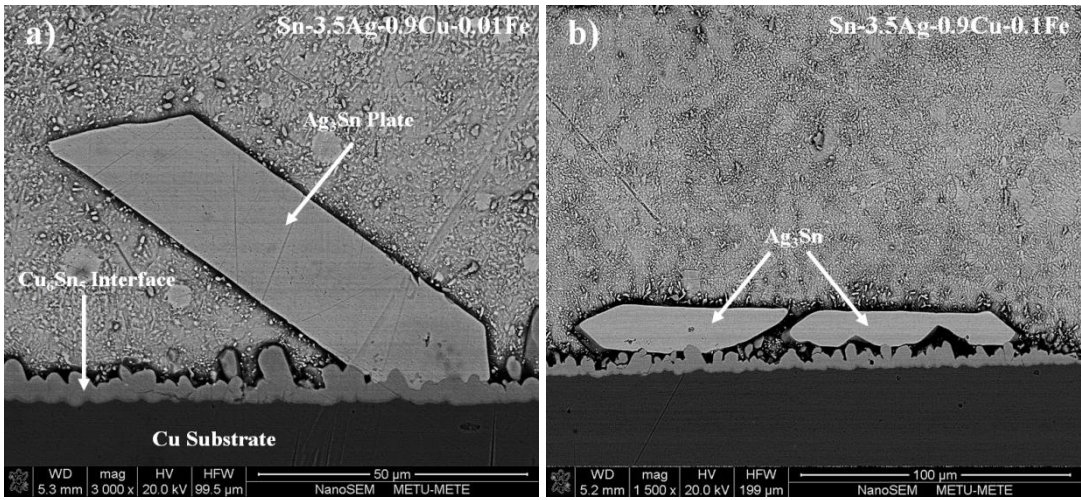

Figure 4.11. BSE images of solders cooled with 0.017 °C/sec.
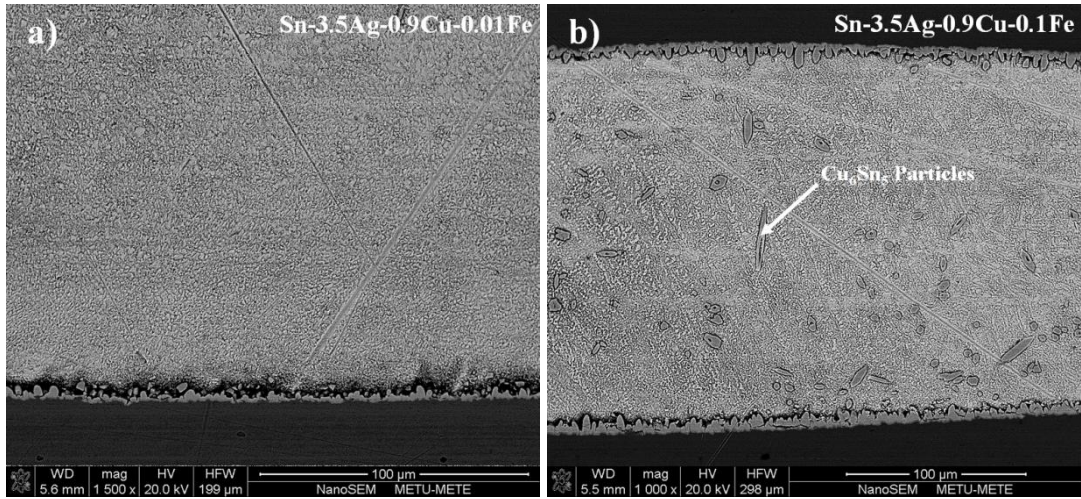

Figure 4.12. BSE images of solders cooled with 1.7 °C/sec.

At high cooling rates, the growth of large Ag_3Sn plates are suppressed, since formation of large IMC crystals are limited by the diffusion of the atoms. However, one of the major disadvantages of rapidly cooling the solder joints is the unwanted thermal stress and strain created between the substrate and the solder. Subsequent stress relieving annealing procedures may badly affect the electronic components on the circuit boards.

4.3. Mechanical Analysis

Mechanical properties of alloys were determined and compared by mainly two different test methods. Single-lap joint shear test was performed to determine the strength of the alloys that are subjected to shear type loading and micro-hardness test was applied to determine the hardness of the alloys. The results of those mechanical tests were reported below.

4.3.1. Single-Lap Joint Shear Test

All samples were failed in cohesive type of failure as shown in **Figure 4.13**, which also indicates that complete wetting of the lap surfaces and good adhesion of solder was achieved during reflow of the copper plates.
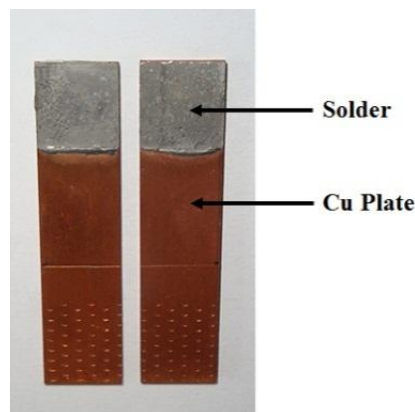

Figure 4.13. Cohesive type of failure after shear test.

Single-lap joint shear test was first performed on the solder alloys that are reported in **Figure 4.14**. Those alloys consist of:

- The lead-free solder alloys that were produced in the laboratory (eutectic, near eutectic; aluminum, iron and titanium modified) specimens
- A commercial lead free solder alloy (SAC 305).
- A commercial near-eutectic lead-tin solder alloy (Sn-40Pb)

In the first group of solders, shown in **Figure 4.14**, the eutectic SAC alloy and SAC+0.05Fe alloy has shear strengths very close to each other, which were measured as 28 and 29 MPa respectively. However, the addition of 0.05 wt. % Al has decreased the shear strength of the alloy to 20 MPa. This result was interpreted as a potential evidence of a microstructural evolution by the addition of Al. The shear strength of near-eutectic SAC alloy was measured as 25 MPa, which was measured as 41 MPa in an earlier study [57]. Similarly, the there is a great difference in shear strength of commercial SAC 305 alloy in this thesis research and an earlier study [57], which was found as 28 and 40 MPa, respectively. This difference is due to the different testing method that were used, where in this study shear strengths were measured with single-lap joint shear tests but asymmetric four points bend (AFPB) shear strength tests were done in the earlier study.
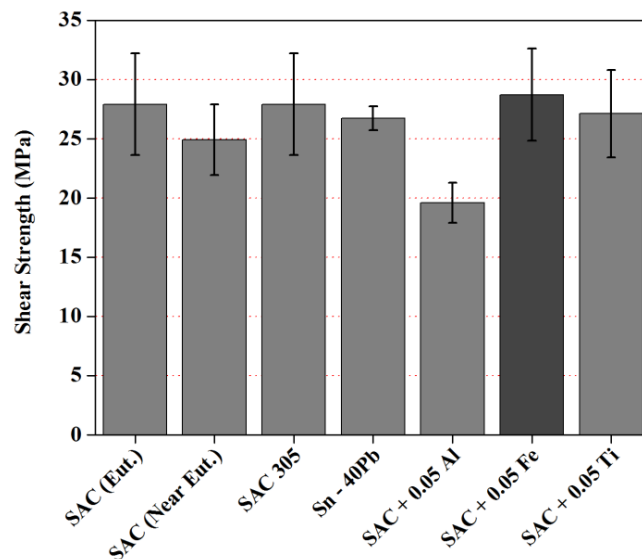

Figure 4.14. Shear strengths of first group alloys, SAC 305 and Sn-40Pb.

One important point to be underlined is the relatively high standard deviations in shear strength measurements. Both in the literature and in the current study, the

measured standard deviations are high because of the chaotic nature of the microstructure. If the standard Sn-40Pb with a high amount of eutectic is considered, one will notice the decrease in standard deviation. In some sense, this figure alone shows the importance to control the nucleation and growth of the unwanted IMC phases.

In the previous section, the crucial role of cooling rate has been determined by using Fe modified SAC alloys. The decrease in cooling rate decreases the corresponding undercooling while the driving force for the non-faceted phase growth becomes limited. The one for faceted phase can be increased by the presence of heterogeneous catalyst. For the shear test, relatively large amount of solder alloy was reflowed onto copper lap specimens. As compared to previous microstructural analysis, relatively low cooling rates are expected because of the increase in solder amount that were used. When the fracture surface was investigated after the test, the effect of cooling rate becomes apparent for Al addition. Although, no major changes were observed for other compositions, SAC+0.05Al solidifies to a new kind of IMC phase as shown in **Figure 4.15**.
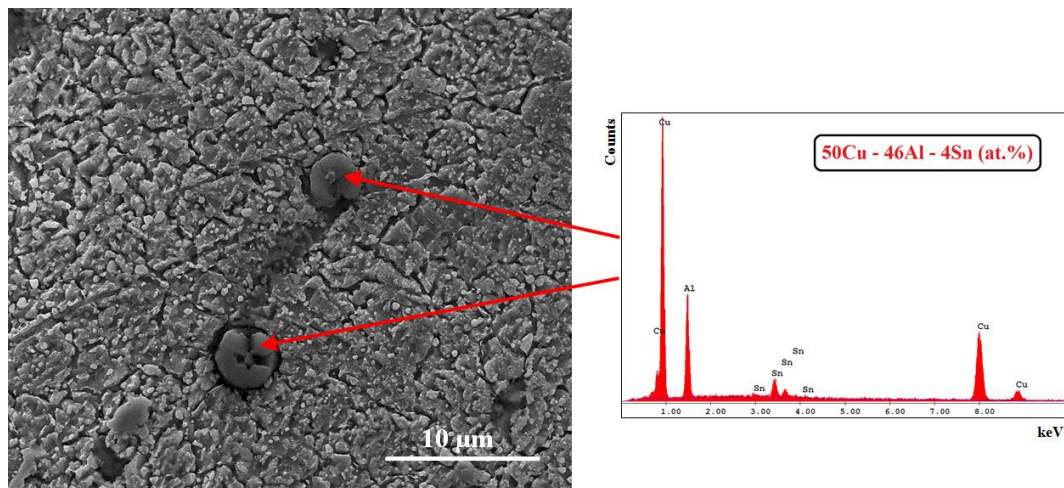

Figure 4.15. Back-scattered electron image of shear test specimen of SAC+0.05Al and EDS spectrum belonging to the phase shown.

The composition was determined to be 50Cu-46Al-4Sn (at. %) with EDS. The other effects of having such IMC can be seen in the results of shear tests. SAC+0.05Al has the lowest shear strength values. When standard deviations are considered, even

the strongest SAC+0.05Al sample is weaker than all the other composition. Remarkably, SAC+0.05Al composition having lower shear strength than eutectic SAC composition proves that, Al addition may affect the mechanical properties negatively by altering the microstructure in an undesired way.

The second group of shear test samples, which are all Fe modified samples, has shear strengths higher than the entire first group of solders. The results are shown in **Figure 4.16**, where shear strength of SAC+0.05Fe alloy is also included for the ease of comparison with the first group of solders. SAC+0.01Fe and SAC+0.07Fe solders was found to have the highest shear strengths, which are 36 and 34 MPa, respectively. It was also determined that, even the weakest Fe modified solder has higher shear strength than the eutectic, Al modified and Ti modified SAC solders. This result is consistent with the microstructural analysis, where SAC+0.01Fe and SAC+0.07Fe alloys have better dispersed IMC than the other solder alloys as seen in **Figure 4.7** and **Figure 4.8**. These compositions also have fine microstructure with wide eutectic regions. Some preferred orientation of β-Sn is observed SAC+0.05Fe alloy, which may result anisotropy of mechanical properties, which may be the reason of lower shear strength of this composition, compared to other Fe micro-alloyed samples as seen in **Figure 4.16**.
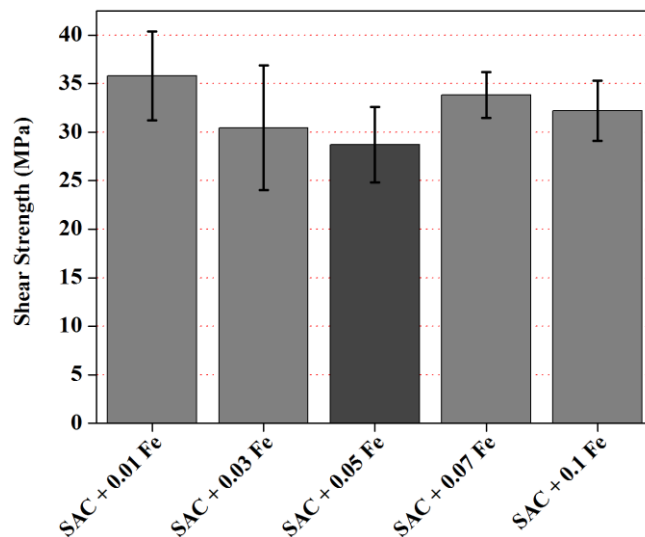

Figure 4.16. Shear strengths of second group alloys.

4.3.2. Hardness Test

The same alloy compositions that were tested and reported in the previous section were also tested for determination of their hardnesses. The results are shown in **Figure 4.17**.
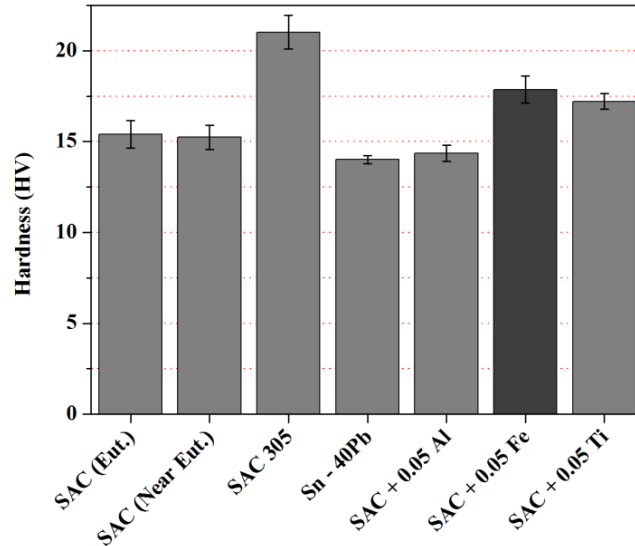

Figure 4.17. Hardnesses of first group alloys, SAC 305 and Sn-40Pb.

For micro-hardness measurements, special care has been taken, in order to collect the data from the matrix but not from any observable IMCs within the limitation of optical microscope (40 x magnifications). Therefore a high micro-Vickers hardness value should indicate a refined microstructure such as small pro-eutectic dendrites and finer eutectic structure. Among all of the specimens, commercial SAC305 alloy has shown the maximum harness values. This alloy contains less silver (3.0 wt. %) and less copper (0.5 wt. %) compared to other alloys. Therefore, it may be concluded that increasing silver and copper content decreases the hardness of the alloy after some concentration. The shear strength of SAC305 alloy was found to be nearly equal with the eutectic SAC alloy, however, hardness of the matrix is ~30 % higher compared to eutectic SAC. This difference in the hardness may be the sign of some detrimental structures formed in the bulk volume of SAC305 alloy, which may result stress concentration around these structures and reduce the shear strength of the alloy. 0.05Fe and 0.05Ti additions increased the hardness considerably, similar with the shear test results of these alloys as seen in **Figure 4.13**. It is

reasonable to expect such coherence in the results of shear test and hardness tests, since no large IMCs were observed in the microstructure of these alloys, which would cause a reduction in shear strength of these alloys, as discussed above.

Iron modified lead-free solder alloys that were referred in **Chapter 4.3** were also tested for the determination of their hardness. The results are shown in **Figure 4.18**.
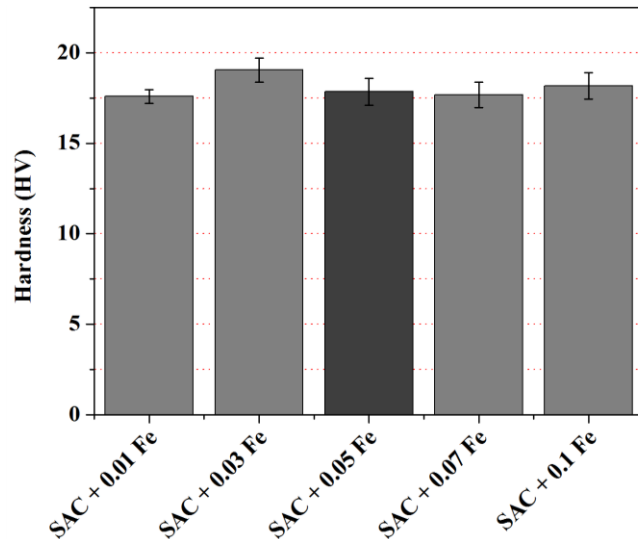

Figure 4.18. Hardnesses of second group alloys.

Hardnesses of the iron micro-alloyed samples are almost equal with similar standard deviations. SAC+0.03Fe alloy is slightly harder than others. Note that as discussed and shown earlier in **Figure 4.7**; this alloy has the finest β-Sn microstructure.

4.4. Wetting Analysis

Wetting was measured for different alloy compositions. It was applied by area and angle measurement as explained in **Chapter 3.5**. The wetting measurement results were given in **Table 4.5**. Wetting results of Sn-40Pb solder was also included for comparison.

There are many factors influencing the wettability of solder alloys. The most important parameters are the surface properties of the substrate and the alloy composition. In order to measure wetting angle, sophisticated technique can be

used; such as goniometer method, which involves deposit of a liquid droplet onto the sample surface with a vertically pointing syringe and capturing a high resolution image to measure the contact angle [89].

For this study by keeping the surface properties constant, change in alloy composition was monitored with corresponding wetting area and angle measurements. The lead-free alloys have wetting angles and areas close to each other. The maximum wetting is represented with higher wetting area and lower wetting angle. The maximum area was achieved by SAC+0.05Al and minimum wetting angle was achieved by SAC+0.05Al, SAC+0.05Ti, SAC+0.01Fe and SAC+0.03Fe.

Table 4.5. Average wetting areas and wetting angles of solders.

Sample Name	Average Area (mm^2)	Average Angle (Degrees)
SAC (Eutectic)	7.3	38.3
SAC (Near Eut.)	7.3	37.3
SAC 305	6.6	34.6
Sn – 40Pb	10.9	16.0
SAC + 0.05Al	7.9	35.9
SAC + 0.05 Fe	6.9	33.3
SAC + 0.05 Ti	7.4	29.5
SAC + 0.01 Fe	6.6	29.6
SAC + 0.03 Fe	7.2	32.6
SAC + 0.07 Fe	7.1	33.0
SAC + 0.1 Fe	7.0	30.0

The surface tension and higher viscosity of lead-free solders results in poor wetting as compared to conventional Sn-40Pb alloy. It should be noted that most of the micro-alloyed SAC solders result in decreased wetting angle by increasing the wetting area. This may be the outcome of the decrease in the undercooling. Since the freezing temperatures increase by fourth element addition, the relevant viscosity just before solidification decreases. This may result in smaller surface tension between the solder and the substrate.

4.5. Thermal Shock Analysis

Thermal shock resistances of the alloys were tested by two different methods. In the first method, the solders were applied onto copper pieces and polished surfaces of their cross-sections were prepared for microscopy analysis prior to the test. The second method includes the use of PBCs instead of copper pieces, where solder joints were subjected to realistic thermal loads during the test. Unlike the first method, the cross-sections of the solder joints were prepared after the test was completed. Results derived from these two methods are given below.

4.5.1. Solder-Copper Joint Thermal Shock Resistance Test

Thermal shock resistance test results were discussed on the SEM images that were taken every 500 cycles. Discussion was made on some selected cycles and the rest of the images were included in **Appendix B**.

SAC (Eutectic)

Figure 4.19.a shows the images taken after 500 cycles and it reveals that the dissociation between interface and matrix was started. The cracking was not observed after 1000 cycles, however as shown on **Figure 4.19.b**, the cracks are visible after 1500 cycles. The intermetallic at interface was almost detached.
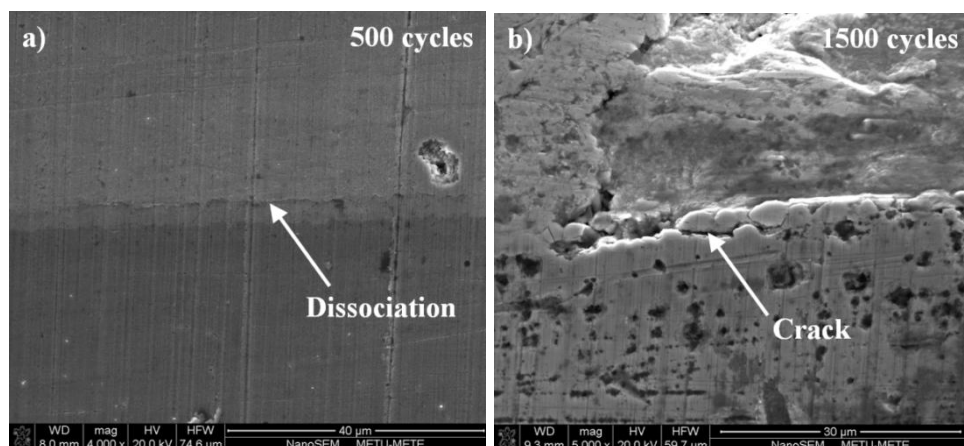

Figure 4.19. Eutectic SAC alloy after 500 and 1500 thermal shock cycles.

SAC (Near-Eutectic)

Figure 4.20.a shows the image taken at 500 cycles and it reveals that the dissociation between interface and matrix was started, similar to eutectic SAC alloy. However, in this alloy, the detachment of the interface was observed earlier, after 1000 cycles as seen on **Figure 4.20.b**. Mechanically, near-eutectic SAC alloy was found to be weaker compared to eutectic SAC alloy in the means of shear strength.
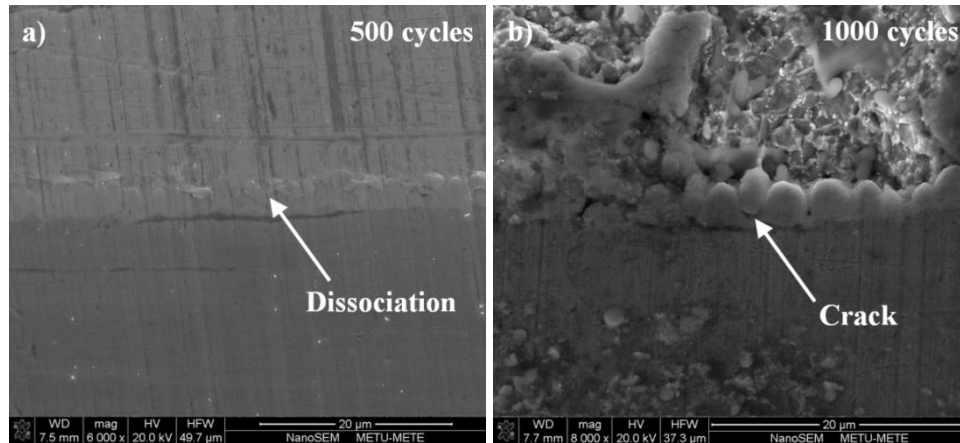

Figure 4.20. Near-Eutectic SAC alloy after 500 and 1000 thermal shock cycles.

SAC 305

Figure 4.21.a shows the image taken at 500 cycles and it shows that the interface was micro-cracked both on the substrate side and the matrix side. **Figure 4.21.b**, taken after 1500 cycles, shows that the cracks were propagated and the interface was almost dissociated.
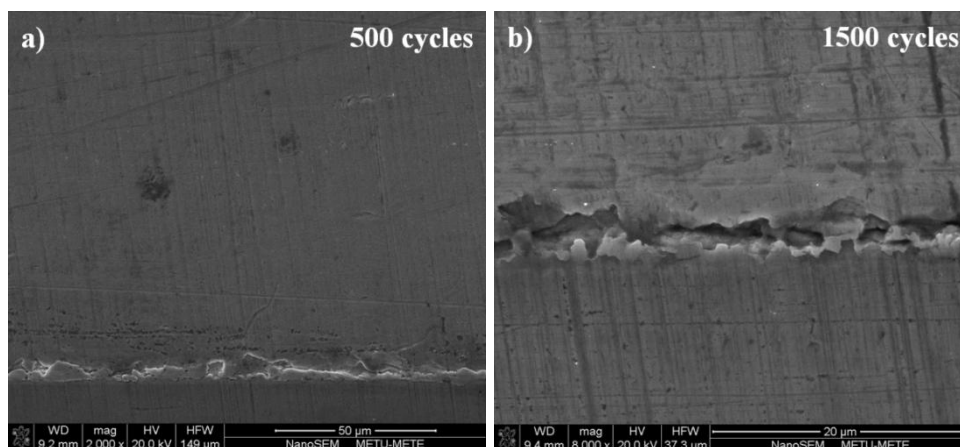

Figure 4.21. SAC305 alloy after 500 and 1500 thermal shock cycles.

SAC + 0.05Al

Figure 4.22 shows the image taken before thermal shock. It can be seen the interface is smooth with no irregularities. **Figure 4.22.b**, taken from the same region after 500 cycles shows that Cu near the interface started to dissociate. When images taken at higher magnifications were evaluated, no cracking was observed between the solder and the Cu substrate. As a result, this alloy may said to be thermal shock resistant among the other compositions.
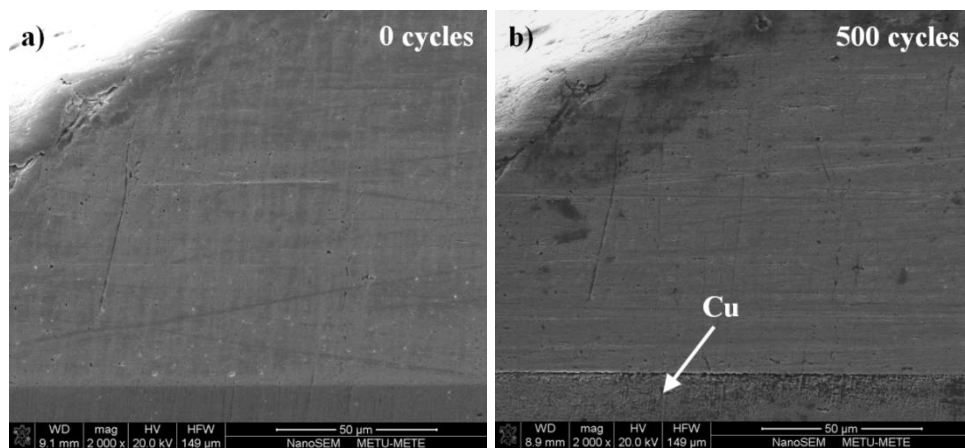

Figure 4.22. SAC+0.05Al alloy before test and after 500 thermal shock cycles.

SAC + 0.05 Ti

Figure 4.23.a shows the image taken before thermal shock. It can be seen the interface is smooth with no irregularities. No initiation of micro-cracks was observed after 500 cycles. However, as seen on **Figure 4.23.b**, after 1000 cycles, the detachment of interface scallop was observed very similar to the type of failure seen in near-eutectic SAC alloy on **Figure 4.20.b**. Both alloys were observed with the same type of cracking after same number of cycles although SAC+0.05Ti alloy has both higher shear strength and higher hardness.
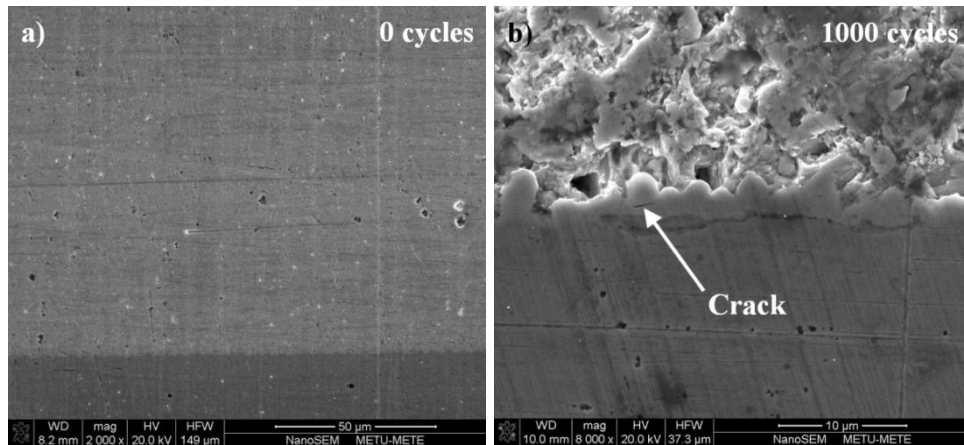
Figure 4.23. SAC+0.05Ti alloy before test and after 1000 thermal shock cycles.

SAC + 0.01Fe

Figure 4.24.a, shows the image taken before thermal shock. **Figure 4.24.b** shows the same region and the cracking at the interface is visible after 500 cycles. No further propagation of the crack was observed.

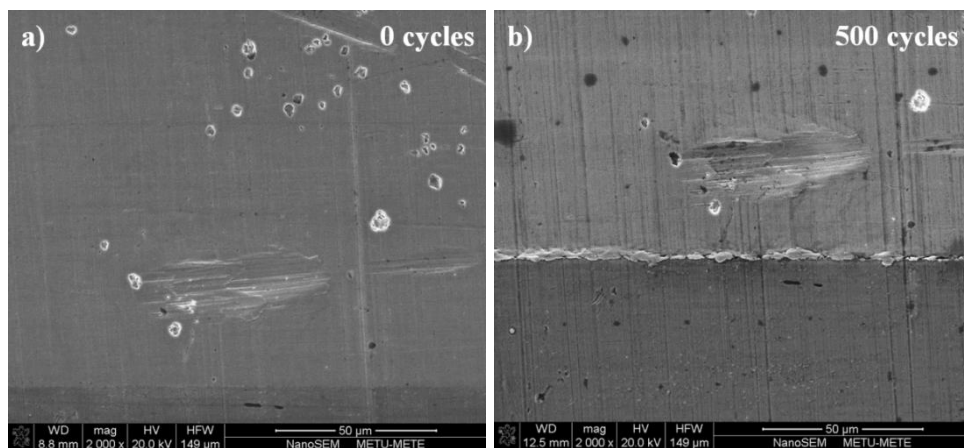**Figure 4.24.** SAC+0.01Fe alloy before test and after 500 thermal shock cycles.

SAC + 0.03Fe

Figure 4.25.a shows the visible cracks formed after 500 cycles at the tip of the solder. The cracks were determined to be propagated when **Figure 4.25.b**, taken after 1000 cycles were investigated. This is the hardest iron modified alloy. No further propagation was observed after 1500 cycles.
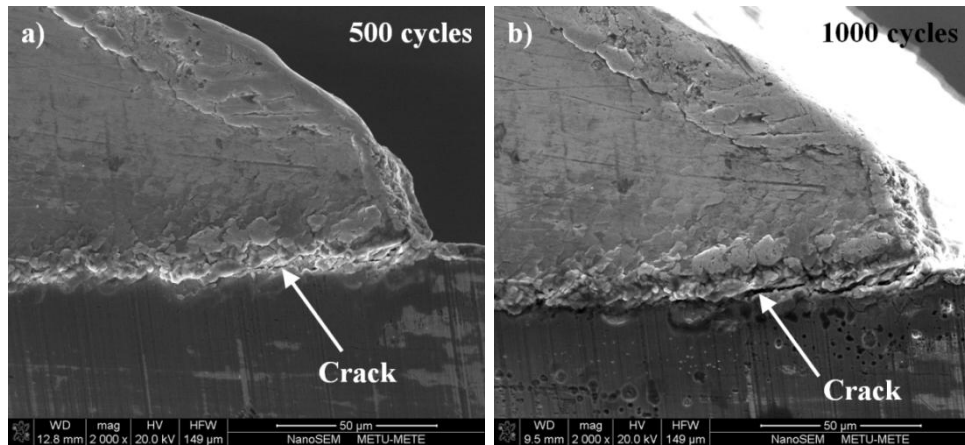
Figure 4.25. SAC+0.03Fe alloy after 500 and 1000 thermal shock cycles.

SAC + 0.05Fe

Figure 4.26.a, shows the image taken before thermal shock. No initiation of micro-cracks was observed after 500 cycles. However, as seen on **Figure 4.26.b**, after 1000 cycles, the detachment of interface scallop was observed very similar to the type of failure seen in near-eutectic SAC alloy on **Figure 4.20.b** and SAC+0.05 Ti alloy seen in **Figure 4.23.b**. All of these alloys were observed with the same type of cracking at the same number of cycles although SAC+0.05 Fe alloy has both higher shear strength and higher hardness.
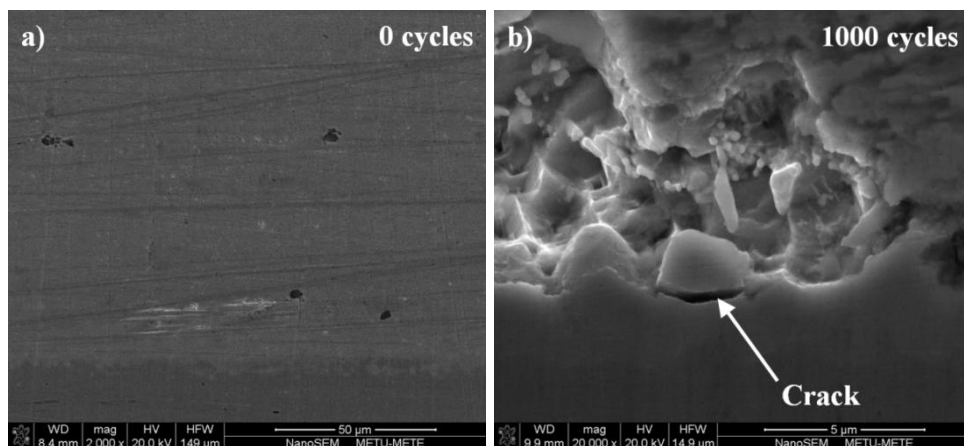

Figure 4.26. SAC+0.05Fe alloy before test and after 1000 thermal shock cycles.

SAC + 0.07Fe

Figure 4.27 shows the image taken before thermal shock. No crack initiation was observed at 500 cycles. However, micro-cracking of the matrix was observed at 1500 cycles as seen in **Figure 4.27**.
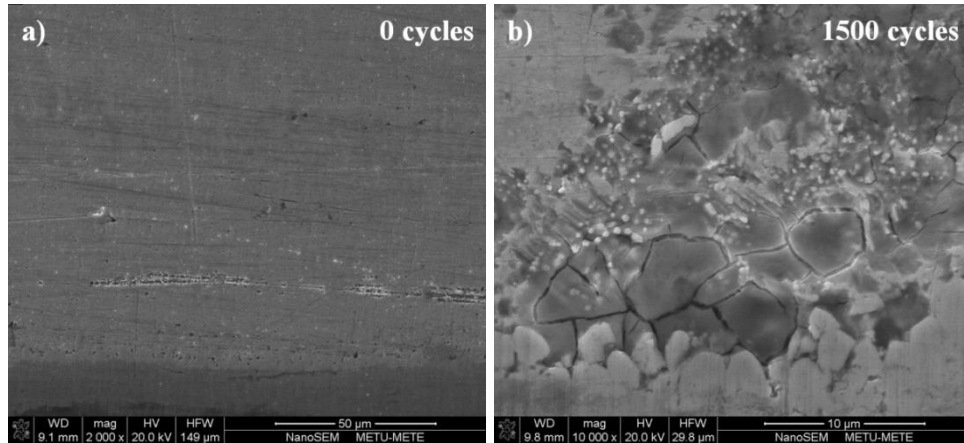

Figure 4.27. SAC+0.07Fe alloy before test and after 1500 thermal shock cycles.

SAC + 0.1Fe

Figure 4.28.a shows the visible cracks formed after 500 cycles at the interface and the matrix. There may be a critical iron concentration which, further iron addition may be causing the cracking of matrix, since this observed only in SAC+0.07Fe and SAC+0.1Fe alloys. The crack were observed to further propagate after 1000 cycles of thermal shock and shown in **Figure 4.28.b**, but no further propagation was determined after 1500 cycles.
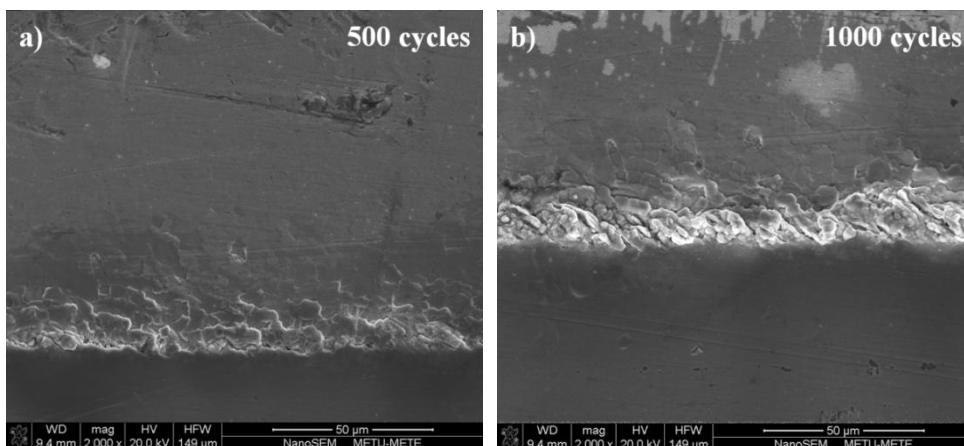

Figure 4.28. SAC+0.1Fe alloy after 500 and 1000 thermal shock cycles.

Table 4.6. The results of thermal shock resistance test.

Alloy	0 cycles	500 cycles	1000 cycles	1500 cycles	Result
SAC(Eutectic)	No Cracks	Initiation	-	Propagation	Failed
SAC (Near Eut.)	No Cracks	Initiation	Propagation	Propagation	Failed
SAC305	No Cracks	Initiation	Propagation	Propagation	Failed
SAC+0.05Al	No Cracks	-	-	-	Not Failed
SAC+0.05Ti	No Cracks	-	Initiation	Propagation	Failed
SAC+0.01Fe	No Cracks	Initiation	-	-	Failed
SAC+0.03Fe	No Cracks	Initiation	Propagation	-	Failed
SAC+0.05Fe	No Cracks	-	Initiation	Propagation	Failed
SAC+0.07Fe	No Cracks	-	-	Initiation	Failed
SAC+0.1Fe	No Cracks	Initiation	Propagation	-	Failed

As summarized in the **Table 4.6.**, for most of the tested lead-free solder alloys, crack initiation was observed even after 500 cycles of thermal shock. The only alloy that no micro-cracking was observed is SAC+0.05Al and this alloy comes out as the *thermal shock resistant* solder alloy at the testing conditions of this study, however depending on the testing conditions and further thermal shock cycles, different results may also be reached.

4.5.2. Performance Test on Printed Circuit Board

Soldering operation for this test was performed in collaboration with Arçelik using hand soldering technique which involves pin through hole application by a soldering iron. The reason why this technique was chosen is the disability of producing 500-600 kg of solder alloys for melting pots of wave soldering units in Arçelik facilities. Unlike other sophisticated soldering methods (namely reflow soldering and wave soldering) this method highly depends on the skills and experience of the person who is doing the soldering operation. Appliance of the heat to the solder and the solder flux at right amounts and positions is important. The joints prepared for this test was not prepared fully successful. Therefore, after thermal shock testing of the circuit boards, visual test of the joints gave no useful results.
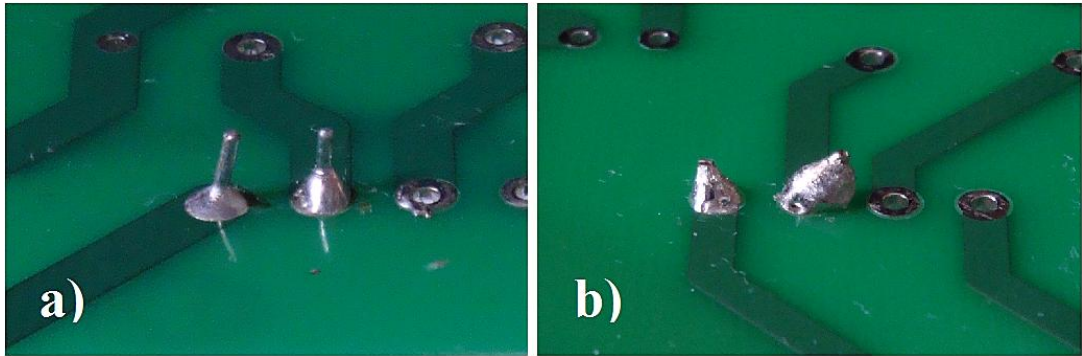
Figure 4.29. a) Good and **b)** bad examples of hand soldered joints produced by Arçelik.

On the other hand, some of the better joints were selected for microstructural analysis and cross-sections of the joints were prepared by metallographic preparation techniques. Microstructural analysis was done at two different regions on these samples. Those regions were labeled as **A** and **B** and positions of those regions on cross-sections of solder joints with different compositions were shown on **Figure 4.30** through **Figure 4.38**.

SAC (Eutectic)

Figure 4.31 and **Figure 4.32** show that the solidification routine of solder alloy on the real circuit boards is much more complicated. Two major interfaces of solder-substrate couples namely A and B, indicates different microstructures.

β-Sn grains are considerably larger at region B, this region may said to provide a slower cooling to the solder. At region A, the dendrites seem to have an orientation, which they grew parallel to each other (similar to directional solidification). The same orientation can be observed on both of the images taken after 100 and 400 cycles in **Figure 4.31** and **Figure 4.32**. As seen in **Figure 4.32**, after 400 cycles, the interface at B region was observed to have grown in the shape of irregular scallops. β-Sn grains seems to have grown and combined at both regions A and B.

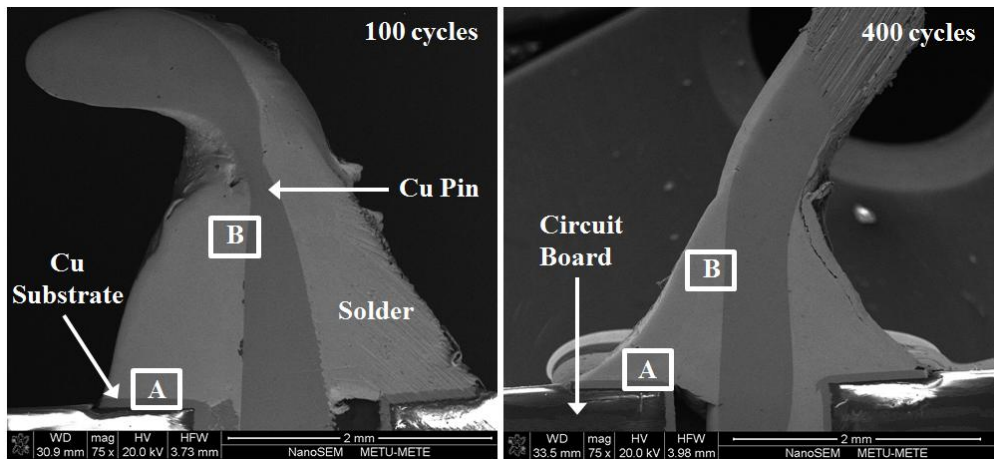**Figure 4.30.** Cross-sections of eutectic SAC solder joints.
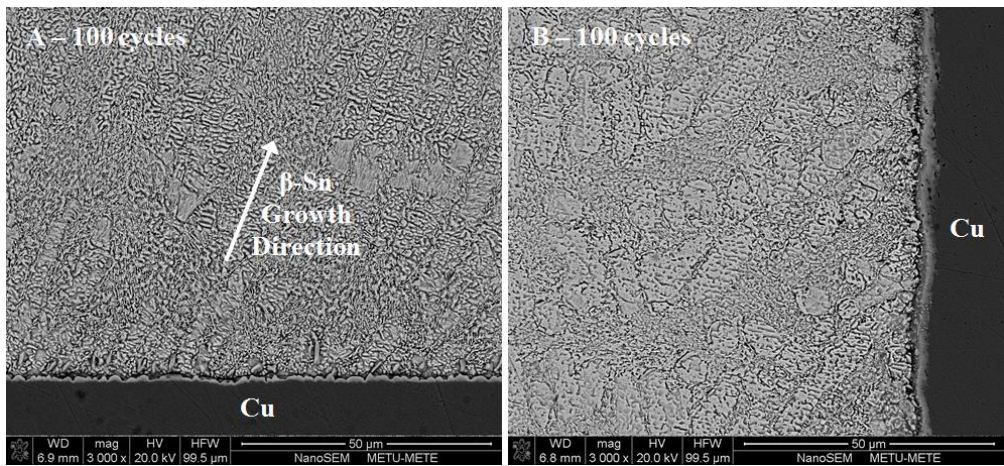

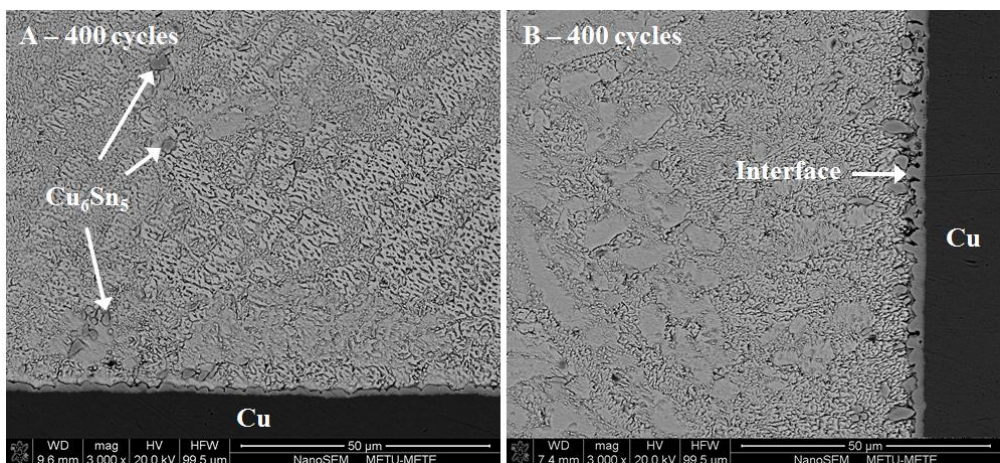**Figure 4.31.** BSE images of eutectic SAC solder joints after 100 cycles.

Figure 4.32. BSE images of eutectic SAC solder joints after 400 cycles.

SAC + 0.01Fe

The SEM images of SAC+0.01Fe joints after 100 and 400 thermal shocks are shown in **Figure 4.34** and **Figure 4.35**, respectively. This alloy was selected for thermal shock resistance test, since it appears to have the best mechanical properties in all tested alloys. It seems that large eutectic phase form at both of regions A and B. Some IMCs are visible in both of the regions after 100 and 400 cycles. Orientation of β-Sn grains is visible at region A after 400 cycles but it is not as visible as in the eutectic SAC alloy. No difference in the interface thickness was observed in region B as in eutectic SAC alloy. Region A has a larger, irregular interface after 100 cycles compared to after 400 cycles, which is not expected. This difference may be due to the soldering conditions of different samples.
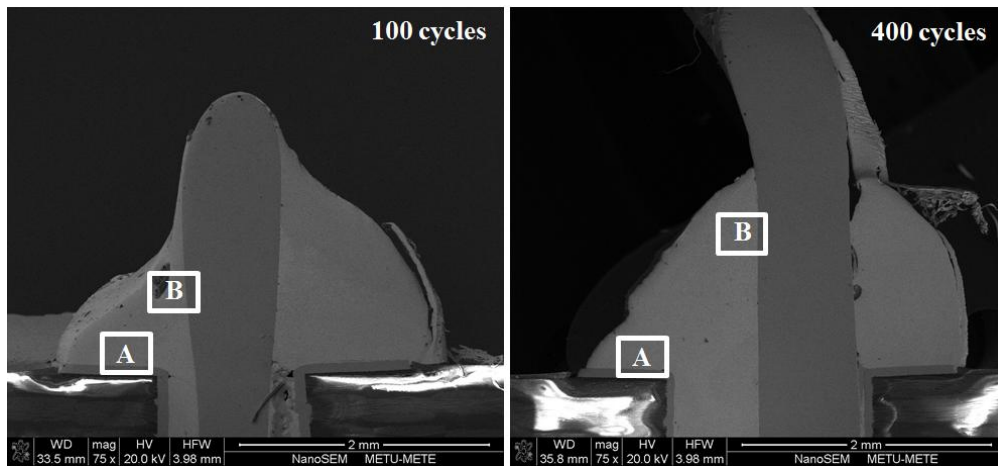

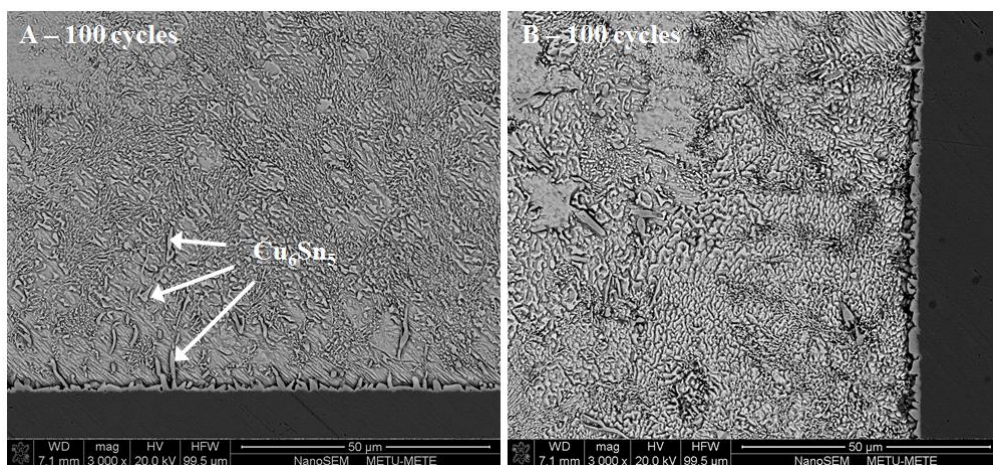**Figure 4.33.** Cross-sections of SAC+0.01Fe solder joints.

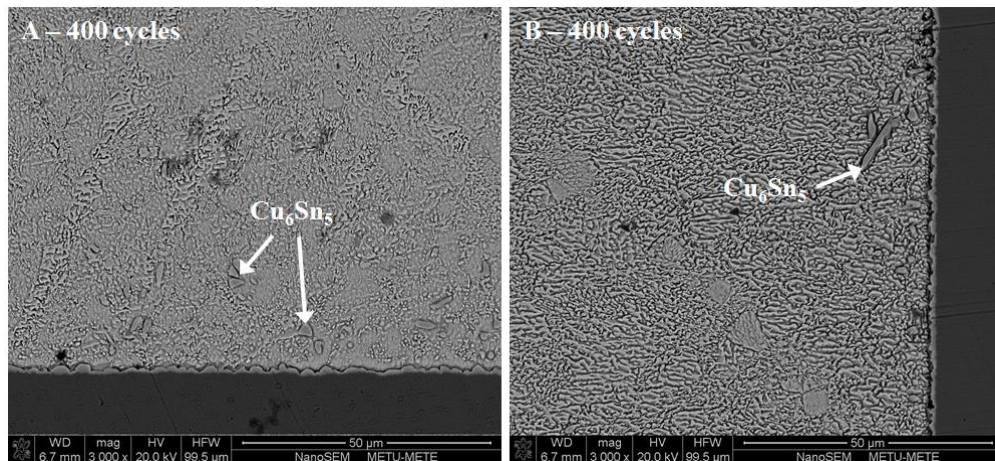**Figure 4.34.** BSE images of SAC+0.01Fe solder joints after 100 cycles.

Figure 4.35. BSE images of SAC+0.01Fe solder joints after 400 cycles.

SAC + 0.05Al

This alloy was selected for thermal shock resistance test, since it has the lowest shear strength and lowest hardness compared to other lead-free solders that were tested. A porous structure was determined on the samples, which were subjected to 100 cycles. The interface is very thin in both of the regions A and B. The microstructure of region A is highly eutectic with some β-Sn grains at the porous regions. However in regions B, very large β-Sn grains were observed, similar to other alloys. After 400 cycles, some large IMCs were observed in region B as seen in **Figure 4.38**. The IMCs were analyzed with EDS and it was found that they are Cu_6Sn_5. The dark spots in these IMCs were also analyzed and their compositions were found as 44Cu-28Sn-26Al (at. %). Actually this is an interesting result. In the previous sections it has been shown that SAC+0.05Al is the only composition to develop metastable Al rich IMC upon decreasing the cooling rate. In this set of experiment, relatively Al rich IMCs formed upon thermal cycling (in some sense annealing) and the faceted Cu_6Sn_5 nucleated on these IMC. Although it has not been observed within this study, the formation of such a phase may be problematic during real service of any electronic equipment by acting as a powerful heterogeneous catalyst.
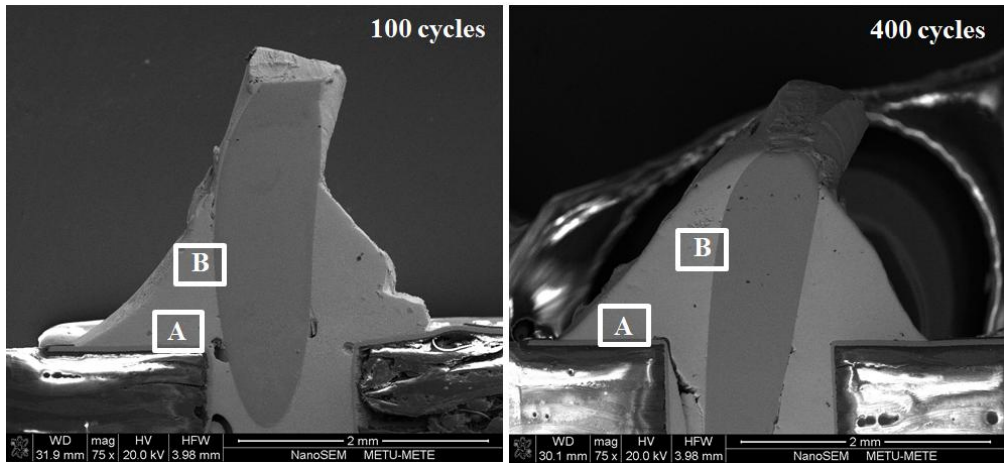
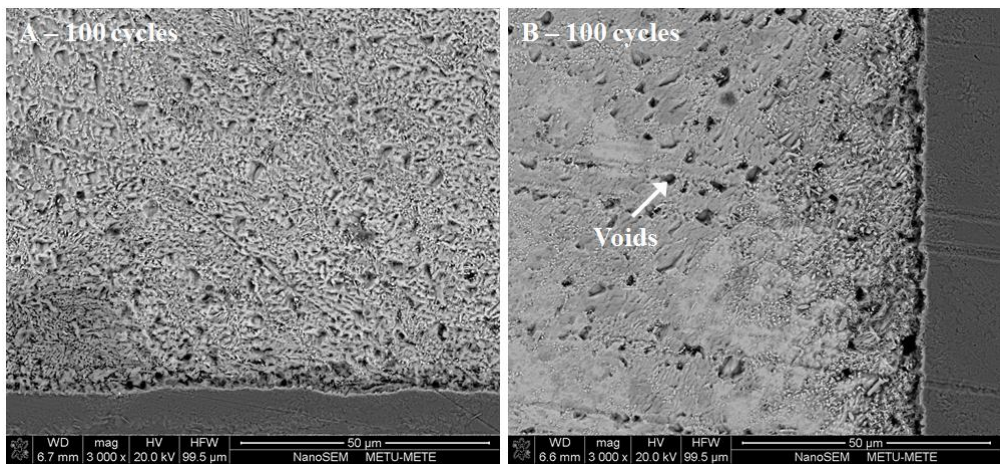**Figure 4.36.** Cross-sections of SAC+0.05Al solder joints.

Figure 4.37. BSE images of SAC+0.05Al solder joints after 100 cycles.
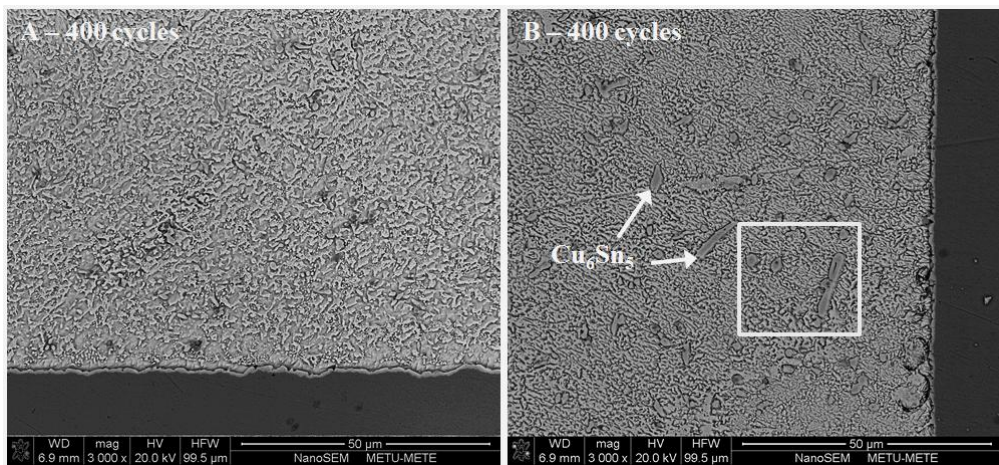
Figure 4.38. BSE images of SAC+0.05Al solder joints after 400 cycles. The region in the square is magnified in **Figure 4.36**.
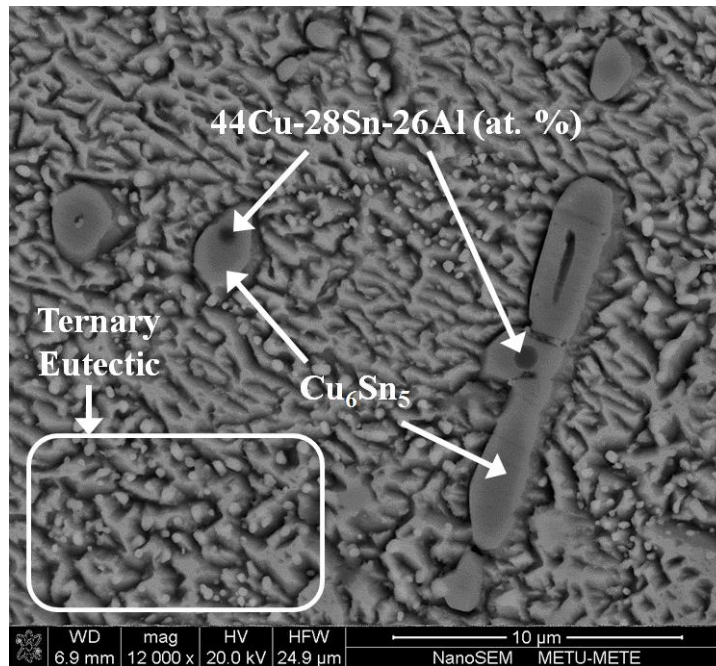
Figure 4.39. IMCs formed at region B.

Beside the formation of faceted IMC within the matrix, the cooling rate differences between region A and B may cause serious problems. One of the most common types of failure mechanisms seen in the wave soldered joints can be related to the microstructure difference created in region A and B (**Figure 4.30**, **Figure 4.33** and **Figure 4.36**). Since solidification starts from region A and B in this joint geometry, there will be a sudden change in the grain size when these zones intersect. Those zones were determined to intersect usually at the path shown in **Figure 4.37**. This result was supported with the SEM image shown in **Figure 4.38**, that was taken from top of the joint, which was may be cracked because of the applied thermal shocks.
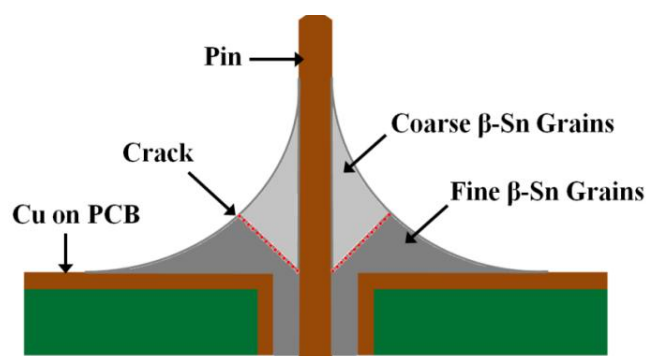
Figure 4.40. Schematic view of cross-section of a soldered pin on PCB.
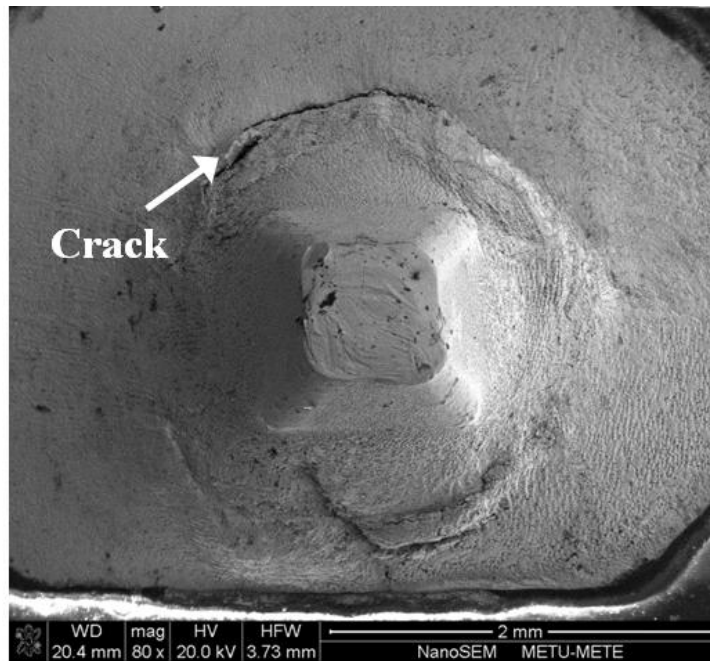
Figure 4.41. Secondary electron image of top view of a pin soldered with SAC 305 alloy.

This type of cracks is quite common in thermal shocked samples of joints, produced with wave soldering method. These macro-cracks are also visible to naked eye without the aid of a microscope. In **Figure 4.39**, cracks are shown on soldered pins of electronic components on a PCB. This type of failure is independent of alloy compositions. The remedy of the problem is related to the process parameters of soldering which is left out of the scope of the current study.
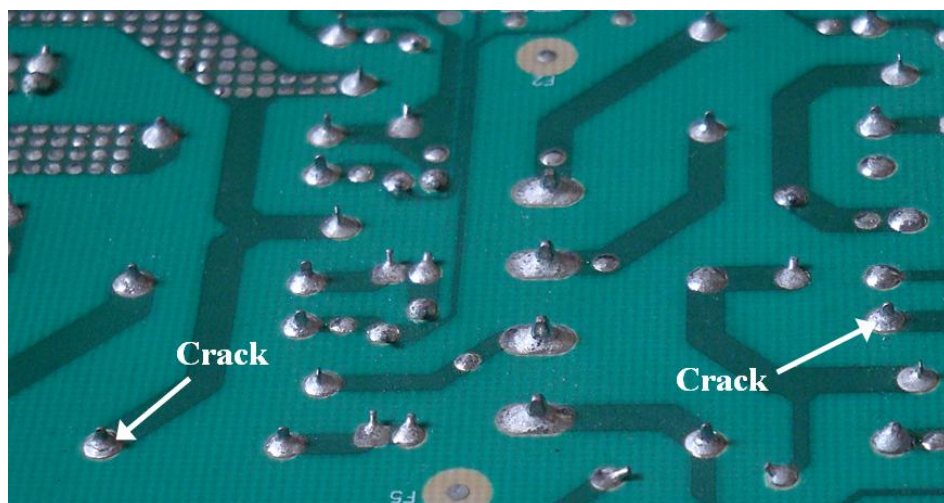
Figure 4.42. Visually detectable cracks as a result of thermal shock.

CHAPTER 5

CONCLUSION & FUTURE RECOMMENDATIONS

5.1. Conclusion

In this thesis study, the problems with existing lead-free solders were investigated and new lead-free alloy compositions were proposed to overcome those problems.

At the first stage of this study, micro alloying effect of *aluminum*, *iron* and *titanium* on the level achievable undercooling was investigated. Among all the alloys, Fe added ones resulted in the smallest undercoolings. This was a desirable effect and it was resulted in an improvement of microstructure for Fe micro-alloyed specimens.

The second stage of the study was mainly focusing on determination of the *Iron* concentration that should be added to create the *better* improvement in the means of all performance and reliability related properties. Lowest volume of IMC and finer microstructure was achieved with SAC+Fe alloys. In terms of shear and hardness tests SAC+0.01Fe and SAC+0.07Fe alloys gave better results. Having the lowest shear strength and hardness in all of the tested alloys, *Aluminum* addition was found to make no practical improvements under the testing conditions of this research.

Titanium addition also made some positive effects on microstructure, mechanical properties and thermal properties, but those improvements were found to be less effective compared to improvements created by *Iron* addition. Moreover, when the costs of *Titanium* and *Iron* are compared, *Titanium* addition seems to be a less practical solution.

In terms of thermal shock induced crack propagation SAC+0.05Al, SAC+0.01Fe and SAC+0.07Fe gave best results. In collaboration with Arçelik, some of the selected solder alloys were applied onto commercial PCBs and subjected to shock cycles. The microstructural analysis indicated the cracking of solders, applied on

PCBs, are mainly originate from different cooling rates acting on different regions (i.e. near substrate and near pin of electronic component) of the solder joints. This may create microstructures with different β-Sn grain size and because of the applied thermal shock cycles, the cracking may occur at the transition zone of fine to coarse grain size.

As a result of microstructural, mechanical and thermal tests; **SAC+0.01Fe** and **SAC+0.07Fe** alloys were found to be the best candidates to be used as a reliable solder for electronics industry.

All the properties of the produced lead-free solders were also compared with a commercially available, traditional near-eutectic tin-lead (Sn-40Pb) solder. While mechanical properties and thermal shock resistance of the lead-free solders are better than Sn-Pb solder, the wetting of Sn-Pb solder was found to be undisputedly higher than all the lead-free solder.

5.2. Future Recommendations

This thesis study was focused on Sn-Ag-Cu (SAC) based lead-free solders. Silver (Ag) is a precious metal with increasing price, which 1 troy ounce (~31.1 grams) of silver's price has increased from 4.60 USD to 32.58 USD in the last 10 years. All the solders that were produced for this research contain at least 3.5 wt. % silver. When scale of industrial production is considered, this small amount of silver would gain importance in reducing the cost of solder alloy. Therefore, a new, Sn based, silver-free solder may be investigated for electronics industry.

Thermal shock performance test on PCB did not give the expected results, since hand soldering was used while preparing the samples. Joints may be prepared with other soldering techniques such as reflow soldering or wave soldering. However, both of these methods require sophisticated equipment for the production and forming of alloys in the laboratory scale. For reflow soldering, solder alloys should be in the form of nanometer/micron sized powder. This powder is then mixed homogenously with a viscous, liquid solder paste prior to the reflow operation. The other method, namely as wave soldering, requires a molten solder bath and some automated parts for the dipping of bottom of PCB into the molten solder wave,

which the wave should be created with the help of pumps. In the industrial scale, wave soldering machines require at least 600 kg of solder alloy for their operation. In the laboratory scale, this machine may be built to operate with as low as a few kilograms of solder. Future studies may contain the fabrication of SAC solder joints by using such devices.

In this thesis study, solder-copper joint thermal shock resistance test, which was discussed in **Chapter 4.5**, was performed on reflow soldered copper pieces. In thermal shock resistance test, the mechanical loads created due to mismatch of the components attached to each other. In a real electronic system, the mismatch between PCB, electronic component and the solder is higher compared to mismatch between copper chip and solder used in this study. Therefore, small PCB pieces and some electrical component may be soldered and tested for the determination of thermal shock resistance of produced solders.

Single-lap joint shear test was one of the methods used for mechanical testing of the alloys in this study. All shear tests were done at room temperature. However, in electronic systems, the operation temperatures are commonly above or below room temperature, depending on purpose and environmental conditions of device's use. Thus, testing the solders below and above room temperature would provide valuable data for development of new and better solder alloys for specific purposes. Moreover, tensile tests can be included to determine the yield and tensile strength of the novel lead-free alloys.

Soldering flux plays an important role on wetting and reliability of solder alloys. However, the effect of flux type was not investigated in this study. A new flux composition may be needed for a new solder alloy since chemical consistency of solder and flux is necessary. A research project may be carried out in collaboration with chemical engineering department for the development of a new flux composition.

REFERENCES

[1]   Resmi Gazete, 30.05.2008, http://www.resmigazete.gov.tr/eskiler/2008/05/ 20080530-3.htm (Last Visited on: 06.11.2012).

[2]   IPC Market Research Services, Global Consumption of Tin/Lead Versus Lead Free Solder, IPC, Quarterly Survey (2011).

[3]   Wikipedia, 2012, "Welding", http://en.wikipedia.org/wiki/Welding (Last Visited on: 17.11.2012).

[4]   Manko H.H., Solder and Soldering, 2nd Edition, McGraw-Hill, New York, (2001).

[5]   Shabtay Y.L., Ainali M., Lea A., New Brazing Processes Using Anneal-Resistant Copper And Brass Alloys, Materials and Design 25 (2004) 83–89.

[6]   Abtew M., Selvaduray G., Lead-Free Solders in Microelectronics, Materials Science and Engineering 27 (2000) 95-141.

[7]   Harrison M.R., Vincent J.H., Steen H.A.H., Lead-Free Reflow Soldering for Electronics Assembly, Soldering & Surface Mount Technology 13/3 (2001) 21-38.

[8]   Suganuma K., Advances in Lead-Free Electronics Soldering, Current Opinion in Solid State and Materials Science 5 (2001) 55-64.

[9]   Ulrich R.K., Advanced Electronic Packaging 2nd Edition, John Wiley & Sons, (2006).

[10]   Sundelin J.J., Nurmi S.T., Lepistö T.K., Ristolainen E.O., Mechanical and Microstructural Properties of SnAgCu Solder Joints, Materials Science and Engineering A, 420 (2006) 55-62.

[11]   Walleser J.K., Microstructure Control of The Tin-Silver-Copper-X Solder Alloy System Through Nucleation Catalysis of Tin, M.Sc. Thesis, Materials Science and Engineering, Iowa State University (2008).

[12]   Arulvanan P., Zhaowei Z., Shi X., Effects of Process Conditions on Reliability, Microstructure Evolution and Failure Modes of SnAgCu Solder Joints, Microelectronics Reliability, 46 (2006) 432-439.

[13] Zeng K., Tu K.N., Six Cases of Reliability Study on Pb-Free Solder Joints in Electronic Packaging Technology, Materials Science and Engineering R 38 (2002) 55-105.

[14] Tu K.N., Gusak A.M., Li M., Physics and Materials Challenges for Lead-Free Solders, Journal of Applied Physics 93/3 (2003) 1335-1353.

[15] Kim H.K., Liou H.K., Tu K.N., Morphology of Instability of the Wetting Tips of Eutectic SnBi, Eutectic SnPb and Pure Sn on Cu, Journal of Materials Research 10 (3) (1995) 497-504.

[16] Karakaya I., Thompson W.T., Bulletin of Alloy Phase Diagrams 9 (1988) 144-152.

[17] Wood E.P., K.L. Nimmo., In Search of New Lead-Free Electronics Solder, Journal of Electronic Materials 23 (8) (1994) 709-713.

[18] Monsalve E.R., Lead Ingestion hazard in Hand Soldering Environments, in Proceedings of the 8th Annual Soldering Technology and Product Assurance Seminar, Naval Weapons Center, China Lake, CA (1984).

[19] Napp D., Lead-Free Interconnect Materials for the Electronics Industry, in: Proceedings of the 27th International SAMPE Technical Conference, Albuquerque, NM, (1995) p.342.

[20] Nimmo K., Review of Current Issues in Lead-Free Soldering, Proceedings of the Surface Mount International Conference, San Jose, CA (1997) 467-475.

[21] Karakaya I., Thompson W.T., Bulletin of Alloy Phase Diagrams 8 (1987) 340-347.

[22] Puttlitz K.J., Stalter K.A., Handbook of Lead-Free Solder Technology for Microelectronic Assemblies, CRC Press (2004) p. 541.

[23] Harper C.A., Electronic Materials and Processes Handbook, McGraw-Hill (2003) pp. 5–8.

[24] Kapp Alloy and Wire Inc., "Tin-Zinc Solders for Aluminum to Aluminum and Copper", http://www.kappalloy.com/tin-zinc-solder.php (Last Visited on: 07.11.2012).

[25] Prasad R.P., Surface Mount Technology: Principles and Practice, Springer-Verlag GmbH (1997) p. 385.

[26] SmartTec GmbH, "Alloy Information", http://www.smarttec.de/download/Legierungs-Info.pdf (Last Visited on: 07.11.2012).

[27] Indium Corporation, "Gold Solders", http://www.indium.com/solders/gold/ (Last Visited on: 07.11.2012).

[28] Indium Corporation, "Bismuth Alloys", http://www.indium.com/solders/bismuth/alloys/ (Last Visited on: 07.11.2012).

[29] Indium Corporation, "Indium Wire", http://www.indium.com/solders/wire/indium-wire/ (Last Visited on: 07.11.2012).

[30] Minges, M.L., Electronic Materials Handbook: Packaging, ASM International (1989) p. 758.

[31] Glazer J., Metallurgy of Low Temperature Pb-Free Solders for Electronic Assembly, International Materials Reviews, 40 (2) (1995) 65-93.

[32] Hua F., Glazer J., Lead-Free Solders for Electronic Assembly: Design & Reliability of Solders and Solder Interconnections, Proceedings of a TMS Symposium, ed. R. K. Mahidhara et al.., Orlando, Fl. (1997) pp. 65-73.

[33] Artaki I., Finley D.W., Jackson A.M., Ray U., Vianco P.T., Wave Soldering with Lead-Free Solders, Proceedings of the Technical Program on Advanced Electronics Manufacturing Technologies, SMI Surface Mount International, San Jose, CA (1995) 495-510.

[34] Lee N.C., Slattery J., Sovinsky J., Artaki I., Vianco P., A Novel Lead-Free Replacement, Circuits Assembly 6 (10) (1995) 34-44.

[35] Jackson A.M., Vianco P.T., Artaki I., Manufacturing Feasibility of Several Lead-Free Solders with Electronic Assembly, Proceedings of the 7th International SAMPE Electronics Conference, Parsippany, NJ, (1994) 381-391.

[36] McCormac M., Jin S., Progress in the Design of New Lead-Free Solder Alloys, Journal of Materials 45 (7) (1993) 36-40.

[37] Knorr D.B., Felton L.E., Designing Lead-Free Solder Alloys for Advanced Electronics Assembly, Proceedings of the Design for Manufacturability Conference, New York (1994) 27-34.

[38] Ames Laboratory, "Alternatives to Lead-Based Solders", https://www.ameslab.gov/files/LeadFreeSolder_Foundation.pdf (Last Visited on: 07.11.2012).

[39] Anderson I.E., Sn-Ag-Cu: A Lead Free Solder For Board Applications, Proceedings of the NEPCON, Anaheim, CA, (1996) 882-887.

[40] Miller C.M., Anderson I.E., Smith J.F., A Viable SnPb Solder Substitute: Sn-Ag-Cu, Journal of Electronic Materials 23 (7) (1994) 595-601.

[41] Kariya Y., Otsuka M., Mechanical Fatigue Characteristics of Sn-3.5Ag-X solder alloys, Journal of Electronic Materials 27 (11) (1998) 1229-1235.

[42] Frear D.R., The Mechanical Behavior of Interconnect Materials for Electronic Packaging, JOM 48 (5) (1996) 49-53.

[43] Moon K.W. et al., Experimental Thermodynamic Assessment of Sn-Ag-Cu Solder Alloys, Journal of Electronic Materials 29 (10) (2000) p. 1122.

[44] Loomans M.E. Fine M.E., Metallurgical and Materials Transactions A, Physical Metallurgy and Materials Science 31A (4) (2000) p. 1155.

[45] Moon K.-W., Boettinger W. J., Kattner U. R., Biancaniello F. S., Handwerker C. A., Journal of Electronic Materials 29 (2000) 1122–1136.

[46] Ye L.L., Lai Z., Liu J., Tholen A., Microstructural Coarsening of Lead-Free Solder Joints During Thermal Cycling, Proceedings of Electronic Components and Technology Conference, Las Vegas (2000) p. 134.

[47] Wu C.M.L., Wong Y.W., Lead-Free Electronic Solders, Springer US (2007) 77-91.

[48] National Electronics Manufacturing Initiatives (NEMI), Lead-Free Assembly Projects (1999).

[49] Japan Electronics and Information Technology Industries Association (JEITA), Roadmap 2002 for Commercialization of Lead-Free Solder (2002).

[50] Wang. F.-J., Gao F., Ma X., Qian Y.-Y., Depressing Effect of 0.2wt.%Zn Addition, Journal of Electronic Materials 35 (10) (2006) 1818-1824.

[51] Kang. S.K. et al., Ag_3Sn Plate Formation in the Solidification of Near-Ternary Eutectic Sn-Ag-Cu, JOM 55(6) (2003) 61-65.

[52] Harris P.G., Chaggar K.S., The Role of Intermetallic Compounds in Lead-Free Soldering, Soldering and Surface Mount Technology 10 (3) (1998) 38-52.

[53] Kang. S.K. et al., Controlling Ag_3Sn plate formation in near-ternary-eutectic Sn-Ag-Cu solder by minor Zn alloying, JOM 55(6) (2003) 34-38.

[54] Kang. S.K. et al., Microstructure and mechanical properties of lead-free solders and solder joints used in microelectronic applications, IBM Journal of Res.& Dev. 49 (4/5) (2005) 607-620.

[55] Kim K.S., Huh S.H., Suganuma K., Effects of Cooling Speed on Microstructure and Tensile Properties of Sn–Ag–Cu Alloys, Materials Science and Engineering A 333 (2002) 106-114.

[56] Frear D.R., Jang J.W., Lin J.K., Zhang C., Pb-Free Solders for Flip Chip Interconnects, JOM 53 (6) (2001) 28-33.

[57] Anderson I.E., Cook B.A., Harringa J., Terpstra R.L., Microstructural Modifications and Properties of Sn-Ag-Cu Solder Joints Induced by Alloying, Journal of Electronic Materials 31 (2002) 1166-1174.

[58] Kim K.S., Huh S.H., Suganuma K., Effects of Intermetallic Compounds on Properties of Sn-Ag-Cu Lead-Free Soldered Joints, Journal of Alloys and Compounds 352 (2003) 226-236.

[59] Anderson I.E., Development of Sn-Ag-Cu and Sn-Ag-Cu-X Alloys for Pb-Free Electronic Solder Applications, Journal of Materials Science: Materials in Electronics 18 (2007) 55-76.

[60] Anderson I.E., Harringa J.L., Journal of Electronic Materials 33 (2004) 1485-1496.

[61] Hume-Rothery W., Powell H.M., Z. Kristallographie 91 (1935) 23.

[62] Wikipedia, 2012, "Hume-Rothery Rules", http://en.wikipedia.org/wiki/Hume-Rothery_rules (Last Visited on: 09.11.2012).

[63] Darken L.S., Gurry R.W., Physical Chemistry of Metals, McGraw-Hill, New York, (1953).

[64] Anderson I.E., Harringa J.L., Suppression of Void Coalescence in Thermal Aging of Tin-Silver-Copper-X Solder Joints, Journal of Electronic Materials 35 (1) (2004) 1-13.

[65] Kim K.S., Huh S.H., Suganuma K., Effects of Fourth Alloying Additive on Microstructures and Tensile Properties of Sn-Ag-Cu Alloy and Joints with Cu, Microelectronics Reliability 43 (2003) 259-267.

[66] Lin L.-W., Song J.-M., Lai Y.-S., Chiu Y.-T., Lee N.-C., Uan J.-Y., Alloying Modification on Sn-Ag-Cu Solders by Manganese and Titanium, Microelectronics Reliability, 49 (2009) 235-241.

[67] Anderson I.E., Walleser J.W., Harringa J.L., Laabs F., Kracher A., Nucleation Control and Thermal Aging Resistance of Near-Eutectic Sn-Ag-Cu-X Solder Joints by Alloy Design, Journal of Electronic Materials, 38 (12) (2009) 2770-2779.

[68] Anderson I.E., Walleser J., Harringa J.L., Observations of nucleation catalysis effects during solidification of SnAgCuX solder joints, JOM 59 (7) (2007) 38-43.

[69] Anderson I.E., Bloomer T.E., Foley J.C., Terpstra R.L., Proceedings of IPC '99, IPC, Northbrook, IL, S-03-5 (1999).

[70] Wang Y.W., Lin Y.W., Tu C.T., Kao C.R., Effects of Minor Fe, Co, and Ni Additions on the Reaction Between SnAgCu Solder and Cu, Journal of Alloys and Compounds 478 (1-2) (2009) 121-127.

[71] Wynblatt P., The Effects of Interfacial Segregation on Wetting in Solid Metal-on-Metal and Metal-on-Ceramic Systems, Acta Materialia 48 (2000) 4439–4447.

[72] Chen S.-W., Wang C.-H., Lin S.-K., Chiu C.-N., Phase Diagrams of Pb-Free Solders and Their Related Materials Systems, Journal of Materials Science: Materials in Electronics 18 (2007) 19-37.

[73] Vianco P.T., Rejent J.A., Properties of Ternary Sn-Ag-Bi Solder Alloys, Part II: Wettability and Mechanical Properties Analyses, Journal of Electronic Materials 28 (1999) 1138-1143.

[74] Loomans M.E., Vaynman S., Ghosh G., Fine M.E., Investigations of Multicomponent Lead-Free Solder, Journal of Electronic Materials 23 (1994) 741-746.

[75] Suganuma K., Niihara K., Shoutoku T., Nakamura Y., Wetting and Interface Microstructure between Sn-Zn Binary Alloys and Cu, Journal of Materials Research 13 (1998) 2859-2865.

[76] Vianco P.T., Claghorn A.C., Effect of Substrate Preheating on Solderability Performance as a Guideline for Assembly Process Development Part I: Baseline Analysis, Soldering and Surface Mount Technology 8 (3) (1996) 12-18.

[77] Wu C.M.L., Wu D.Q., Law C.M.T., Wang L., The Wettability and Microstructure of Sn-Zn-RE Alloys, Journal of Electronic Materials 32 (29) (2003) 63-69.

[78] Kang S.K., Choi W.K., Shih D.-Y., Henderson D.W., Gosselin T., Sarkhel A., Goldsmith C., Puttlitz K.J., "Study of Ag$_3$Sn Plate Formation in the Solidification of Near Ternary Eutectic Sn-Ag-Cu Alloys, JOM 55 (6) (2003) 61-65.

[79] Lin C.-K., Teng H.-T., Creep Properties of Sn-3.5Ag-0.5Cu Lead-Free Solder Under Step-Loading, Journal of Materials Science: Materials in Electronics 17 (2006) 577–586.

[80] Dusek M., Wickham M., Hunt C., The Impact of Thermal Cycling Regime on the Shear Strength of Lead-Free Solder Joints, Soldering and Surface Mount Technology 17 (2) (2005) 22–31.

[81] Espec Technologies, The Effect of Ramp Rate on Temperature Cycle Fatigue in Solder Joints, Espec Technology Report No.25 (2007).

[82] Wikipedia, 2012, "Soldering", http://en.wikipedia.org/wiki/Soldering (Last Visited on: 10.11.2012).

[83] Nogita K., Stabilisation of Cu_6Sn_5 by Ni in Sn-0.7Cu-0.05Ni Lead-Free Solder Alloys, Intermetallics 18 (2010) 145–149.

[84] Hwang C.-W., Suganuma K., Interface Microstructures Between Ni–P Alloy Plating and Sn–Ag–(Cu) Lead-Free Solders, Journal of Materials Research 18, (11) (2003) 2540-2543.

[85] Lee N. T. S., Tan V. B. C., Lima K. M., Structural and Mechanical Properties of Sn-Based Intermetallics From ab-initio Calculations, Applied Physics Letters 89, 141908 (2006).

[86] Carnegie Mellon University, "Crystal Structure Data", http://som.web.cmu.edu/structures/S018-beta-Sn.html (Last Visited on: 17.11.2012).

[87] Wikipedia, 2012, "Electronegativity", http://en.wikipedia.org/wiki/Electronegativity (Last Visited on: 17.11.2012).

[88] Wikipedia, 2012, "Atomic radii of the elements (data page)", http://en.wikipedia.org/wiki/Atomic_radii_of_the_elements_(data_page) (Last Visited on: 17.11.2012).

[89] Wikipedia, 2012, "Sessile drop technique", http://en.wikipedia.org/wiki/Sessile_drop_technique (Last Visited on: 17.11.2012).

[90] ASM Metals Handbook, Volume 3, Alloy Phase Diagrams (1992).

APPENDIX A
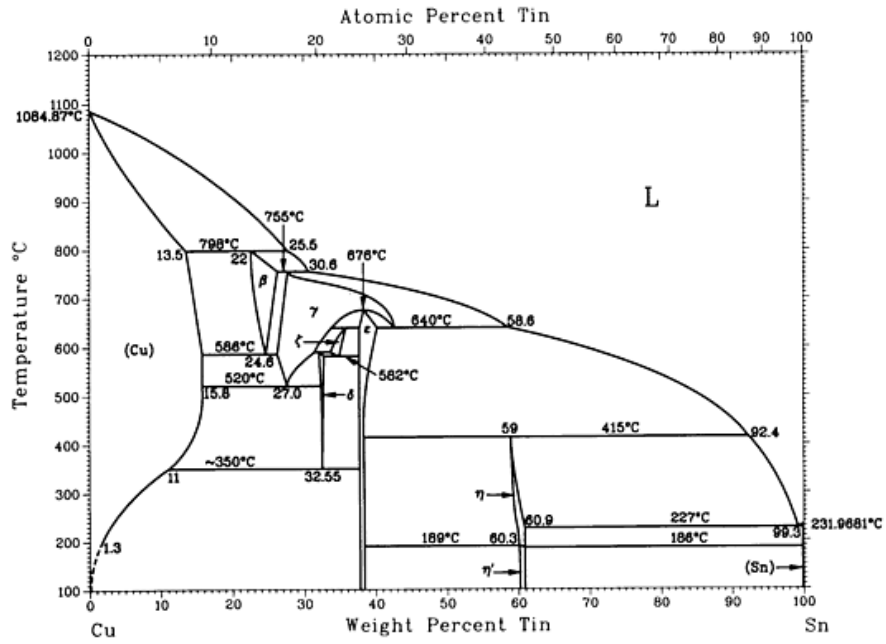
Phase Diagrams (Adapted from **[90]**)

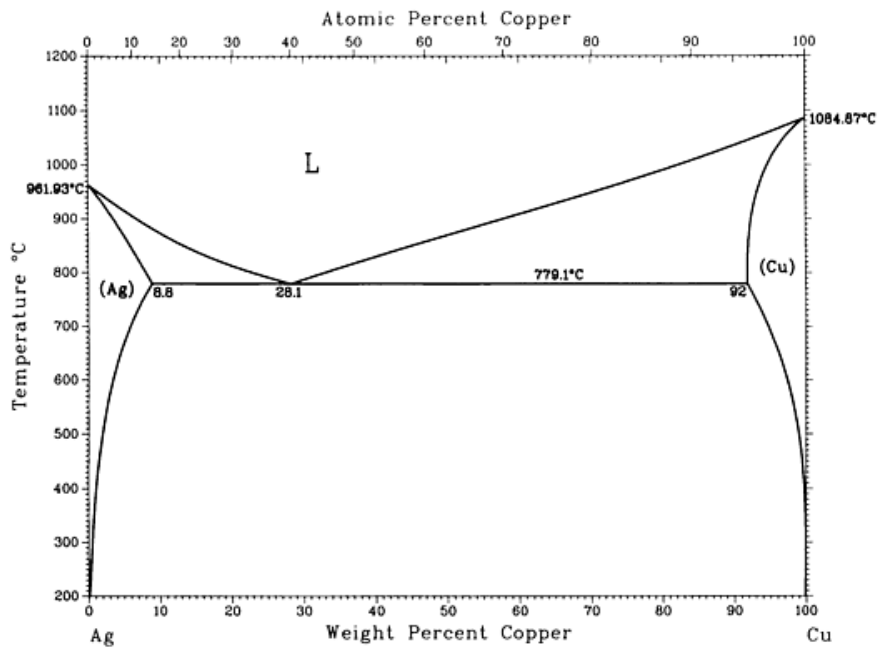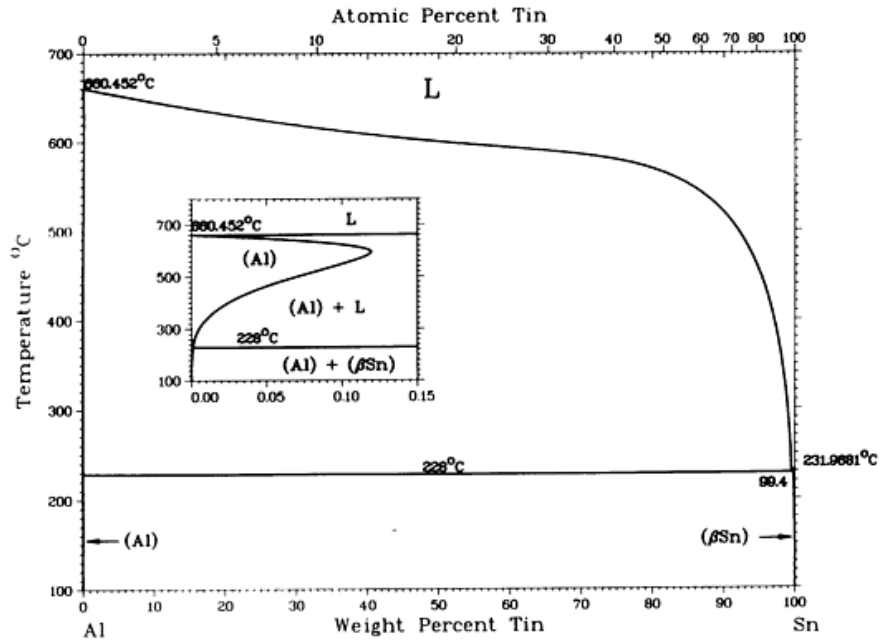**Figure A.1.** Copper-Tin (Cu-Sn) binary phase diagram.

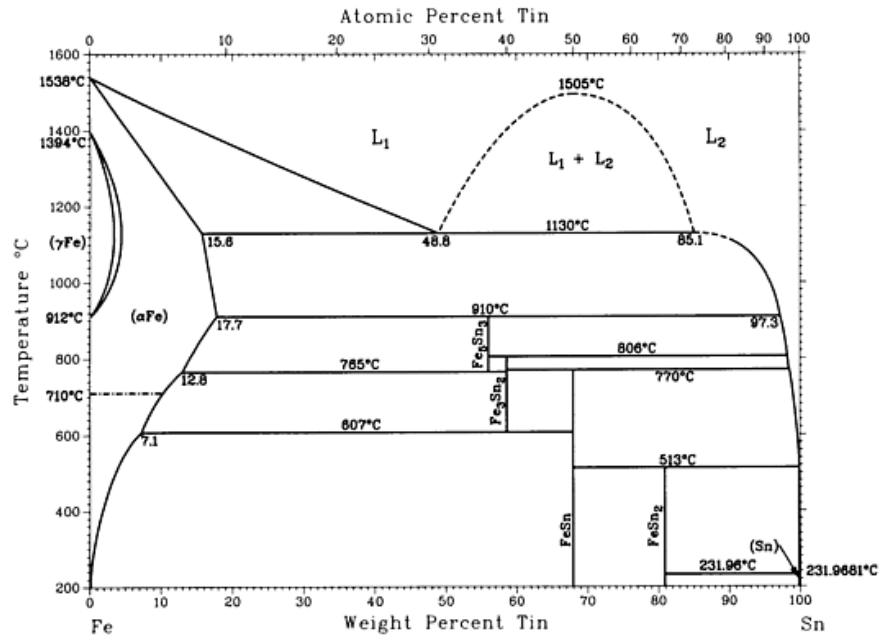**Figure A.3.** Aluminum-Tin (Al-Sn) binary phase diagram.

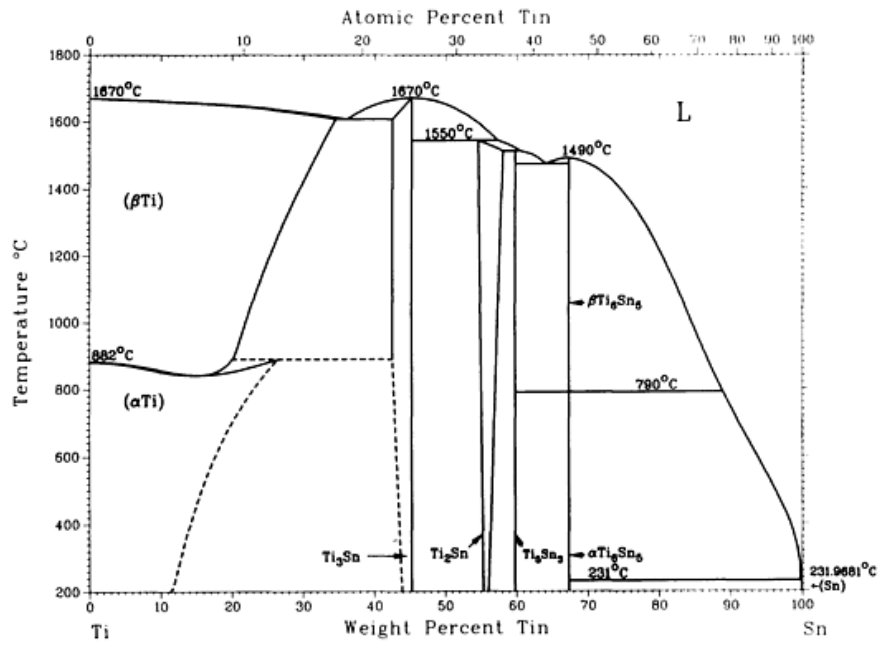**Figure A.4.** Iron-Tin (Fe-Sn) binary phase diagram.

Figure A.5. Titanium-Tin (Ti-Sn) binary phase diagram.

APPENDIX B

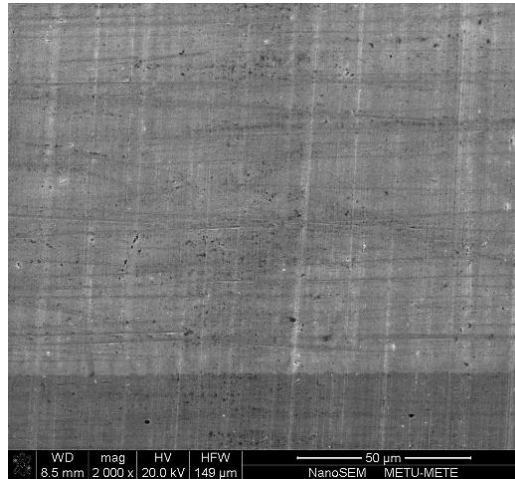## SEM Images of Samples Before and After Thermal Shock Cycles

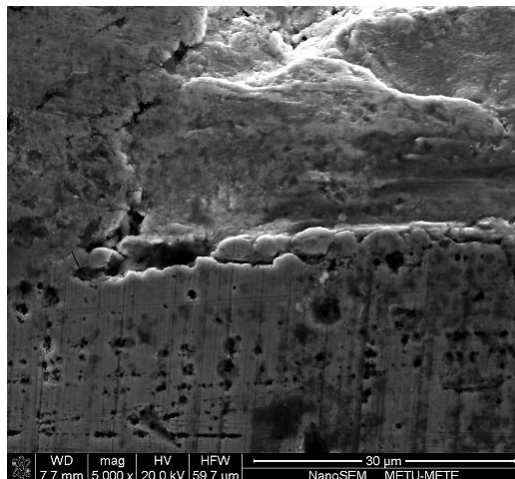**Figure B.1.** Alloy with Sn-3.5Ag-0.9Cu composition before thermal shock.

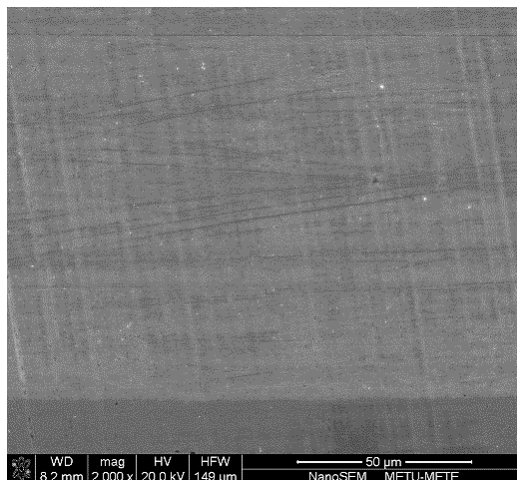**Figure B.2.** Alloy with Sn-3.5Ag-0.9Cu composition after 1000 cycles.

Figure B.3. Alloy with Sn-3.7Ag-0.9Cu composition before thermal shock.
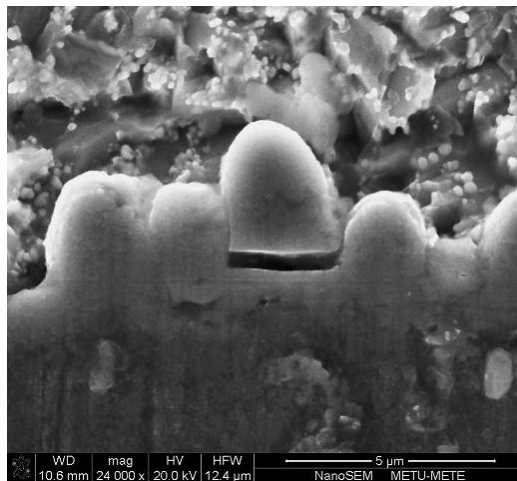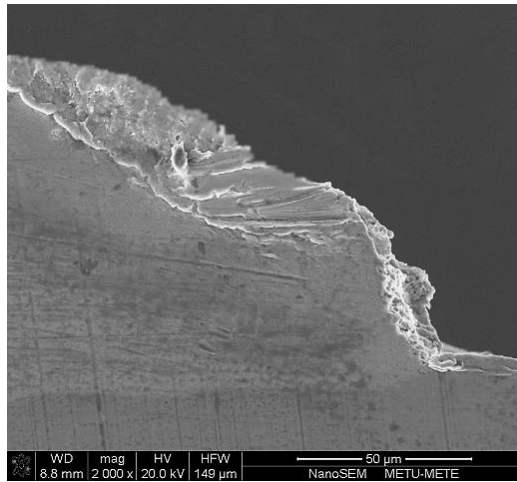

Figure B.4. Alloy with Sn-3.7Ag-0.9Cu composition after 1500 cycles.

Figure B.5. Alloy with Sn-3.0Ag-0.5Cu composition after 1500 cycles.

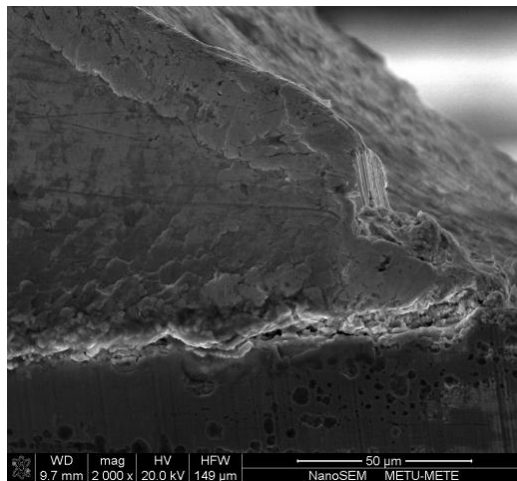**Figure B.6.** Alloy with SAC+0.03Fe composition before thermal shock.

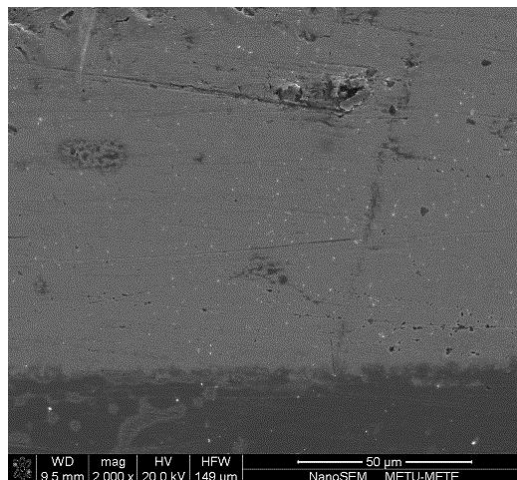**Figure B.7.** Alloy with SAC+0.03Fe composition after 1500 cycles.

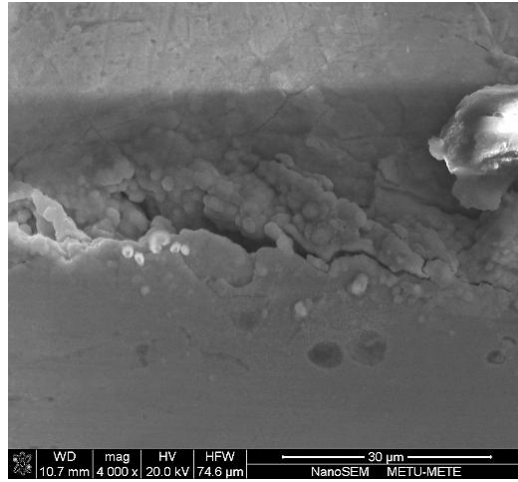**Figure B.8.** Alloy with SAC+0.1Fe composition before thermal shock.

Figure B.9. Alloy with SAC+0.1Fe composition after 1500 cycles.